



This work is protected by copyright and other intellectual property rights and duplication or sale of all or part is not permitted, except that material may be duplicated by you for research, private study, criticism/review or educational purposes. Electronic or print copies are for your own personal, non-commercial use and shall not be passed to any other individual. No quotation may be published without proper acknowledgement. For any other use, or to quote extensively from the work, permission must be obtained from the copyright holder/s.

A STUDY OF COHERENCE PHENOMENA  
IN AN AMMONIA MASER

Thesis submitted to the  
University of Keele for  
the Degree of Doctor of Philosophy  
by  
William Stanley Bardo

Department of Physics,  
University of Keele.  
November 1969.



## ACKNOWLEDGEMENTS

The Author would like to thank

Professor D. J. E. Ingram for the provision of experimental facilities.

Dr. D. C. Lainé for his guidance and enthusiastic encouragement.

His colleagues in the Maser Group, Dr. C. A. Scott and Mr. G. D. S. Smart, for the benefit of many helpful discussions.

The technical staff of the Department and of the University Workshop for their continued help.

The S.R.C. and the University for personal finance.

His wife, Susan, who typed this thesis and prepared the diagrams.

Mr. M. Cheney for the photographic work.

## ABSTRACT

The design and operation of an advanced ammonia beam maser is described. Special features of the design permit operation of the device as an oscillator without the benefit of pumping with liquid nitrogen. Further, one novel feature allows variation of the beam geometry, while the system is under vacuum, to suit different conditions of operation. By virtue of these developments the device has a relatively high efficiency compared with other ammonia masers when it is operated with liquid nitrogen pumping.

The investigations described here are part of a wider exploration of the analogies that exist between various electric dipole and magnetic dipole systems. In particular, it has proved possible to produce two effects for which theory suggests a very small chance of occurrence in an ammonia maser: the transient that follows switching on (and off) of the oscillation; and the oscillation pulsations (spiking) consequent upon periodic modulation of the oscillation condition. These are familiar adjuncts of laser and maser action in many solid-state systems.

A second resonant microwave cavity is employed to monitor the effects on the beam of coherent transitions occurring in the first cavity for a range of beam intensities. The change in relative populations between the two levels is followed by operating

the second cavity in the spectroscopic mode, and looking for absorption or stimulated emission in the beam. A complementary study of the polarisation imparted to the beam by the first cavity is made by observing the change in oscillation level within the second cavity as a function of the frequency detuning of the first resonator. The relationship between the spectroscopic observations and the polarisation effects is clarified in a general treatment for the detuning phenomena. Predictions are made for new types of detuning phenomena, and some tentative support is offered for these predictions.

The analysis of the partial saturation behaviour in the first cavity leads to a proposal for a method of producing a beam composed predominantly of relatively slow molecules. The technique is general in scope and is not restricted to maser media. It offers possibilities of application in frequency standards and in high resolution gas spectroscopy.

1.1	Introduction	66
1.2	Stimulated Emission and Absorption	67
1.3	Steady-State Level Populations	69
1.4	Theories of Spontaneous Emission and Absorption	71
1.5	Two-Level Transition Probabilities	72
1.6	Transient Properties of Two-Level Behaviour	81
1.7	Two-Cavity Detuning Phenomena	93
	References	102

# CONTENTS

	Page
ACKNOWLEDGEMENTS	
ABSTRACT	
PREFACE	i
References	ix
CHAPTER I	
COHERENCE	1
References	28
CHAPTER II	
THE AMMONIA BEAM MASER	
2.1	Introduction 29
2.2	The Ammonia Molecule 30
2.3	The Maser 33
2.4	Microwave System 52
2.5	Electronic Equipment 55
2.6	Operation of the Maser 56
References	64
CHAPTER III	
THEORIES OF MASER BEHAVIOUR	
3.1	Introduction 66
3.2	Dehmelt's Macroscopic Maser 67
3.3	Eberly's Pendulum Analogue 69
3.4	Theorem of Feynman, Vernon and Hellwarth 71
3.5	Two Level Transition Probabilities 79
3.6	Transient Aspects of Two Level Behaviour 81
3.7	Two Cavity Detuning Phenomenon 93
References	105

CHAPTER IV	THE EXPERIMENTAL INVESTIGATION OF TRANSIENT EFFECTS	
4.1	The Oscillation Transient	108
4.2	Induced Spiking	115
4.3	The Spectroscopic Investigation of the State of the Beam Emerging from the First Cavity	119
4.4	Further Investigations of the Beam	127
4.5	Suggestions for Further Work	134
	References	141
	KEY TO SYMBOLS	142
APPENDIX A	ELECTROFORMING CAVITIES	144
APPENDIX B	METHOD FOR DETERMINING Q FACTORS	145

## PREFACE

The invention of the molecular beam maser constituted a major advance in microwave spectroscopy, and presaged the growth of a new field of physical electronics-quantum electronics. The characteristic feature of the new discipline is that it utilises quantum properties of matter in the construction of amplifiers and oscillators, whereas classical electronics is concerned with the charge properties of matter.

All the active quantum electronics devices, maser amplifiers and oscillators, depend upon the phenomenon of stimulated emission: the emission of radiation from atoms or molecules induced by a signal field, and coherent with that field. The concept of induced emission was introduced in 1917 by Einstein. However, it was not until 1954 that a device operating on the principle of stimulated emission was constructed.

For a substance in thermal equilibrium the populations of its energy levels are governed by the Boltzmann distribution, and of two energy levels the lower has a greater population. Irradiation of a system in thermal equilibrium with a signal field of a frequency corresponding to the energy separation of the two levels yields a net absorption. Amplification of the signal demands a non-equilibrium distribution of populations, with a greater number of molecules or atoms in the upper energy level

than in the lower. Such a system is sometimes described as having a negative temperature, from a formal interpretation of the Boltzmann equation, though it should be noted that it is a non-equilibrium situation and in relaxing towards thermal equilibrium the system passes through an infinite temperature. Negative temperature implies "hotness" rather than coldness. If the method of inversion involves the irradiation of the system with a pulse then, strictly, a temperature should not be assigned to the inverted system until a time of the order of the transverse relaxation time ( $T_2$ ) has elapsed. Immediately after the pulse there exist phase relationships between the "spins" (the off-diagonal elements of the density matrix are non-zero) which require a time of the order of  $T_2$  to approach the condition of internal thermal equilibrium.

A variety of methods have been devised to achieve the desired non-thermal population imbalance: these are reviewed in standard textbooks such as those by Singer (1959) and Vuylsteke (1960). The method employed in the ammonia maser is perhaps the simplest in concept, and involves the removal of the molecules populating the lower of the two levels involved in the microwave transition.

A proposal for a maser oscillator was presented by A. H. Nethercot on behalf of C. H. Townes at a symposium on sub-millimetre waves at the University of Illinois in May, 1951.

There followed an outline of a proposed gas beam device in the Columbia Radiation Laboratory Quarterly Progress Report for December 31, 1951. Transient stimulated emission from an inverted system was observed by Purcell and Pound (1951), but involved no amplification. The principle of obtaining amplification of electromagnetic waves by means of non-equilibrium quantum systems is described in a patent granted in 1951 to Fabrikant, Vudynskii and Butaeva. In 1953 Weber examined (independently of Townes) the possibilities of obtaining amplification and oscillation with non-Boltzmann populations. Basov and Prokhorov (1954) discussed a design for a molecular amplifier and oscillator, together with a theoretical treatment. In the same year Gordon, Zeiger and Townes published their first results from an ammonia beam maser operating at 24GHz., reporting a very low noise amplifier ( $< 10^0\text{K}$ ), a very stable oscillator (with a fractional frequency stability of better than  $10^{-10}$ ), and a gas spectrometer with a resolution ( $\sim 7\text{kHz.}$ ) nearly an order of magnitude better than previously achieved. It was they who coined the acronym MASER (Molecular Amplification by Stimulated Emission of Radiation).

Since that time the maser principle has been exploited over a wide range of the frequency spectrum, for electric dipole and magnetic dipole transitions, and in all states of media, gaseous, liquid and solid.



In 1957 Feynman, Vernon, and Hellwarth established a rigorous analogy between electric and magnetic dipole two-level non-interacting systems. They provided a geometric representation of the Schrödinger equation which invested the equations of motion of the density matrix with an intuitive interpretation. It is possible to view the behaviour of an electric dipole system under irradiation as the analogue of the behaviour of a magnetised gyroscope precessing about a static magnetic field while subject to a time varying magnetic field. The pre-eminent exemplar of this correspondence is the observation and interpretation of the photon echo, the optical analogue of the spin echo of nuclear magnetic resonance (Kurnit, Abella, and Hartmann, 1964).

In recent years the Keele maser group, which includes the author, has been investigating the analogies which exist between various electric dipole and magnetic dipole systems.

Since, for the purpose of most discussions, the ammonia beam maser is a good approximation to a two-level system of molecules interacting with a radiation field, it has served as a model for a number of theoretical discussions concerning transient behaviour of quantum electronic amplifiers and oscillators. However, experimental confirmation of some of the theoretical predictions has so far depended upon other maser systems. Interest in transients springs also from the consideration that their analysis

permits measurement of relaxation times for population changes ( $T_1$ ) and for dephasing effects ( $T_2$ ).

This dissertation is principally concerned with two transients - the oscillation transient and the related phenomenon of induced spiking. The former has been observed in laser systems and in the hydrogen beam maser. The latter is closely related to the spiking behaviour observed in a number of solid state lasers and masers.

The transient behaviour reflects the partial saturation behaviour of the maser: molecules are induced to make several coherent transitions between the two levels during their time of flight through the resonator. This behaviour is further examined by analysing with a second microwave cavity the state of the beam emerging from the first. The beam is examined for its relative populations, and for the polarization it receives in the first resonator.

Analysis of microwave electric dipole maser behaviour in terms of a nuclear magnetic resonance analogue has a dual appeal. Firstly, the behaviour of a perturbed magnetized gyroscope is more readily visualised than the motion of vectors in an abstract space that describes the time development of an electric dipole system. The behaviour of nuclear magnetic resonance systems has been studied very thoroughly, and much of the theoretical treatment is readily

translated into a form suitable for discussion of the electric dipole case. Secondly, nuclear magnetic resonance systems have many desirable experimental features that are denied to the microwave maser systems. One instance may serve to illustrate this aspect. Acting on a suggestion by D. C. Laine<sup>1</sup> that liquid flow n.m.r. masers should provide an analogue for the two-cavity ammonia beam maser the present writer examined the possibility of adapting such a maser. A maser devised by Benoit (1958, 1959) proved ideal for the purpose and W. H. U. Krause constructed a liquid nuclear maser at Keele, and converted it to the two-cavity analogue by adding a second coil downstream from the first emission coil. Krause (1969) has proceeded to demonstrate in a series of elegant experiments the analogues of much of the behaviour of a microwave two-cavity maser, and extended the theoretical treatment developed by the French school to include the two-coil case. The n.m.r. liquid maser possesses many virtues: it does not require a vacuum system, there are no problems of beam divergence, the velocity distribution is comparatively simple under conditions of laminar flow, the frequency of a few kiloHertz is convenient for processing of the signals with conventional circuitry, and the  $Q$  of the "cavities" is readily varied by means of  $Q$  multipliers. One disadvantage is its enhanced sensitivity to inhomogeneities in the magnetic field, compared with the ammonia maser.

The thesis has been organized into four chapters. Since the concepts of induced and spontaneous emission are crucial to an understanding of maser action, theoretical treatment of these topics is reviewed in Chapter I in preparation for the discussions that follow in the other chapters. The relationship between the concepts of coherence employed in optical studies and in microwave work is often not clear. It might seem reasonable to argue that for microwave fields temporal coherence is assured because the microwave sources produce a continuous train of waves of high monochromaticity, and that spatial coherence exists because apparatus dimensions are usually about the same order of magnitude as the wavelength. However, the discussions here are concerned with the interaction of molecular systems with the field, and not counter detection of photon correlations. Molecular systems subjected to irradiation with coherent pulses may be correlated so that they subsequently emit radiation of varying degrees of coherence. Spatial distribution of the molecules is an important factor in the nature of the radiation emitted by the molecules: for instance, the shape of the gas cell affects the distribution of radiation emitted from an assembly of molecules in a super-radiant state.

In Chapter II the special features of design of the maser which render the transient effects accessible are described.

Chapter III is devoted to a review of theoretical investigations of one- and two-cavity maser behaviour, giving particular attention to the analogy that exists between electric dipole and magnetic dipole systems.

Chapter IV details the experimental investigations of the transient effects, and the conclusions which emerge from their analysis. Suggestions are made for methods of extending the capabilities of the maser for further study of these transients, and of others, and for the investigation of maser components, such as new forms of focuser.

REFERENCES

Einstein, A. (1917), Phys. Z. 18, 121.

Singer, J. R. (1959), Masers, New York, John Wiley.

Vuylsteke, A. A. (1960), Elements of Maser Theory, Princeton,  
van Nostrand.

Purcell, E. M., Pound R.V. (1951), Phys. Rev., 81, 279.

Fabrikant, V. A., Vudynskii, M. M., and Butaeva, F. A. (1951),  
Patent Cert. No. 148441 (576749/26 of 18 July 1951)

Weber, J. (1953), Trans. I.R.E.P.G.E.D., 3, 1.

Basov, N. G., Prokhorov, A. M. (1954), Sov. Phys. - J.E.T.P., 27, 431.

Gordon, J. P., Zeiger, H. J., and Townes, C. H. (1955), Phys. Rev.,  
99, 1264.

Feynman, R. P., Vernon, F. L., and Hellwarth, R. W. (1957),  
J. Appl. Phys., 28, 49.

Kurnit, N. A., Abella, I. D., and Hartmann, S. R. (1964),  
Phys. Rev. Lett., 13, 567-8.

Benoit, H. (1958), Comptes rendus, 246, 2123.

Benoit, H. (1959), Ann. Physique, 4, 1439.

Krause, W. H. U. (1969), doctoral thesis, University of Keele.

## CHAPTER I

### COHERENCE

The advent of lasers provided theoreticians with a considerable incentive to extend the study of the coherence properties of an electromagnetic radiation field. The salient advance made in the quantum mechanical treatment of photon distributions is the systematic use of a particular set of nonstationary states for the harmonic oscillator representing a mode of the field. These are the eigenstates  $|\{\alpha_k\}\rangle$  of the photon annihilation operators  $a_k$ . These "coherent states" obey the relations

$$a_k |\{\alpha_k\}\rangle = \alpha_k |\{\alpha_k\}\rangle ,$$

for all  $k$ , where the  $\{\alpha_k\}$  are an arbitrary set of complex numbers.

They can be constructed from number eigenstates

$$|\alpha\rangle = \sum_{n=0}^{\infty} |n\rangle \langle n|\alpha\rangle ,$$

whence

$$|\alpha\rangle = \exp\left(-\frac{1}{2} |\alpha|^2\right) \sum_{n=0}^{\infty} \frac{\alpha^n}{(n!)^{\frac{1}{2}}} |n\rangle .$$

They can also be generated by the action of a unitary displacement operator on the ground state

$$|\alpha\rangle = \exp\left[\alpha a^\dagger - \frac{1}{2} |\alpha|^2\right] |0\rangle .$$

These states form a subset of the set that minimise the uncertainty product. In the Schrödinger picture they evolve in time

according to

$$|\alpha(t)\rangle \equiv e^{-iHt} |\alpha\rangle = \exp[\alpha a e^{i\omega t} - \frac{1}{2} |\alpha|^2] |\alpha\rangle.$$

This describes a displaced ground state wavefunction which vibrates back and forth with frequency  $\omega$  without any change of shape or spreading (Henley and Thirring, Carruthers and Nieto).

The utility of the coherent states for the investigation of photon correlations may be ascribed to two main features:

(a) the states are eigenstates of the complex field operator, and permit the reduction of the operator to a c-number, thus facilitating the construction of suggestive analogies between the classical and quantum-mechanical behaviour of fields (the degree of equivalence between the two is a matter of lively controversy- see the paper by Glauber);

(b) the coherent states form an overcomplete set, and thus the density operator  $\rho$  can be expanded in terms of these states as a basis. The coherence properties of the quantized field are described by means of a hierarchy of correlation functions for the complex field operators,

$$G^{(n)}(x_1 \dots x_n, x_{n+1} \dots x_{2n}) = \text{tr} \{ \rho E^{(-)}(x_1) \dots E^{(-)}(x_n) E^{(+)}(x_{n+1}) \dots E^{(+)}(x_{2n}) \},$$

where  $E^{(-)}(x)$  and  $E^{(+)}(x)$  are the negative- and positive-frequency parts of the electric field operator, and  $x_j$  stands for both the arguments  $\underline{r}_j$  and  $t_j$ . A field is said to possess



m th-order coherence if the correlation functions of order up to and including m factorize according to the scheme

$$G^{(n)}(x_1, \dots, x_{2n}) = \prod_{j=1}^n \mathcal{E}^*(x_j) \mathcal{E}(x_{j+n}),$$

where  $\mathcal{E}(x)$  is a complex function of  $x$ , independent of  $n$ . Other pure states can fulfil the full coherence conditions, but the coherent states satisfy certain stringent restrictions on factorization.

Klauder and Sudarshan give a detailed pedagogical treatment of these formulations of coherence properties.

Fortunately, this dissertation is concerned with observations and interpretations of coherence effects occurring at microwave frequencies, for which less esoteric and more intuitively accessible concepts of coherence will serve very well. Here one is concerned with the effect of microwave fields on an assembly of two-level systems. The coherent excitation puts the "spins" into a coherent superposition of states

$$|\psi\rangle = a(t) |\frac{1}{2}\rangle + b(t) |-\frac{1}{2}\rangle,$$

where  $a(t)$  and  $b(t)$  are found by solving the Schrödinger time-dependent equation. These are periodic functions of time which are locked in phase to the r.f. field. Where before the dipole oscillators had random phase, the r.f. field has ordered the phases to give an oscillating macroscopic polarization, which further reacts on the field.

In terms of the density matrix formalism; initially the  $a$ 's and  $b$ 's of different atoms have random phase, the density matrix of the system is diagonal, and the properties one can observe of the system are those of atoms in pure states. On the application of the r.f. field coherence properties appear, and the non-diagonal elements of the density matrix,  $ab^*$  and  $ba^*$  are no longer zero. When the external locking agent is removed the coherence decays with the characteristic relaxation time  $T_2$ .

For these purposes, then, one can define a coherent oscillation as a sinusoidal oscillation with a well-defined phase. By coherent radiation from a molecule, one means radiation for which the field oscillates coherently, with the phase determined by the state of the molecule or by the coherent field to which the molecule is coupled. If the state of the molecule and / or coupled field do not determine the phase of the radiation, then the phase is a random variable and the radiation is incoherent. Only coherent radiation will contribute to an average of the radiation field over many similar systems, but the incoherent radiation will appear in the average of the square of the field. Thus the dispersion in field  $(\langle E^2 \rangle - \langle E \rangle^2)$  is a measure of the incoherence.

These latter considerations appear to have little in common with the concept of coherence discussed in the early paragraphs in the context of photon correlations. The coherent states

can serve to mediate between the two viewpoints. It can be shown, using Dirac's radiation theory, in which the molecule and the field are quantized, that the spontaneous emission by the molecule, if it is initially in the excited state ( $b = 1, a = 0$ ), is completely incoherent. The incoherence is due to the uncertainty in the positions of the charged particles in the molecule when the molecule is in a stationary state. Consider a dipolar harmonic oscillator in the energy eigenstate  $|n\rangle$ , with energy  $E_n$ . The field emitted in the spontaneous decay to the state  $|n-1\rangle$  is completely incoherent. In the state  $|n\rangle$ , the dipole moment of the oscillator is equally likely  $\pm \mu$ , and hence the field at any one point in space equally likely  $\pm E$ . In consequence the expectation value of the field operator vanishes at any given time. However, if the oscillator is in a coherent state  $|\alpha\rangle$  such that its energy is the same as in state  $|n\rangle$ ,  $\langle \alpha | \mathcal{H} | \alpha \rangle = E_n$ , the rate of emission by the oscillator is the same as when in the state  $|n\rangle$ , but the field is completely coherent.

The ammonia maser poses a number of interesting theoretical problems concerning coherence. It reduces essentially to a study of the behaviour of a coherently oscillating radiation field which is in resonance (or near resonance) with a group of similar molecular systems which are coupled with one another solely via the field, by means of their electric dipole moments. In particular one wishes

to examine induced emission, incoherent and coherent spontaneous emission, and correlation effects between molecules. The discussion which follows is based mainly on the treatment of these aspects of microwave spectroscopy given by Dicke (1954) and Senitzky (I-1958, II-1959).

Senitzky's approach is based on a perturbation treatment to various orders of dynamical variables, in which both molecules and field are treated quantum-mechanically. In I the cavity is assumed lossless, but in II losses are included to permit a calculation of amplitudes and time dependence of induced and spontaneous emissions. For the lossless case only an initial field need be assumed, but for the lossy case the initial field would be damped, and so a driving field must be provided. The assumed driving field mechanism is a classical dipole in resonance with the cavity and two-level molecules.

The field is described by

$$\underline{E} = -4\pi c \underline{P}, \quad \underline{H} = \nabla \wedge \underline{A},$$

$$\underline{A} = Q(t) \underline{u}(\underline{r}), \quad \underline{P} = P(t) \underline{u}(\underline{r}),$$

where  $P$  and  $Q$  are the quantum-mechanical field variables, obeying the commutation rule  $[Q, P] = i\hbar$ . The initial state of the field, which describes a coherently oscillating field, is chosen to be the pure state,

$$\phi(P, 0) = \left( \frac{4c^2}{\hbar \omega} \right)^{\frac{1}{4}} \exp \left[ -\frac{4\pi c^2}{\hbar \omega} \left( \frac{1}{2} P^2 - \frac{E_0}{4\pi c} P \right) \right].$$

The initial state of the molecules is described by

$$\psi = \prod_{m=1}^N [a_1(m) \phi_1(m) + a_2(m) \phi_2(m)],$$

where  $\phi_1(m)$  and  $\phi_2(m)$  are the two energy states of the  $m$ th free molecule, and

$$|a_1(m)|^2 + |a_2(m)|^2 = 1.$$

The electric dipole moment of the  $m$ th molecule is specified by  $\underline{\gamma}_m$  which, since the molecule has no permanent dipole moment, has only off-diagonal elements. The Hamiltonian for the combined system is

$$\mathcal{H} = 2\pi c^2 P^2 + \frac{\omega^2}{8\pi c^2} Q^2 + \sum_{m=1}^N \mathcal{H}_m - \sum_m \underline{\gamma}_m \cdot \underline{E}(\underline{r}_m).$$

The Heisenberg equations of motion for the field variables are

$$\begin{aligned} \dot{P} &= -\left( \frac{\omega^2}{4\pi c^2} \right) Q, \\ \dot{Q} &= 4\pi c^2 P + 4\pi c \sum_m \underline{\gamma}_m \cdot \underline{u}(\underline{r}_m). \end{aligned}$$

In integral form these equations become

$$Q(t) = Q^{(0)}(t) + 4\pi c \sum_m \int_0^t dt_1 \underline{\gamma}_m(t_1) \cdot \underline{u}(\underline{r}_m) \cos \omega(t-t_1),$$

$$P(t) = P^{(0)}(t) - \frac{\omega}{c} \sum_m \int_0^t dt_1 \underline{\gamma}_m(t_1) \cdot \underline{u}(\underline{r}_m) \sin \omega(t-t_1),$$

where  $P^{(0)}(t)$  and  $Q^{(0)}(t)$  represent the field in the absence of interaction with the molecules.

The dynamical variables are expanded in powers of the coupling constant (contained in  $\underline{\gamma}$ ). Thus, setting  $P(t) = P^{(0)}(t) + P^{(1)}(t) + P^{(2)}(t) + \dots$  and similarly for  $Q(t)$  and  $\underline{\gamma}(t)$ ,

$$Q^{(n)}(t) = 4\pi c \sum_m \int_0^t dt_1 \gamma_m^{(n-1)}(t_1) \cdot \underline{u}(\underline{r}_m) \cos \omega(t-t_1),$$

$$P^{(n)}(t) = \frac{\omega}{c} \sum_m \int_0^t dt_1 \gamma_m^{(n-1)}(t_1) \cdot \underline{u}(\underline{r}_m) \sin \omega(t-t_1).$$

The expectation values for  $Q^{(1)}(t)$  and  $P^{(1)}(t)$  are

$$\langle P^{(1)}(t) \rangle \simeq -(\omega/c) \sum_m |a_1(m) a_2(m)| \tilde{\gamma}_m t \sin(\omega t + \Theta_m),$$

$$\langle Q^{(1)}(t) \rangle \simeq 4\pi c \sum_m |a_1(m) a_2(m)| \tilde{\gamma}_m t \cos(\omega t + \Theta_m),$$

where  $\tilde{\gamma}_m = \gamma_{m12} = \gamma_{m21}^*$  are the matrix elements of  $\gamma_m^{(0)}(0)$

( $\gamma_m$  is the component of  $\underline{\gamma}_m$  along  $\underline{u}(\underline{r})$ ), and  $\Theta_m$  is the

difference in phase between  $a_2(m)$  and  $a_1(m)$ . Here, in first order, is spontaneous emission, with each molecule acting (on the

average) as a classical oscillator of well-defined phase,

and amplitude which is proportional to  $|a_1(m) a_2(m)|$ . This

amplitude is a maximum when  $|a_1(m)| = |a_2(m)| = 2^{-1/2}$ ; in

other words, when the molecule is in the superposition state with

equal amounts of each of the two energy states. Also, the amplitude

vanishes when the molecule is completely in either one of the energy states.

Proceeding to higher orders, the expectation values are

$$\langle \gamma_m^{(1)}(t) \rangle \simeq E_0 u \hbar^{-1} \tilde{\gamma}^2 t [|a_2(m)|^2 - |a_1(m)|^2] \cos \omega t,$$

$$\langle P^{(2)}(t) \rangle \simeq -\frac{E_0}{8\pi c} \frac{E_0(t)}{\hbar \omega} \sin \omega t \sum_m [|a_2(m)|^2 - |a_1(m)|^2],$$

where  $\mathcal{E}_0(t) \equiv 2\pi\omega^2 u^2 \tilde{y}^2 t^2$ .

This is induced radiation, which is in phase (emission) or  $180^\circ$  out of phase (absorption) with respect to the inducing field, depending upon whether the molecule is mostly in the upper energy state or the lower energy state.

The entire expression (up to the second order) for the expectation value of the electric field is

$$\begin{aligned} \langle E \rangle &= E_0 u \sin \omega t \\ &+ E_0 u \frac{\mathcal{E}_0(t)}{2\hbar\omega} \sum_m [|a_2(m)|^2 - |a_1(m)|^2] \sin \omega t \\ &+ 4\pi\omega u^2 t \tilde{y} \sum_m |a_1(m) a_2(m)| \sin(\omega t + \theta_m). \end{aligned}$$

The expectation value for the energy of the field is,

$$\begin{aligned} \langle \mathcal{H}_{\text{field}} \rangle &= 2\pi c^2 \langle P^2 \rangle + \left( \frac{\omega^2}{8\pi c^2} \right) \langle Q^2 \rangle, \\ &= \frac{E_0^2}{8\pi} + \frac{E_0^2}{8\pi} \frac{\mathcal{E}_0(t)}{\hbar\omega} \sum_m [|a_2(m)|^2 - |a_1(m)|^2] \\ &+ E_0 \omega \tilde{y} u t \sum_m |a_1(m) a_2(m)| \cos \theta_m \\ &+ \mathcal{E}_0(t) \sum_m |a_2(m)|^2 \\ &+ \mathcal{E}_0(t) \sum_{m \neq m'} |a_1(m) a_2(m)| |a_1(m') a_2(m')| \\ &\quad \times \cos(\theta_m - \theta_{m'}) + \frac{1}{2} \hbar \omega. \end{aligned}$$

The first term is the energy of the initial field. The second



term is induced radiation (emission or absorption). The third term is the interaction between the initial oscillation of the molecule and the field which exists in the cavity. The fourth and fifth terms are spontaneous emission, and the last term is the zero-point energy of the field (which is independent of the molecules).

In order to determine the coherent and incoherent contributions to the field energy it is necessary to examine the dispersion,  $(\langle E^2 \rangle - \langle E \rangle^2)$ , as discussed earlier.

The first term in the expression for the energy corresponds to the square of the first term in  $\langle E \rangle (\sin^2 \omega t$  is combined with  $\cos^2 \omega t$  contributed by the magnetic part of the energy). This is the coherent energy of the initial field. The second and third terms in  $\langle \mathcal{H} \text{ field} \rangle$  correspond with the cross-products in the square of  $\langle E \rangle$ , and therefore represent coherent energy. There remains for consideration the square of the last term in  $\langle E \rangle$ , for which the corresponding term in the energy would be

$$\begin{aligned} \mathcal{E}_0(t) & \sum_{m, m'} |a_1(m) a_2(m)| |a_1(m') a_2(m')| \cos(\theta_m - \theta_{m'}) \\ & = \mathcal{E}_0(t) \left\{ \sum_{m \neq m'} |a_1(m) a_2(m)| |a_1(m') a_2(m')| \cos(\theta_m - \theta_{m'}) \right. \\ & \quad \left. + \sum_m [ |a_2(m)|^2 - |a_2(m)|^4 ] \right\}. \end{aligned}$$

Part of this appears as the fourth term and the entire fifth term of  $\langle \mathcal{H} \text{ field} \rangle$ , and is the coherent spontaneous emission energy.

The remainder is  $\mathcal{E}_0(t) \sum_m |a_2(m)|^4$ ,



and represents the incoherent spontaneous emission energy.

It should be noted that the first order part of  $\langle E \rangle$ , and the coherent part of the spontaneous emission energy, are the field and energy of a classical radiation field coupled to a classical oscillating dipole moment,  $\langle \gamma(t) \rangle$ .

A distinction should be made between the use here of the term "coherence" in the context of Senitzky's treatment, and the connotation the word may normally carry. Consider the situation where there is a random distribution of initial states. Then the "coherent" radiation of each molecule has random phase, and is more properly described as "incoherent", in keeping with the classical notion of incoherence resulting from an assembly of oscillators with random initial phase.

Consider next a number of situations which are of particular relevance to this thesis. For simplicity assume that the amplitudes of oscillation of all the radiators are equal; that is  $|a_1(m)a_2(m)| = |a_1(m')a_2(m')|$ . Let  $M$  molecules have one phase and the remainder have opposite phase. The coherent spontaneous emission energy is then proportional to  $[M - (N - M)]^2$ . If  $M = \frac{N}{2}$  then the coherent spontaneous emission vanishes. However, there still remains the incoherent spontaneous radiation which is completely independent of the phase of the molecules. The energy of this emission is a function of the total number of

molecules. For the case of  $M=N$ , when all the molecules are in phase, the energy of the coherent emission is proportional to  $N^2$ , and when  $|a_1(m)a_2(m)| = \frac{1}{2}$ , it is a maximum.

Coherent spontaneous emission (otherwise known as "molecular ringing") is observed to follow the application of a short microwave pulse to an assembly of molecules. The driving field orders the state phases of the molecules to produce an induced oscillating dipole with a well-defined phase dependent upon the amplitude and duration of the primary field. When this field is cut off the induced emission does not cease instantaneously, for the dipole moment now gives rise to "spontaneous coherent emission". The molecules are now driven by their own radiation. The amplitude of the ringing field is proportional to the rate of change of the state populations, which in turn is dependent upon the ringing field. Bloom (1956) has made a time-dependent perturbation calculation employing this self-consistency condition, and has shown that the ringing power varies as a  $\text{sech}^2$  function. Furthermore, depending upon the strength and duration of the driving pulse the ringing may exhibit a delayed maximum. This occurs when the ringing field has driven the populations to an instantaneous equality. (This phenomenon is discussed further in a later chapter.)

It will be perceived that the only distinction between induced emission and coherent spontaneous emission lies in the

manner in which the driving mechanism, the induced oscillating dipole moment, is produced. A treatment including higher orders in the perturbation expansion reveals that the energy radiated in induced emission is proportional to  $N^2$ , as in the molecular ring-ing.

The treatment reviewed so far has employed molecular states which are products of one-molecule states, and are therefore uncorrelated. In principle, measurements of the state of each molecule are independent of one another. Correlated states, which are linear combinations of products of one-molecule states, must be employed if the underlying symmetries of the field-molecule system are to be exploited to the full.

Dicke (1954) has investigated co-operative phenomena arising as a result of transitions between energy levels corresponding to correlations between molecules. His treatment of the collection of molecules as a single quantum-mechanical system reveals that there are "super-radiant" and "subradiant" states for which the radiation rates are, respectively, higher and lower than the incoherent emission rate.

The formalism employs operators  $R_1$ ,  $R_2$ , and  $R_3$ , which are analogues of the Pauli spin operators. They operate on the  $j$  th molecule according to the rules:

$$\begin{aligned}
 & \begin{array}{c} j \\ \downarrow \end{array} \\
 R_{j1} [\dots \pm \dots] &= \frac{1}{2} [\dots \mp \dots], \\
 R_{j2} [\dots \pm \dots] &= \pm \frac{1}{2} i [\dots \mp \dots], \\
 R_{j3} [\dots \pm \dots] &= \pm \frac{1}{2} [\dots \pm \dots].
 \end{aligned}$$

They appear in combination as

$$R_k = \sum_{j=1}^n R_{jk}, \quad k = 1, 2, 3,$$

and

$$R^2 = R_1^2 + R_2^2 + R_3^2.$$

Consider initially that the molecular gas is enclosed in a resonant cavity the dimensions of which are much smaller than the wavelength. Assume that the gas molecules have only two non-degenerate levels  $E_+$  and  $E_-$  ( $E_+ > E_-$ ). The radiation is calculated in the dipole approximation. It is further assumed that the wavefunctions of the molecules do not overlap, so that the Pauli conditions on symmetrization of the wavefunctions can be relaxed. The Hamiltonian of the system of molecules, neglecting the radiation field, may then be written as

$$\mathcal{H} = \mathcal{H}_0 + E \sum_{j=1}^n R_{j3} = \mathcal{H}_0 + E R_3,$$

where  $E = \hbar \omega_0 = E_+ - E_-$ ,  $\mathcal{H}_0$  operates on the coordinates of the centre of mass of the molecules and represents the energy of translational motion of the molecules and the energy of intermolecular interaction,  $E R_{j3}$  is the internal energy of the  $j$ th molecule and has the eigenvalues  $\pm \frac{1}{2} E$ .

$\mathcal{H}_0$  and all the  $R_{j3}$  commute with each other.

Consequently it is possible to choose eigenfunctions of the energy operator which will simultaneously be eigenfunctions of  $\mathcal{H}_0, R_{13}, R_{23}, \dots$

These eigenfunctions have the form

$$\psi_{gm} = \psi_g(\underline{r}_1, \underline{r}_2, \dots, \underline{r}_n) [ + + - \dots + - ]$$

Here  $\underline{r}_1 \dots \underline{r}_n$  are coordinates of the centres of mass of the  $n$  molecules, and the  $+$  and  $-$  symbols represent the internal energies of the various molecules. If the numbers of  $+$  and  $-$  symbols are designated by  $n_+$  and  $n_-$  respectively, then  $m$  is defined as

$$m = \frac{1}{2}(n_+ - n_-)$$

$$n = n_+ + n_- = \text{number of gas molecules.}$$

The total energy of the gas is

$$E_{gm} = E_g + E_m,$$

where  $E_g$  is the energy of translational motion and interaction of the molecules.  $E_{gm}$  is degenerate of multiplicity

$$\frac{n!}{n_+! n_-!} = \frac{n!}{(\frac{1}{2}n + m)! (\frac{1}{2}n - m)!}$$

In the Hamiltonian  $\mathcal{H}_0$  operates on the coordinates of

the centres of mass so that

$$H_0 U_g = E_g U_g ,$$

and  $R_{j3}$  acts on the + and - symbols in the jth place in

$$[+ + - \dots + -] . \text{ Further note that } R_3 \psi_{gm} = m \psi_{gm} .$$

The operator representing the energy of interaction of the jth molecule with the radiation field is

$$- \underline{A}(\underline{r}_j) . \sum_k \frac{e_k}{m_k c} \underline{P}_k ,$$

where  $\underline{A}(\underline{r}_j)$  is the vector potential of the radiation field at the centre of mass of the jth molecule;  $e_k, m_k$  and  $\underline{P}_k$  are respectively the charge, mass and momentum of the kth particle in the molecule. In the approximation detailed earlier the dependence of  $\underline{A}$  on the coordinates may be neglected, and the interaction term becomes

$$- \underline{A}(0) . \sum_k \frac{e_k}{m_k c} \underline{P}_k .$$

Since the internal energy of the molecule may assume only two values,  $\pm \frac{1}{2}E$ , the interaction operator may be represented as a Hermitian matrix of second order with vanishing diagonal elements, and written in the form

$$- \underline{A}(0) . (\underline{e}_1 R_{j1} + \underline{e}_2 R_{j2}) .$$

The vectors  $\underline{e}_1$  and  $\underline{e}_2$  are constants depending on the type of molecules. The total interaction energy becomes

$$H_1 = - \underline{A}(0) . (\underline{e}_1 R_1 + \underline{e}_2 R_2) .$$

The operators  $\hbar R_1$ ,  $\hbar R_2$  and  $\hbar R_3$  obey the same commutation relations as the three components of angular momentum. In consequence, the operator of the interaction energy obeys the selection rule  $\Delta m = \pm 1$ , and has non-vanishing matrix elements only between the given states and other states which differ in  $m$  by 1. In order to simplify the calculation of the probability of spontaneous transitions stationary states are introduced; chosen so that the interaction energy operator has non-vanishing matrix elements only for transitions between the given state and two other states with higher and lower energies. These stationary states are devised as follows: the operators  $\mathcal{H}$  and  $R^2$  commute. Therefore it is possible to choose eigenstates of  $R^2$  as stationary states. These states will be linear combinations of the states  $\psi_{gm}$ .  $R^2$  has the eigenvalues  $r(r+1)$ , where  $r$  is an integral or half-integral number satisfying

$$|m| \leq r \leq \frac{1}{2} n.$$

The quantum number  $r$  is termed the co-operation number of the gas.

In terms of the spin analogue,  $R$  is the total spin of the system,  $r$  is a constant spin  $s$ , and  $m$  the projection of the spin on the  $z$  axis.

The new eigenstates, designated  $\psi_{gmr}$ , satisfy

$$\mathcal{H} \psi_{gmr} = (E_g + mE) \psi_{gmr},$$

$$R^2 \psi_{gmr} = r(r+1) \psi_{gmr}.$$



The introduction of  $R^2$  does not remove the degeneracy completely.

Dicke, in Fig.1. of his paper, gives a classification which, as

Gamba (1958) explains, reflects a permutation symmetry.

Functions with the same  $r$  have the same properties with respect to permutations: the functions with the highest  $r$  are completely symmetric, those with the lowest  $r$  are as antisymmetric as possible for functions of this type.

The matrix elements of the interaction energy operator are

$$(g, r, m | \underline{e}_1 R_1 + \underline{e}_2 R_2 | g, r, m \mp 1) \\ = \frac{1}{2}(\underline{e}_1 \pm i\underline{e}_2) \left[ (r \pm m)(r \mp m + 1) \right]^{\frac{1}{2}}.$$

Transitional probabilities are proportional to the square of the matrix elements. Thus, the spontaneous radiation probabilities are

$$I = I_0 (r + m)(r - m + 1)$$

where  $I_0$  is the radiation rate of a gas composed of one molecule in its excited state ( $r = m = \frac{1}{2}$ ). For all  $n$  molecules excited

$$(m = r = \frac{1}{2}n)$$

$$I = nI_0.$$

Coherent radiation is emitted when  $r$  is large but  $|m|$  small. For instance, for even  $n$  let  $r = \frac{1}{2}n$ ,  $m = 0$ , then  $I = \frac{1}{2}n (\frac{1}{2}n + 1)I_0$ .

This is the largest rate at which a gas with an even number of molecules can radiate spontaneously, and for large  $n$  is proportional



to the square of the number of molecules.

The general expression for the radiation rate of a superposition state is

$$I = I_0 \langle (R_1 + iR_2)(R_1 - iR_2) \rangle .$$

In all radiative transitions of the system the co-operation number  $r$  does not change since the operator  $R^2$  is a constant of the motion,

$$\frac{dR^2}{dt} = \frac{i}{\hbar} [\mathcal{H} + \mathcal{H}_1, R^2] = 0 .$$

States with low cooperation number are highly correlated to have abnormally low radiation rates. Indeed, a gas in the state  $r = m = 0$  does not radiate at all. Dicke remarks that this state (which is realised only for even  $n$ ) is analogous to the classical system of an even number of oscillators swinging in pairs oppositely phased.

Dicke calls the states with  $m \sim 0$  "super-radiant" because they radiate spontaneously at an abnormally high rate. These states may be prepared in a number of ways. If, for instance all the molecules be excited, the gas is in the state with  $r = m = \frac{1}{2}n$ . As the system radiates  $m$  decreases towards the super-radiant region  $m \sim 0$ .

Alternatively, the gas in its ground state

$r = -m = \frac{1}{2}n$  can be irradiated with a pulse to lift it into a

superposition state with  $m \sim 0$  (what is normally termed a  $90^\circ$  pulse). Normally, of course, the experiment is conducted with the gas in thermal equilibrium; for which, Dicke shows, the system may be considered to be in the state  $r = m \sim -\frac{nE}{4kT}$ . Spectroscopic equipment based on pulse excitation was developed by Dicke and Romer (1955).

Although the intensity of spontaneous radiation depends upon the state of the gas ( $r, m$ ), the stimulated emission rate is normal and is always proportional to the number of active molecules. The external field induces transitions with a reduction in  $m$  ( $m \rightarrow m - 1$ ), and transitions with an increase in  $m$  ( $m \rightarrow m + 1$ ). The intensity of net emission or absorption is then proportional to

$$I(m \rightarrow m - 1) - I(m \rightarrow m + 1)$$

$$(r + m)(r - m + 1) - (r + m + 1)(r - m) = 2m.$$

In order to derive parameters describing the radiation line breadth and shape Dicke utilises a classical model consisting of a spinning top carrying an electric dipole moment, which precesses about the  $z$  axis as a result of an interaction with a static electric field in that direction. This is a valid model when large quantum numbers are involved.

The principal result to emerge from this analysis is that the commonly held notion that the natural linewidth for microwave transitions may be neglected can be in error when coherence effects are involved.

If  $\theta$  is the polar angle (between the spin axis and the z axis) then

$$m = r \cos \theta.$$

As the system radiates  $\theta$  increases, and the radiation intensity varies with  $\theta$  as

$$\begin{aligned} I &= I_0 (r + m)(r - m + 1), \\ &\sim I_0 (r^2 - m^2), \text{ if } r - |m| \gg 1, \\ &= I_0 r^2 \sin^2 \theta. \end{aligned}$$

The internal energy of the gas is

$$mE = rE \cos \theta.$$

Equating the rate of energy loss to the radiation rate gives

$$-\frac{d}{dt} (mE) = I.$$

Which, since the length of r is constant, yields

$$\dot{\theta} = \frac{I_0 r}{E} \sin \theta.$$

If  $\theta = 90^\circ$  for  $t = 0$ ,

$$\sin \theta = \operatorname{sech} \left( \frac{I_0 r}{E} t \right).$$

The field has the form

$$A(t) = \begin{cases} e^{i\omega t} \sin \theta, & t > 0, \hbar\omega = E \\ 0 & t < 0, \end{cases}$$

As  $\theta$  increases from below  $\frac{\pi}{2}$  the amplitude increases to a maximum at  $\theta = \frac{\pi}{2}$  and then decreases. The Fourier transformation gives a lineshape which is not Lorentzian. The linewidth  $\Delta\omega$  at half-intensity points is of the order of  $r\gamma$ , where  $\gamma$  is the line-

width for the incoherent spontaneous radiation from isolated single molecules. The maximum value for  $r$  of  $\frac{n}{2}$  gives a linewidth of the order of  $\gamma n$  which is usually very much greater than  $\gamma$ , and thus may be far from negligible in some applications. For instance, Gamba remarks that the increased spontaneous decay probability for super-radiant systems should be taken into account when calculating noise figures for gas masers.

Recently, Eberly and Rehler (1969) have extended Dicke's treatment to embrace the optical region, where the assumption that the system of a large number of atoms is confined to a region small compared with the wavelength is untenable. They find that the enhancement factor of the radiation rate over the ordinary incoherent emission rate that super-radiance confers on the large system is smaller than that found for the small system, but still proportional to the total number of emitting atoms.

The spontaneous radiation rate in the direction  $\underline{K}$  is given by

$$I(\underline{K}) = I_0(\underline{K}) \langle R_{\underline{K}+} R_{\underline{K}-} \rangle$$

where  $I_0(\underline{K})$  is the radiation rate of a single excited atom. Here,

$$R_{\underline{K}\pm} = \sum_{j=1}^N R_{\pm j} \exp(\pm i \underline{K} \cdot \underline{r}_j).$$

It is assumed that all the atoms are in their ground states prior to excitation by a short plane wave pulse which turns the pseudo-

atomic dipole moments through an angle  $\Theta$  (using the analogy with nuclear magnetic resonance established by Feynman et al (1957)).

The intensity of the spontaneously emitted radiation is given by

$$I(\underline{k}) = I_0(\underline{k}) \frac{1}{2} N [1 - \cos \Theta + \frac{1}{2} N \sin^2 \Theta \{ \Gamma(\underline{k}, \underline{k}_1) - \frac{1}{N} \}].$$

The function  $\Gamma(\underline{k}, \underline{k}_1)$  takes into account the different times of excitation of the different atoms, and is strongly dependent on the geometry of the system. Explicitly it is

$$\Gamma(\underline{k}, \underline{k}_1) = |\{ \exp [i(\underline{k} - \underline{k}_1) \cdot \underline{r}] \}_{av}|^2$$

where the average is taken over all the positions  $\underline{r}_j$  of the atoms in the system, and  $\underline{k}_1$  is the wavevector of the excitation pulse.

By equating the rate of energy loss by the atomic system to the rate of emission integrated over all directions a non-linear differential equation is obtained:

$$\dot{W} = \frac{\mu}{\tau_0} (W + \frac{1}{2} N)(W - \frac{1}{2} N - \mu^{-1}),$$

where  $W$  is the energy of the system of atoms in units of  $\hbar\omega$ ,  $\tau_0$  is the lifetime of a single atom, and

$$\mu = \left( \frac{\tau_0}{\hbar\omega} \right) \int I_0(\underline{k}) \Gamma(\underline{k}, \underline{k}_1) d\Omega \underline{k} - \frac{1}{N}.$$

The solution is

$$W = -\frac{N}{2} \left[ \left( 1 + \frac{1}{\mu N} \right) \tanh \frac{1}{\tau} (t - t_0) - \frac{1}{\mu N} \right],$$

from which the radiation rate is

$$I(t) = -\hbar\omega\dot{W} = \frac{\hbar\omega}{4\mu\tau_0} (\mu N + 1)^2 \operatorname{sech}^2 \frac{t - t_0}{\tau}.$$

$\tau$  is the radiation pulse width and depends upon the shape of the system and  $N$ ,

$$\tau = \frac{2\tau_0}{(\mu N + 1)}.$$

$t_0$  is defined so that  $W(0) = \frac{1}{2}N$ , and is given by

$$t_0 = [\tau_0(\mu N + 1)^{-1}] \log \mu N.$$

Again, the radiation rate is proportional to  $N^2$  for large  $N$ , but the factor  $\mu$  exerts a strong influence. It approaches a limit,  $\mu \rightarrow 1 - \frac{1}{N}$ , as the volume of the radiating system is decreased.

Dicke terms radiation coherent if the radiation rate is proportional to  $N^2$ , and makes no distinction, as Senitzky does, between radiation of well-defined phase and that of random phase.

It is worthwhile examining Senitzky's treatment of correlation effects, for it serves to delineate the concepts of coherence and correlation: terms which are employed loosely in the literature.

Consider a system of two molecules. The two possible correlated states are

$$\begin{aligned} \psi_s &= 2^{-\frac{1}{2}} [\phi_1(1)\phi_2(2) + \phi_2(1)\phi_1(2)], \\ \text{and} \\ \psi_a &= 2^{-\frac{1}{2}} [\phi_1(1)\phi_2(2) - \phi_2(1)\phi_1(2)]. \end{aligned}$$

These are symmetric and antisymmetric respectively, but this has no significance in terms of the Pauli principle, since there is assumed to be negligible overlap of spatial wavefunctions.

An uncorrelated state is

$$\psi_u = \phi_1(1) \phi_2(2).$$

All three are eigenstates of the energy with the same eigenvalue. However, the expectation values for the field energies are

$$\langle \mathcal{H}_{\text{field}} \rangle_s = 2\mathcal{E}_0(t), \langle \mathcal{H}_{\text{field}} \rangle_a = 0, \langle \mathcal{H}_{\text{field}} \rangle_u = \mathcal{E}_0(t).$$

Now, the expectation value for the field strength vanishes in all three cases, indicating that any radiation from these molecules must be incoherent spontaneous emission. It would appear then that, although the phase of oscillation cannot be predicted for a correlated energy state, the phase relationship between the molecules is fixed: the incoherent oscillations are equal and in phase for the symmetric state, but equal and out of phase for the antisymmetric state.

Consider next a system of  $N$  molecules with  $N/2$  molecules in the upper state and  $N/2$  in the lower state. For a symmetric correlated state the energy is

$$\left(\frac{1}{4}N^2 + \frac{1}{2}N\right)\mathcal{E}_0(t).$$

For an uncorrelated state the spontaneous emission energy is

$$\frac{1}{2}N\mathcal{E}_0(t).$$



Thus, for the correlated state the incoherent energy is proportional to  $N^2$ , while for the uncorrelated state it is proportional to  $N$ . Again, although the radiation does not have a well-defined phase (and is hence termed incoherent), it does have the same phase for all molecules in the correlated state, and random phase relationships between molecules in the uncorrelated state.

Contrast this with the spontaneous emission energy from  $N$  molecules oscillating coherently. These are in the uncorrelated state.

$$\psi = \prod_{m=1}^N [a_1(m) \phi_1(m) + a_2(m) \phi_2(m)],$$

with  $|a_1(m)| = |a_2(m)| = 2^{-\frac{1}{2}}.$

All the molecules are oscillating with the same well-defined phase and maximum amplitude. The total spontaneous emission energy is

$$\frac{1}{4} (N^2 + N) \mathcal{E}_0(t),$$

with the  $N^2$  term coherent, and the  $N$  term incoherent.

It is seen that both incoherent and coherent radiation may have an  $N^2$  dependence: the incoherent case arising from correlation while the coherent radiation corresponds to the classical case of an assembly of oscillators all having the same phase. (Quantum mechanical correlation should be distinguished from a classical type of correlation which might be said to exist between the phases of such an assembly of oscillators).

Senitzky asserts that, as a corollary of the uncertainty



principle, coherence and correlation are mutually exclusive and obey a conjugate variable relationship. More correlation implies less coherence and vice versa.

It is interesting to note that Yariv, in his textbook "Quantum Electronics" (1967), employs the term "super-radiance" in a sense quite different from that intended by Dicke. Yariv describes a phenomenon which he calls "super-radiant narrowing". This occurs when a laser diode is operated at high current levels, but is kept below oscillation threshold by removing the optical feedback. Under these conditions the spontaneous recombination radiation is incoherently amplified as it passes through the medium. The line narrowing results because frequencies near the lineshape maximum are amplified more strongly than those further away.

One final point can be made. The photon correlations discussed in the preceding pages are but one aspect of a quantum mechanical effect; boson condensation. The probability that a boson will enter a particular state is enhanced by a factor  $(n + 1)$  if there are already  $n$  identical bosons in that state. The cooperative effects exhibited by superfluid  $\text{He}^4$  are another manifestation of the phenomenon.

## REFERENCES

- Henley, E. M., Thirring, W., (1962), Elementary Quantum Field Theory, New York, McGraw-Hill, Ch. 2.
- Carruthers, P., Nieto, M. M. (1965), Am. J. Phys., 33, 537-544.
- Glauber, R. J. (1966), Physics of Quantum Electronics, 788, New York, McGraw-Hill.
- Klauder, J. R., Sudarshan, E. C. G. (1968), Fundamentals of Quantum Optics, New York, Benjamin.
- Dicke, R. H. (1954), Phys. Rev., 93, 99-110.
- Senitzky, I. R. (1958), Phys. Rev., 111, 3-11.
- Senitzky, I. R. (1959), Phys. Rev., 115, 227-237.
- Bloom, S. (1956), J. App. Phys., 27, 785-8.
- Gamba, A. (1958), Phys. Rev., 110, 601-3.
- Dicke, R. H., Romer, R. H. (1955), Rev. Sc. Ins., 26, 915-28.
- Eberly, J. H., Rehler, N. E. (1969), Phys. Lett., 29A, 142-3.
- Feynman, R. P., Vernon, F. L., Hellwarth, R. W. (1957), J. App. Phys. 28, 49-52.
- Yariv, A. (1967), Quantum Electronics, New York, J. Wiley.

## CHAPTER II

### THE AMMONIA BEAM MASER

#### 2.1 Introduction

A simple ammonia beam maser features four components: a nozzle, a focuser, and a microwave cavity, within a vacuum chamber continuously pumped to below a pressure of about  $10^{-5}$  torr to permit a long mean free path. Gas effuses from the nozzle, and part of this effusion is captured by the state focuser which focuses upper energy molecules into a beam, and deflects lower state molecules out of the beam. The beam consisting predominantly of upper state molecules passes then into a high-Q microwave cavity. Therein a signal within the linewidth can induce the molecules to emit coherently with the signal, thus providing amplification if the resonator wall losses are small. With an increase in the beam intensity the power emitted by the molecules becomes greater than that dissipated in the walls and lost through the coupling hole, the process becomes self-supporting and auto-oscillation is observed.

After a brief review of the properties of the ammonia molecule, consideration is given to the design features of the components of the maser which confer particular efficiency. The detection scheme which is used for the observation of transient effects is also described.

## 2.2 The ammonia molecule

The ammonia molecule is a non-rigid, oblate symmetric top with the three hydrogen atoms at the apices of the base equilateral triangle and the nitrogen at the apex of the tetrahedron. Various oscillatory and rotational motions are possible. In particular, there are oscillations of the nitrogen atom at right angles to the plane of the hydrogen atoms. The potential energy of the molecule as a function of the distance between the nitrogen and the plane of the hydrogen atoms exhibits the form of a symmetrical curve with a maximum at the origin, separating two minima displaced from the base plane. If the tunnel effect is neglected, then each of the lower oscillation levels is doubly degenerate since there are two equivalent positions for the nitrogen on one side or the other of the potential barrier. The quantum mechanical tunnel effect lifts the degeneracy, and the vibrational spectrum consists of a series of doublets. The higher level of each doublet represents an anti-symmetric state of the system relative to inversion of the vibration coordinate in the centre of mass of the system: the lower level represents a symmetric state. Since the splitting corresponds classically with the motion in which the nitrogen atom oscillates back and forth through the plane of the hydrogen atoms, or in which the molecule inverts periodically, it is termed "inversion" splitting. The analogue of the inversion doublet is the two minima problem of

two weakly coupled pendula, where the two swinging together corresponds to the symmetric state, and the two swinging in opposite directions corresponds to the antisymmetric state.

The level separation in the  $\text{NH}_3$  molecule depends on the rotation of the molecule, which is characterized by three quantum numbers: the total angular momentum,  $J$ ; the projection of the total angular momentum on a space axis,  $M_J$ ; and the projection of  $J$  on the symmetry axis,  $K$ . Rotational states with  $J = K$  have the greatest statistical weight and therefore the inversion spectrum lines corresponding to these are the most intense. The one most frequently used in molecular beam masers is the  $J = 3, K = 3$  of  $\text{N}^{14}\text{H}_3$ , which has a frequency of 23,870 MHz. The 3,3 line has a complicated hyperfine structure as a result of various intramolecular interactions. The electric quadrupole interaction of the  $\text{N}^{14}$  nucleus with the molecular field produces splittings of several megahertz. The spin-spin interaction of the nitrogen and hydrogen nuclei and the interaction of the spins with the magnetic field of the rotating molecule result in splittings up to 100 kHz.

Five quantum numbers are required to characterize the energy levels of the molecules when account is taken of the hyperfine interactions: they are,  $I_H$ ,  $I_N$ ,  $J$ ,  $F_1$ , and  $F$ , where  $I_N$  is the spin vector of the nitrogen nucleus,  $I_H$  is the vector of the total spin of the hydrogen nuclei, and  $\underline{F}_1 = \underline{I}_N + \underline{J}$ ,  $\underline{F} = \underline{F}_1 + \underline{I}_H$ .

The component used in a maser is the most intense component of the inversion transition  $J = 3, K = 3$ , which is diagonal in the quantum numbers  $F_1$  and  $F$  ( $\Delta F_1 = 0, \Delta F = 0$ ).

The constants of the quadrupole and magnetic couplings in ammonia are different for the upper and lower inversion levels (Gordon 1955). As a result the line  $J = 3, K = 3$ ,  $\Delta F_1 = \Delta F = 0$  is split into twelve components corresponding to the twelve possible values of the quantum numbers  $F_1$  and  $F$  for the 3,3 line. For usual linewidths these components are not resolved. The peak position of the line, however, depends on the ratios of the intensities of the individual components and on their frequencies. For a gas in thermal equilibrium the intensities of the components are determined by the thermal distribution of the molecules among the levels.

In the beam emerging from a state focuser the ratios of the intensities of the components are changed, and the peak of the spectral line is shifted relative to that of the line in the gas at equilibrium. The shift is a function of the voltage on the focuser, since the ratios of the intensities of the components depends on the electric field in the focuser. Furthermore, the different components have different values of the dipole matrix element and display different degrees of saturation with change in the electric field in the cavity. Overall, the shift is a

function of beam intensity.

A symmetric top with inversion symmetry, such as ammonia, does not possess a permanent dipole moment. However, in an applied electric field the ammonia molecule acquires an induced dipole moment parallel to the field. The quadratic Stark effect increases the separation of the inversion levels and splits them according to the previously degenerate M levels. Vuylsteke (1960) gives a detailed discussion of the origin of the inversion spectrum, and of the Stark effect.

For low values of J and K the fraction of molecules in a given rotational state under conditions of thermal equilibrium is given by (Townes and Schawlow, 1955),

$$f_{JK} = \frac{S(I, K)(2J+1)}{4I^2 + 4I + 1} \left[ \frac{B^2 C h^3}{\pi (kT)^3} \right]^{\frac{1}{2}}.$$

The population of the 3,3 levels is about 6% that of the total population at room temperature. The ratio of the number of molecules in the lower inversion level to the number in the upper is, from the Boltzmann formula, 1.004.

### 2.3 The maser

Most designs of the ammonia maser feature pumping of the ammonia by means of condensation of the gas on surfaces cooled with liquid nitrogen (the solid has a vapour pressure of about  $10^{-6}$  torr at 77°K), in addition to pumping by diffusion pumps.

When designing and constructing an ammonia maser the condition that it should oscillate without benefit of liquid nitrogen pumping serves as a most stringent criterion of efficient operation of the nozzle, focuser and cavity.

In simple versions of the maser the nozzle, focuser and cavity are housed within one vacuum compartment. Of the total effusion from the nozzle only that within a small solid angle is captured by the focuser. Those molecules not incident on the entrance of the focuser serve only to degrade the vacuum and reduce the mean free path of molecules in the beam. There is, then, considerable advantage to be gained by housing the nozzle in a separately pumped compartment and selecting by means of a diaphragm only those molecules which can be captured by the focuser. Such a differential pumping scheme is employed here. It has been used before in maser designs by White (1959), and Grigor'yants and Zhabotinskii (1961). Skvortsov, Krupnov and Naumov (1960) have operated a maser without liquid nitrogen in a single pumped chamber. An ammonia maser has also been installed in a space satellite, where the ammonia was allowed to escape into the space vacuum (Basov et al, 1966).

It may be inferred from the papers listed above that the motivation in constructing such a device has been to gain longevity and convenience of operation, and enhanced frequency stability



(changes in the beam freezing region consequent upon boiling and subsequent pouring of the liquid nitrogen induce frequency shifts). For the present work it serves merely as a sensitive indication of improvements in design.

(a) General

Figures 2.1 (a) and (b) display the maser together with some of its associated microwave and electronic equipment. (The insulating jackets have been removed from the nitrogen reservoirs).

The maser is mounted horizontally on a wooden table and cushioned with rubber. The pumping system and the ammonia purification system are mounted below the table. The microwave detection apparatus is mounted on an extension of the table, which also serves as a rack for the i.f. amplifier power supply and the cavity stabilisation equipment.

(b) Maser vacuum system and ammonia supply

Figure 2.2 is a diagram of the vacuum system. The main chamber is an aluminium bronze casting, approximately 18" x 8" x 8", which has been sealed with Araldite on the outside surface, and with a silicone varnish on the inside, and cured at 200°C. It is fitted with a brass lid carrying two liquid nitrogen traps, and with a perspex window, and two brass flanges carrying the waveguides to the two microwave cavities. One panel is machined flat to carry electrical and mechanical lead-throughs. All connections are sealed

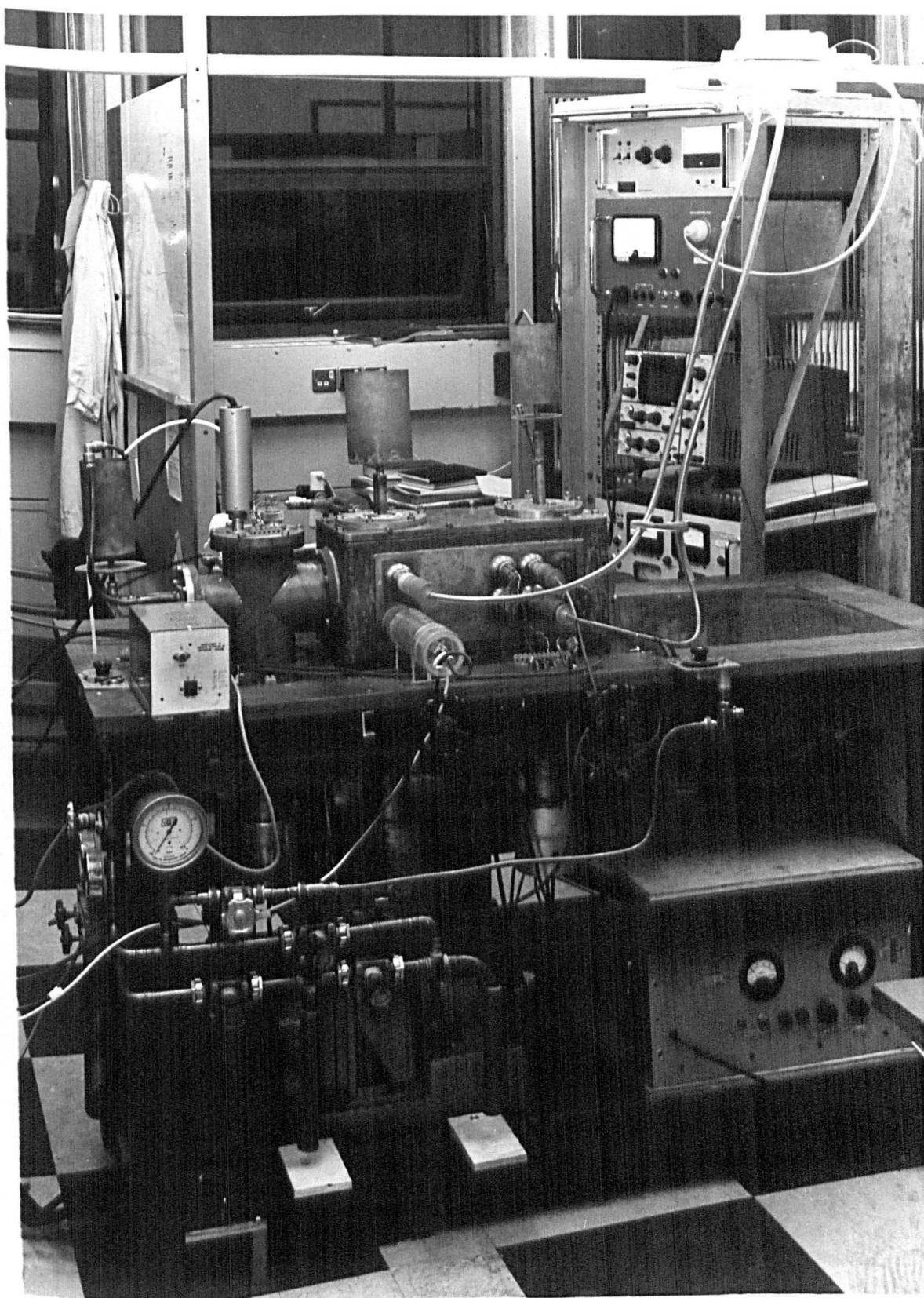


Figure 2.1(a) General view of the maser

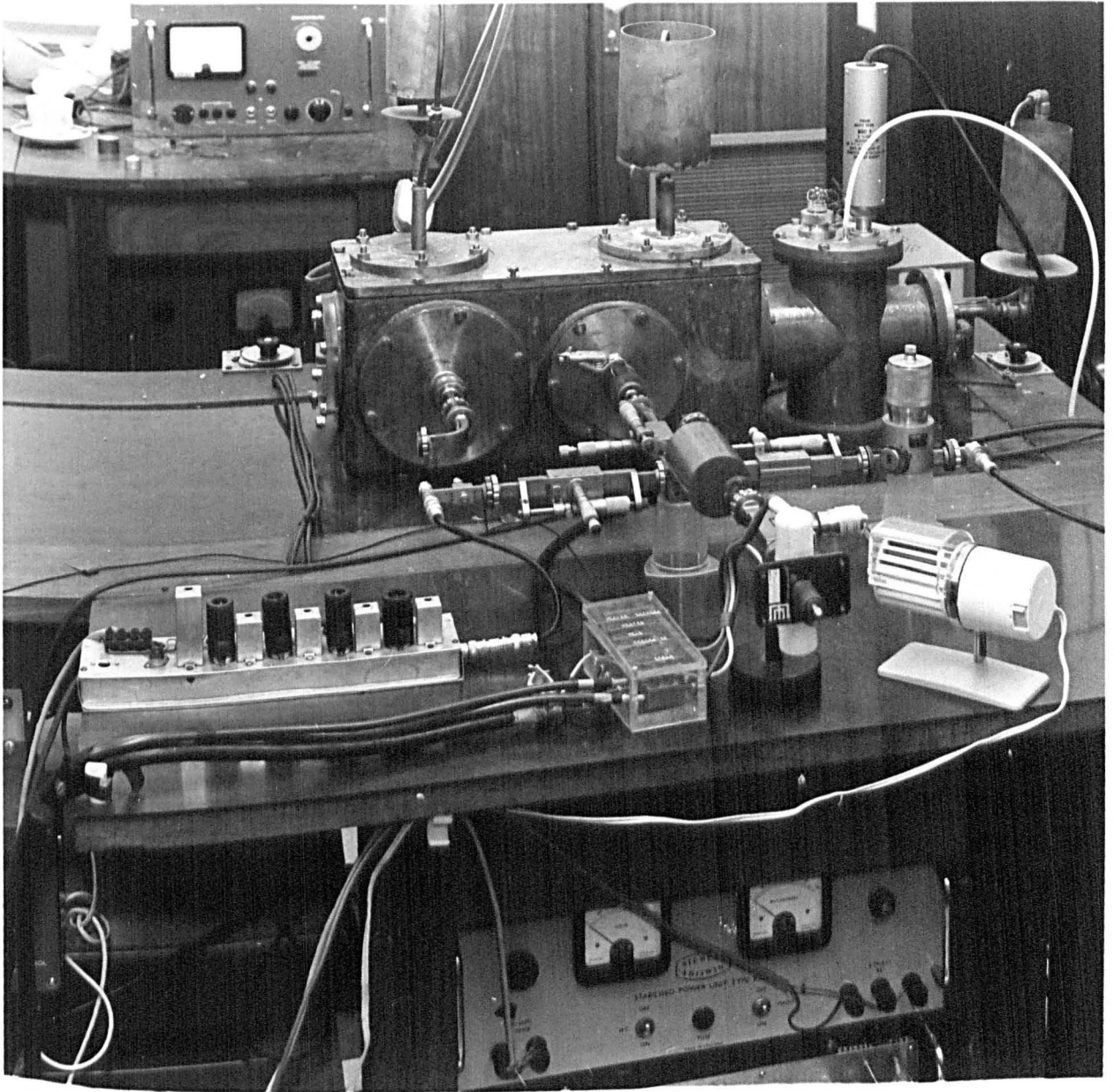


Figure 2.1(b) The microwave bridge

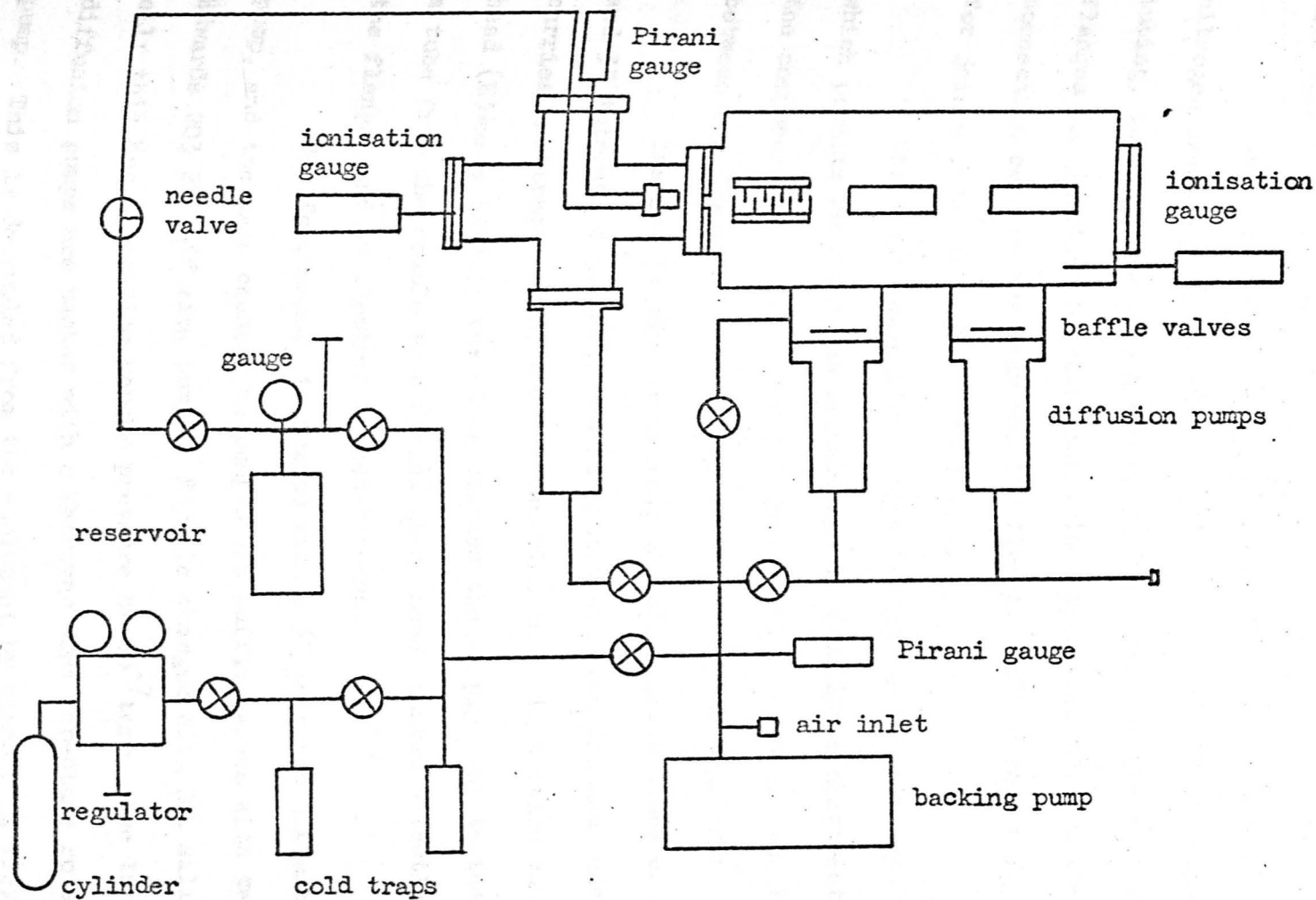


Figure 2.2. Pumping arrangement and gas supply for the maser.

with rubber "O" rings.

In order to minimise the number of soldered joints the nitrogen traps are made with a single continuous coil of copper tubing, to which are attached copper fins. The cooling of the flanges is minimised by employing thin cupronickel tube as the connection between the trap and the flange. Silver solder is used for joints which are subject to thermal cycling.

The K band waveguide passes through an "O" ring seal which permits rotation and translation to facilitate alignment of the components. It is sealed internally with mica discs mounted between the flanges and "O" rings of the waveguide couplings.

The nozzle chamber is made of rolled brass tubes of 4" and 3" internal diameters. It is fitted with two flanges: one carries a nitrogen trap, and a connection to an ionization gauge head (Edwards IG2HB); the other carries the supply line to the nozzle, a tube from the nozzle to a Pirani gauge head mounted directly on the flange, and an electrical lead-through.

The forechamber is pumped with a 3" Metrovac diffusion pump, and the main chamber is pumped via baffle valves with two Edwards 203 2" diffusion pumps. Each is charged with 704 silicone oil; this has a limiting vapour pressure of  $10^{-7}$  torr. The three diffusion pumps are backed with a Metrovac GDR1 two-stage rotary pump. This is decoupled from the equipment by means of a flexible

rubber hose to minimise vibration. The main pumping lines are of 1" copper tubing.

The ammonia source is a lecture size cylinder of anhydrous liquid ammonia. The gas flow is controlled with a pressure reducing valve adjusted for about 30lb/sq. inch output pressure. The ammonia is purified by freezing it in traps cooled with liquid nitrogen.

While it is frozen the traps are pumped to remove gaseous impurities.

It is then allowed to pass to a similar trap. Water vapour is trapped by maintaining the trap below  $0^{\circ}\text{C}$  during the transfer.

The ammonia is then stored in a  $6\frac{1}{4}$  litre pressure cylinder. The flow from the reservoir to the nozzle is controlled by a hand valve and a fine needle valve. The needle valve is connected to the flange by a  $\frac{1}{4}$ " diameter thick walled flexible nylon tube, and thence to the nozzle chamber via a flexible plastic tube. The pressure in the nozzle chamber is measured by an Edwards Pirani gauge (head M5C) mounted on the flange. This is connected to the nozzle chamber via a short length of plastic tubing.

The background pressure in each chamber is monitored with an Edwards IGH2B Ionisation Gauge Head, for which the power supply is an Edwards Model 2 controller. This registers pressures from  $10^{-2}$  to  $10^{-7}$  torr. The pressure in the two chambers can be reduced to about  $5 \times 10^{-6}$  torr after 3 hours of pumping. Addition of liquid nitrogen to the traps further reduces the pressure to about  $3 \times 10^{-6}$  torr.



The two chambers are separated by a variable iris diaphragm. The aperture of this iris is controlled from outside the chamber with an Edwards rotary drive lead-through which is coupled to a screw driven carriage by flexible nylon tube. Rotation of the external control results in translational motion of the carriage, which in turn swivels the lever which sets the iris aperture. By this means the optimum division of molecular flux between the two chambers can be obtained for different experimental conditions.

#### (c) Nozzle

The choice of nozzle is governed primarily by the type of focuser. Pilot experiments established that the nozzle which best suited the ring focuser employed throughout this work was one having a single channel 1mm. in diameter and 1cm. long. This is mounted with its exit 1cm. from the iris aperture. Another type of nozzle which is commonly used is that of the multichannel form fashioned from klystron grid stock. Typically this would be about 5mm. long, 3.5mm. in diameter, consisting of a honeycomb of fine parallel tubes 0.25mm. in diameter.

The nozzle is attached to the source chamber by screwing both into a screwed barrel. The source chamber is mounted in a carriage which, by means of a combination of rotational and sliding action, will permit the nozzle to describe any locus within a

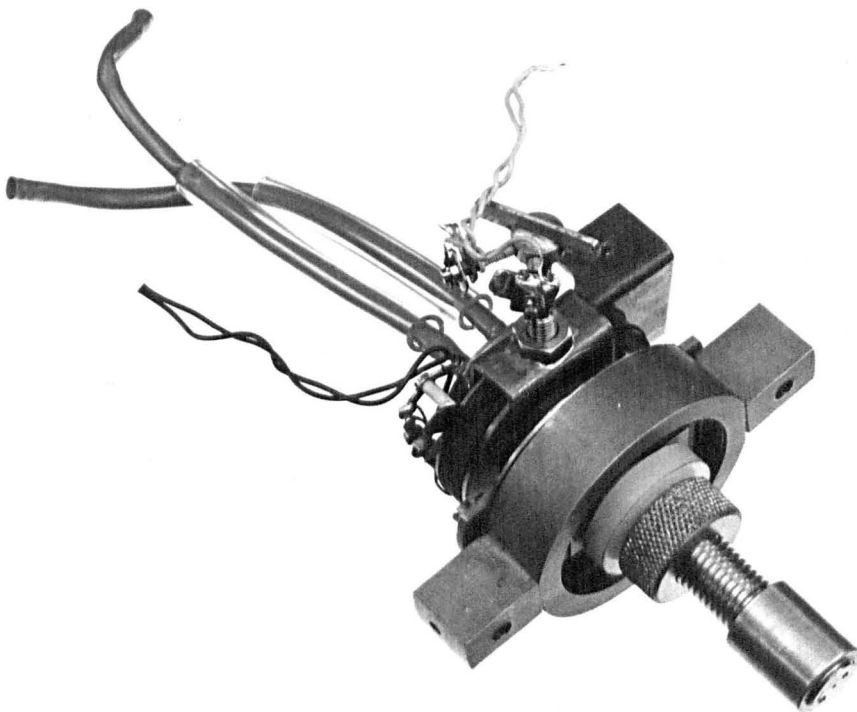


Figure 2.3 Nozzle assembly



circle of  $\frac{1}{2}$ " diameter. The carriage is mounted on two rods which pass through the wall dividing the two chambers. The focuser carriage is mounted on these rods on the other side of the iris aperture.

Figure 2.3 shows the nozzle and its carriage (a temperature sensor and a heater coil are shown).

#### (d) Focuser

The quadratic Stark effect is utilized to effect a separation of molecules in the upper and lower inversion levels.

If a strong field ( $> 1\text{kv. cm.}^{-1}$ ) is applied the inversion is partially quenched and an average dipole moment is created.

Neglecting hyperfine effects the inversion states have energies

$$W = W_0 \pm \left[ \left( \frac{h\nu_0}{2} \right)^2 + \left( \frac{\mu E M_J K}{J(J+1)} \right)^2 \right]^{\frac{1}{2}},$$

where  $W_0$  is the average energy of the upper and lower inversion levels,  $\mu$  is the permanent dipole moment that the molecule would exhibit in the absence of inversion,  $E$  is the electric field strength and  $M_J$  is the projection of  $J$  on the direction of the applied field.

The term "state focuser" is to be preferred to the alternative "state separator" since it can be seen that the degree of separation is dependent upon the quantum number  $M_J$ . States with  $M_J = 0$  are not affected by the applied field but states with  $M_J > 0$  have different energies (greater for upper inversion

states, less for lower inversion states) and in an inhomogeneous field the molecules experience a force

$$\underline{F} = - \text{grad } W.$$

The upper inversion state molecules experience a force directed towards a region of minimum field, and lower state molecules experience one towards a maximum field region.

Upper state focusers are designed to produce a field which increases with radial distance from the axis. Early designs consisted of an array of rod electrodes parallel to the direction of the beam and arranged in a circle. The rods (an even number) are charged alternately positive and negative. They are usually circular in cross-section, though for accurate computational purposes quadrupolar focusers with hyperboloidal cross-sections have been used. Vonbun (1958) has given an analysis of a multipole focuser and calculated the paths of ammonia molecules of various velocities and states. Upper level molecules possessing radial velocities lower than a critical value, dictated by the maximum Stark energy, are trapped in a potential well and describe, to a first approximation, simple harmonic motion about the axis. Lower state molecules are deflected out of the beam.

The sorting field of this type of focuser is purely transverse, and is thus best suited for sorting molecules with moments perpendicular to the axis. Now, throughout the work

described in this thesis a cylindrical cavity operating in the  $TM_{010}$  mode is used. The oscillating electric field in this mode configuration is longitudinal. In consequence, those molecules with moment directed along the axis have the greatest probability of radiating energy on interacting with this field. It would seem desirable to employ a longitudinal field for sorting. Focusers of the ring type, or those of bifilar helix construction, develop fields with both longitudinal and transverse components. These focusers (described below) sort molecules with transverse and longitudinal components of orientation, providing a more complete utilisation of the beam. Mednikov and Parygin (1963) have evaluated the relative effectiveness of the three types of focuser.

The theoretical advantages adduced for the ring focuser in combination with a  $TM_{010}$  cavity may not entirely be realised in practice, for the fringe field at the exit of the focuser may satisfy the adiabaticity condition

$$\frac{\hbar}{(W_2 - W_1)^2} \mu_{12} \frac{\partial E}{\partial t} \ll 1,$$

and the molecule on emerging from the focuser rotates in space, following the electric field. If the fringe fields of the two types of focuser have roughly the same configuration the two systems may evince much the same efficiency (Krupnov and Skvortsov, 1965).

Krupnov and Skvortsov also obtained evidence for a predominantly longitudinal character of the fringe field at the exit of a quadrupole focuser. They used a Fabry-Perot resonator in which the beam may be oriented at any angle with respect to the direction of the electric vector of the microwave field. They found that when the beam was directed along the field the excitation parameter  $\eta = 0.55$ , and when it was directed perpendicular to the field  $\eta = 0.2$  ( $\eta = 1$  corresponds to the threshold of oscillation, and is given by

$$\eta = 4\pi Q_L N a^* \mu^2 \tau^2 \xi / \hbar V,$$

where  $Q_L$  is the loaded Q,  $N a^*$  is the flux of "active" molecules,  $\tau$  is the transit time through the resonator,  $V$  is the volume of the cavity, and  $\xi$  is a filling factor.).

Krupnov (1959) and Becker (1961, 1963) have used ring and spiral separators. The ring focuser consists of a series of rings alternately charged positive and negative, along the axis of which the beam is directed. The spiral separator consists of two parallel spiral wires oppositely charged. The spiral separator has the advantage of greater transparency compared with the ring focuser; in other words, it is a more open structure and presents a smaller scattering surface to the deflected lower state molecules. On the other hand it is a less rigid structure.

Ring and spiral focusers both produce an inhomogeneous

field along the axis, thus providing focusing for axial molecules.

The field in a ring system is given by

$$E = \frac{V_0 \sin \frac{\pi}{2} \left(1 - \frac{2\delta}{L}\right) \frac{2\pi}{L} Z}{I_0 \left(\frac{2\pi R}{L}\right) \frac{\pi}{2} \left(1 - \frac{2\delta}{L}\right)}$$

where

$$Z^2 = I_0^2 \left(\frac{2\pi r}{L}\right) \cos^2 \frac{2\pi z}{L} + (I_0')^2 \left(\frac{2\pi r}{L}\right) \sin^2 \frac{2\pi z}{L}$$

and

$$I_0(x) = 1 + \frac{x^2}{4} - \frac{x^4}{2^4 (2!)^2} + \dots$$

is a modified Bessel function of the first kind of zero order, for which  $1 + \frac{x^2}{4}$  is a good approximation when  $x$  is small.  $L$  is the period of the ring system,  $\delta$  is the ring thickness,  $R$  the ring radius,  $r$  the radial distance, and  $z$  the axial distance.

For  $\delta = 0$

$$E = \frac{4V_0 Z}{\left[1 + \frac{\pi^2 R^2}{L^2}\right] \left[\frac{L}{2}\right]}$$

and  $Z$  varies periodically from

$$\cos \left(\frac{2\pi z}{L}\right) \left(1 + \frac{4\pi^2 r^2}{L^2}\right) \text{ to } \frac{8\pi^2 r}{L^2}$$

along the  $z$  axis, typically a variation between 0 and 150,000 volts.cm<sup>-1</sup>

Becker shows that the diameter,  $z$ , of the molecular beam of upper state molecules is given by

$$z = \frac{eB}{a} \left[ 1 - \frac{a(e - a)}{ef} \right]$$

where  $e$  is the distance between the source nozzle and the diaphragm at the entrance to the resonator,  $a$  is the distance between the nozzle and the centre of the separator (internal diameter  $B$ ),  $f$  is the focal length of the lens equivalent of the focuser given by

$$\frac{B}{f} \approx bmU,$$

where  $U$  is the potential difference between the rings (or spiral wires),  $m$  is the number of rings or windings of a single electrode, and  $b = 0.87 \times 10^{-6}$  per volt for ring and  $1.03 \times 10^{-6}$  per volt for spiral focusers.

Shcheglov (1961) has provided a detailed analysis of ring focusers. Krupnov (1959) indicates that the optimum ratio of ring radius to the ring separation should be of the order of unity.

Much ingenuity has been devoted to devising means of slowing down molecules or selecting slow molecules (for a review of methods see the publication "Soviet Maser Research", 1964). The provision of a beam of slow molecules (relative to the average velocity at room temperature) would increase the frequency stability of maser frequency standards. Strakhovskii and Tatarenkov (1965) suggested a curved ring focuser which would function as a velocity selector. Only upper state molecules with a velocity below a critical value would be focused. Molecules with higher velocities would leave the system. They obtained a weak stimulated emission

signal with such a device. Kazachok (1965) proposed an electro-dynamic method of decelerating molecules by applying a time varying field to a ring focuser having a parabolic dependence of ring radius on axial distance. There appear to be no reports of such a device operating.

The rings usually used in focusers terminate in relatively sharp edges at which breakdown can occur. The focuser designed for the present work is constructed with rings fashioned from the sprung spiral ends of safety pins. The ring section has a smooth profile which decreases the tendency towards breakdown. The two ends of the spiral are mounted in holes in channels filled with solder.

Figure 2.4 shows the focuser. The two sets of rings are mounted on brass strips of dovetail cross-section which fit into slots in the P.T.F.E. formers. This feature allows interchange of focusers. The P.T.F.E. formers are separated with Sintox ceramic tubes. The separation between the two sets is adjusted with nylon screws. Alignment of the device is made with the sections dovetailed into a brass jig in which a metal rod is passed through the rings. The rings are secured with solder by placing the jig on a hotplate. All surfaces are rounded and smoothed.

The combination of P.T.F.E. and ceramic insulation, together with the use of safety pin rings, has permitted operation

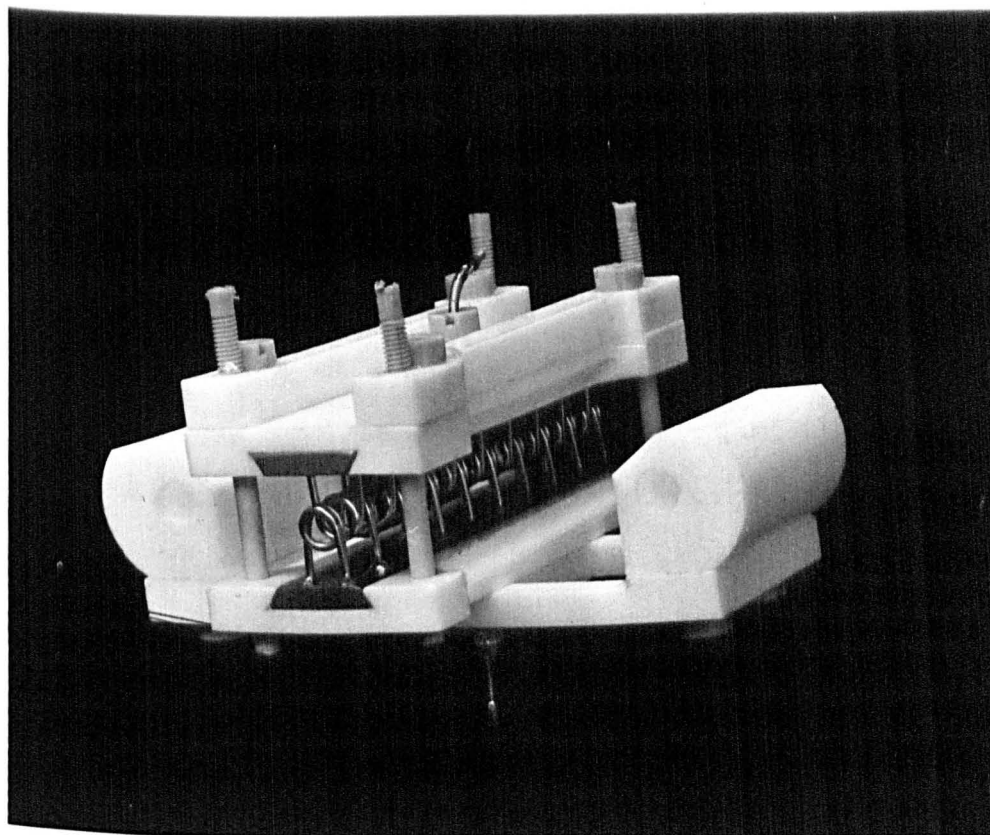


Figure 2.4 Main focuser



of the device with voltages in excess of 50kV between the rings.

The internal diameter of the rings is 0.164" (0.416cm.); and the diameter of the wire is 0.045" (0.114cm.), so that each ring has a thickness of 0.090" at the widest part of the spiral. There is 0.090" (0.228cm.) between adjacent (oppositely charged) rings. This spacing represents a compromise between transparency (50%) and high field strengths (of the order of  $220 \text{ kV. cm}^{-1}$  maximum), with concession to the design principle that the ratio of ring radius to ring separation should be close to unity. There are 10 rings of one sign, interleaved with 9 of the opposite sign. The focuser is 8.45cm. long between the entrance to the first ring and the exit of the last. It is mounted symmetrically between the iris diaphragm and the entrance to the cavity, 1cm. from each.

If it may be assumed that the theory for ring focusers, as detailed above, may be applied to this design (a dubious supposition), then the "focal length" is approximately 5.5cm. for 10kV. and 1.5cm. for 40kV. and the beam diameter is 0.5cm. for 10kV. (the expression becomes negative when the focal length is reduced beyond about 2.8cm.).

Figure 2.5 shows another form of ring focuser, with large diameter rings, mounted on a carriage. This short focuser is used in an experiment to be described later, where strong focusing action is not required.

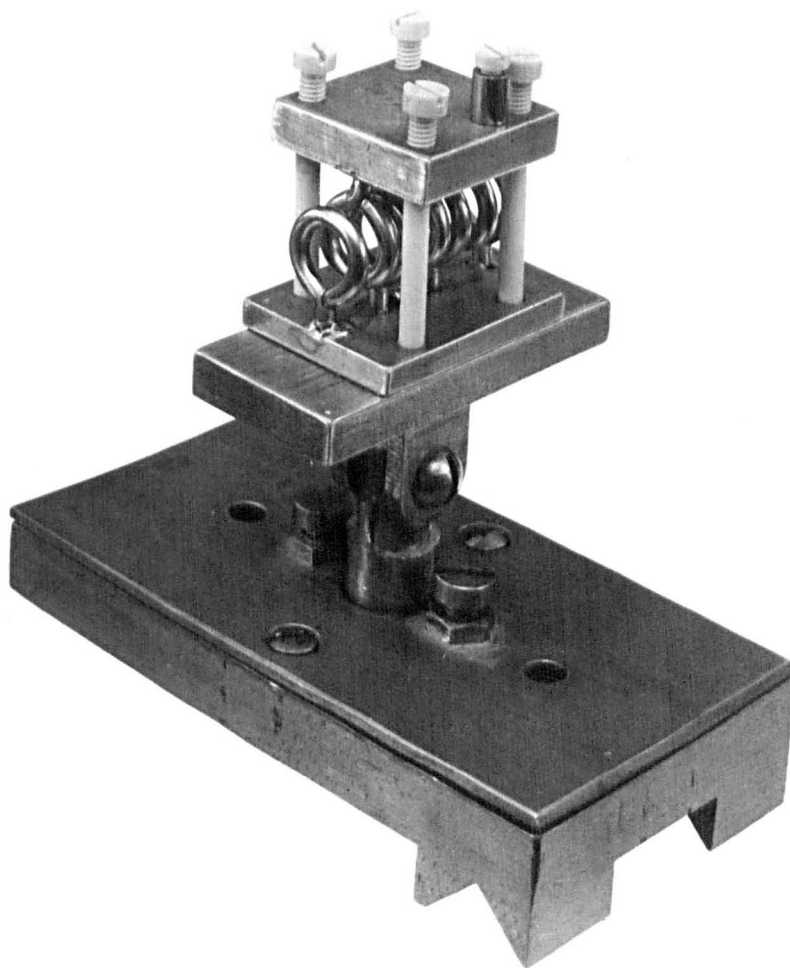


Figure 2.5 Ancillary focuser

(e) Resonant cavity

The mode configurations of a cylindrical cavity can be divided into two classes: TE or H modes where there is no electric field parallel to the axis of the resonator, and TM or E modes where there is no magnetic field parallel to the axis of the resonator. The resonant condition for E modes is given by

$$\lambda_0 = \frac{4}{\left[ \left( \frac{p}{2z_0} \right)^2 + \left( \frac{2U_{m,n}}{\pi a} \right)^2 \right]^{\frac{1}{2}}},$$

where  $p$  is an integer equivalent to the number of half wave variations along the axis of the resonator of length  $2z_0$ ,  $a$  is the radius of the cylinder and  $U_{m,n}$  is the  $n$ th root of the  $m$ th order Bessel function  $J_m(U) = 0$ . If  $p = 0$ , that is for the  $E_{m,n,0}$  mode (where  $m$  is the total number of full period variations of either field component along a circular path concentric with the cylinder wall, and  $n$  is one more than the number of reversals of sign of a field component along a radius)

$$\lambda_0 = \frac{2\pi a}{U_{m,n}}.$$

If  $m = 0$ , then  $2a = 0.9614\text{cm}$ . for a frequency of  $23.87\text{GHz}$ .

A major advantage that accrues from the use of a cavity that operates in the  $E_{010}$  mode is that much of the Doppler effect

is eliminated. The formation of the mode requires that the resonator is very close to cut-off for the  $E_{01}$  wave, the guide wavelength becomes very long and the phase velocity of the wave along the axis becomes infinite. Since the Doppler frequency shift is determined by the ratio of the velocity of the beam molecules to the phase velocity of the waves in the direction of propagation of the beam, the longitudinal Doppler effect disappears and the residual Doppler shift depends upon the angular spread of the beam. The spectral linewidth is determined, via the Uncertainty Principle, by the time of flight through the resonator (however, under saturation conditions, where the molecule can pass from level to level several times, the lifetime on a level is shorter than the time of flight and the spectral width is increased). This argument must be qualified by noting that under maser conditions the radiation emitted by the molecules varies along the cavity, and as a result there is a travelling wave which gives rise to a Doppler shift in frequency. For this reason ammonia maser frequency standards featured opposing identical beams passing through one cavity in which the coupling hole was centrally placed.

Gordon, Zeiger, and Townes (1955) remark that if the cavity is excited in a mode in which there is more than one-half wavelength along the direction of travel of the beam, then the emission line is split with two peaks symmetrically disposed about the transition frequency.

Shimoda, Wang and Townes (1956) show that the parameter  $Q_0 L / A$ , rather than  $Q_0$ , is a measure of sensitivity for resonator design, where  $Q_0$  is the unloaded Q, L is the length of the cavity, and A is the cross-sectional area. Accordingly they define a "figure of merit" M for a resonator

$$M = \left( \frac{L Q_0}{A} \right) \left( \frac{8}{\pi^2} \right)^p ,$$

for p, the axial mode number, having the values 0 or 1. For a broad beam the  $E_{010}$  mode has the highest figure of merit compared with the modes  $E_{011}$ ,  $H_{211}$ ,  $H_{011}$ ,  $H_{111}$ ; and for a narrow beam the advantage is even more pronounced.

Shimoda, Wang and Townes give a value for the unloaded Q,  $Q_0$  of 10,800 for a copper cavity 12cm. long, in the  $E_{010}$  mode at 24 GHz, assuming  $\epsilon = 4.27 \times 10^{-5}$  cm., where  $\epsilon$  is the skin depth multiplied by the specific permeability  $\mu'$  of the wall material,

$$\epsilon = \left( \frac{c}{2\pi} \right) \left( \frac{\mu' \tau}{\gamma} \right)^{\frac{1}{2}} ;$$

here  $\tau$  is the electric resistivity.

The cavity is fashioned by depositing copper electrolytically on to a stainless steel (S80) mandrel (further details are given in Appendix A). When the electroform is about an inch in diameter it is machined, and then removed from the mandrel by

heating it in hot oil.

The cavities are made slightly undersize so that they may be stabilised at the resonance frequency by controlled heating. Though undersized at room temperature the cavities have to be made from mandrels 0.0005cm. greater in diameter than the calculated value (0.9619cm. (0.3788") compared with 0.9614cm.) to allow for end effects of the cavities. The calculated coefficient of variation of frequency with diameter is about 6MHz. per 0.0001 inch; and the observed variation of frequency with temperature is approximately 0.4MHz. per degree C.

The Q factor of the cavity is increased by inserting metal rings (end caps) in each end of the cavity, so that the waveguide is beyond cut-off.

Two cavities have been employed in the work described here, and hereafter are referred to as cavities 1 and 2. Cavity 1 has a physical length of 13.3cm. reduced to an effective length of 12.4cm. by the insertion of 1cm. long end caps to depths of 0.55cm. and 0.35cm. (the Q varies with the positioning of the end caps and these values represent one combination which optimised the Q). The coupling hole is positioned 5.8cm. from one end (that nearest the focuser). This positioning was dictated by the geometry of the box. The cavity is much undercoupled, in order to yield a high loaded Q of  $8,850 \pm 450$  (details of the method used to measure

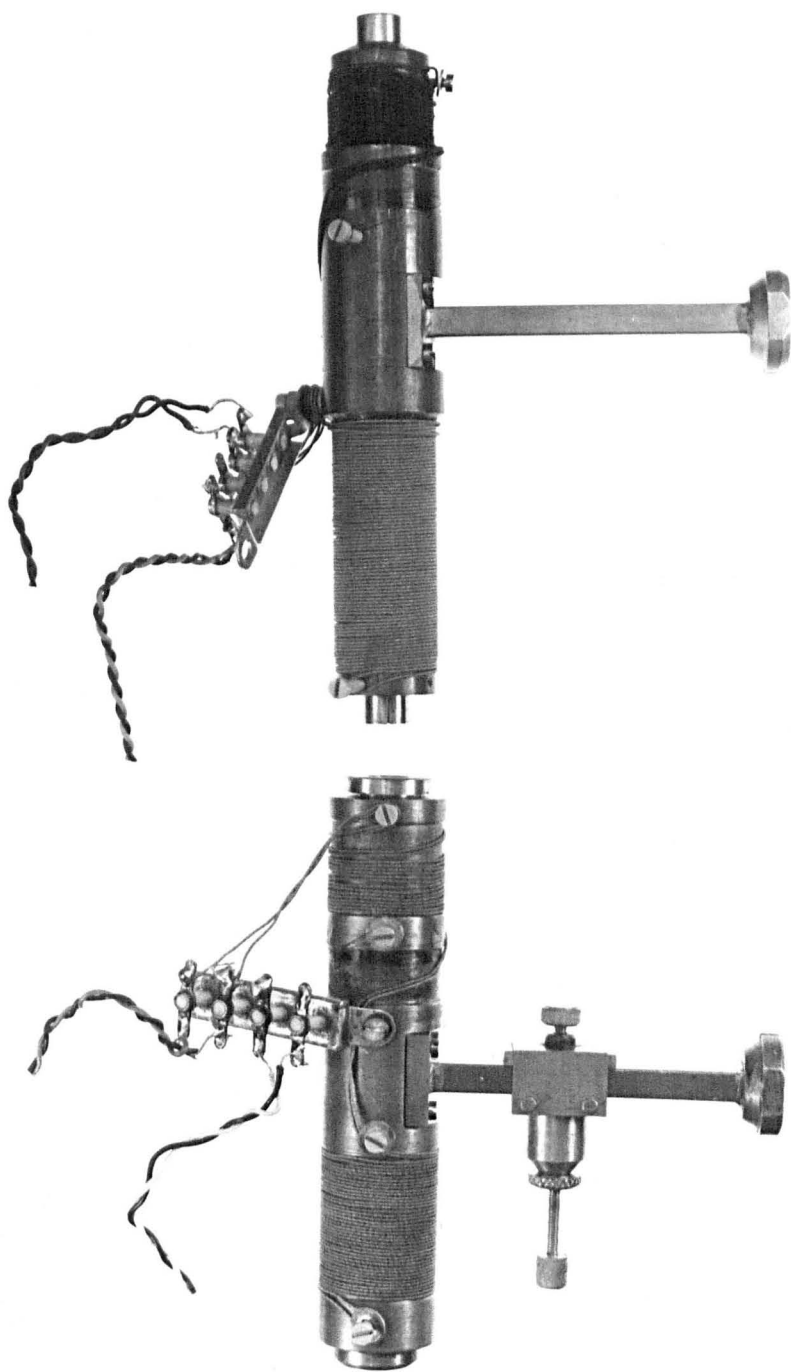


Figure 2.6 Microwave cavities

the  $Q$  are given in Appendix B). The coupling hole parameters are: diaphragm thickness 0.017", hole diameter  $5/64$ ". Cavity 2 has a physical length of 11.4cm. reduced to 10.2cm. by end caps inserted 0.6cm. in each end. The coupling hole is centrally placed, and has a diameter of  $1/10$ " with a diaphragm thickness of 0.008". This cavity is very strongly coupled and has a loaded  $Q$  of  $6,050 \pm 300$ . Figure 2.6 shows the two cavities, wound with heater coils (glass covered Eureka wire) and sensor coils (insulated copper) for stabilised tuning. Cavity 1 is of entirely copper construction, whereas cavity 2 is copper sheathed in brass.

Stabilisation of the cavity temperature to better than  $1/10^{\circ}\text{C}$  is effected with a modified version of an Airmec N.299 Temperature Controller. This circuit variant (due to G. D. S. Smart) gives a continuously variable heating current instead of a relay switched form of control. A further modification by the present writer is a slow motor sweep of a helipot resistance in the "set temperature" arm of the a.c. bridge circuit. The maximum motor speed which can be used to change the tuning of the cavity is governed by the thermal time constants.

Typically the cavities are designed to be operated between  $20$  and  $30^{\circ}\text{C}$  above room temperature in order to maintain positive stabilisation.

Figure 2.7 shows the components mounted in the maser.



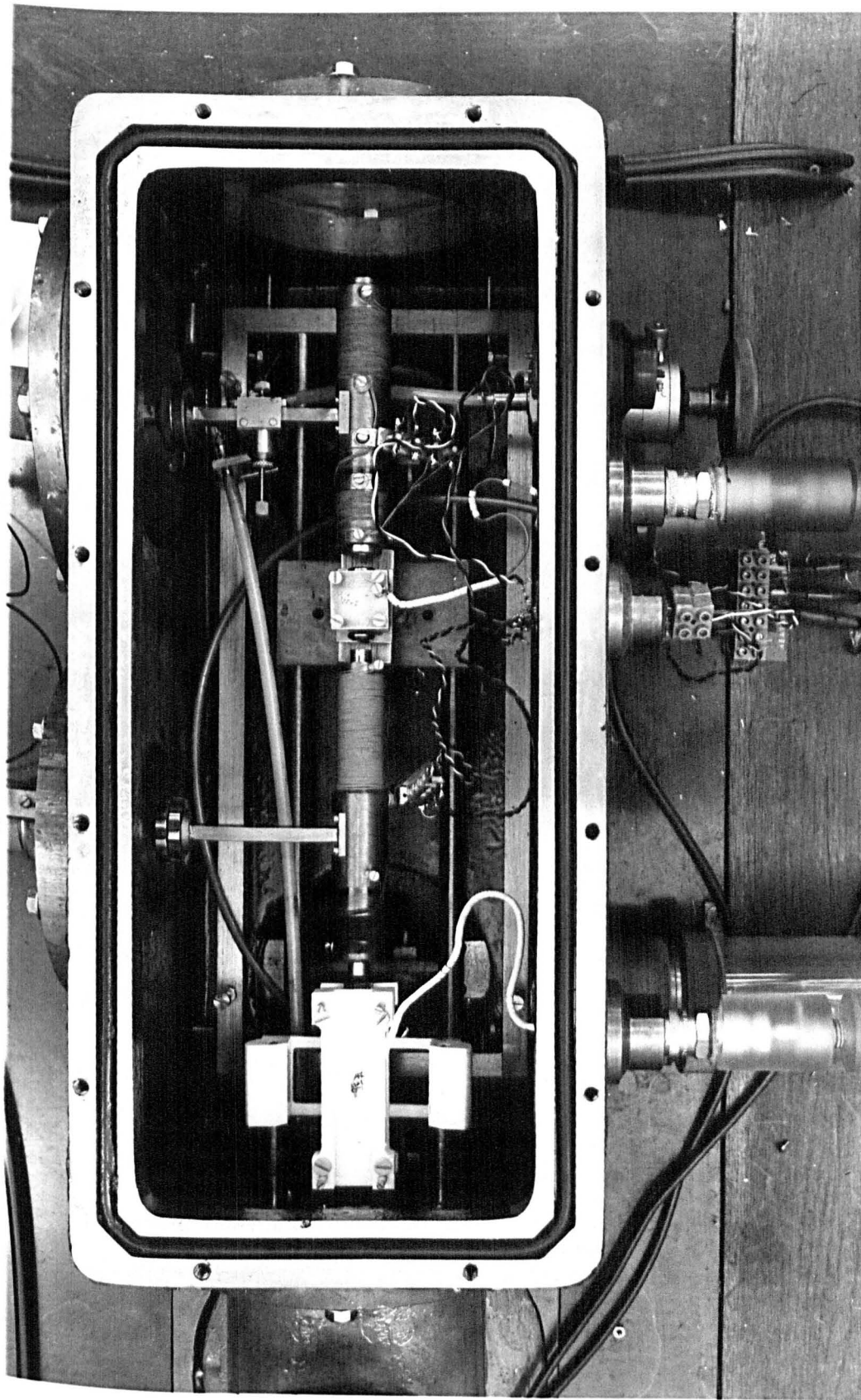


Figure 2.7

## 2.4 Microwave System

There are three modes of operation of the microwave system: crystal video, unstabilised superheterodyne, and stabilised superheterodyne. The first, crystal video, is used only in setting up procedures, such as the tuning of a cavity resonance. The unstabilised superheterodyne mode of operation is employed for most of the experiments conducted in the present investigations since it displays rapid time and frequency variation of signals. The stabilised superheterodyne technique is used to display slow variations of oscillation amplitude with changes in maser parameters.

Figure 2.8 is a schematic representation of the basic microwave bridge employed, together with the electronic detection system. (The microwave circuit appears in the photograph Figure 2.1(a)). The bridge is a version of one designed by Herrmann and Bonanomi (1956).

In the crystal video mode of operation a saw-tooth waveform is applied to the reflector of the klystron: approximately 120 volts peak potential is required to sweep the klystron (Elliot-Lytton 12RK3) through a complete mode. The first detector is connected directly to the oscilloscope (Telequipment D53) vertical audio amplifier, with the timebase triggered by the original 50Hz. saw-tooth. This displays the klystron mode on which may be seen a dip corresponding to the microwave cavity absorption. The bridge

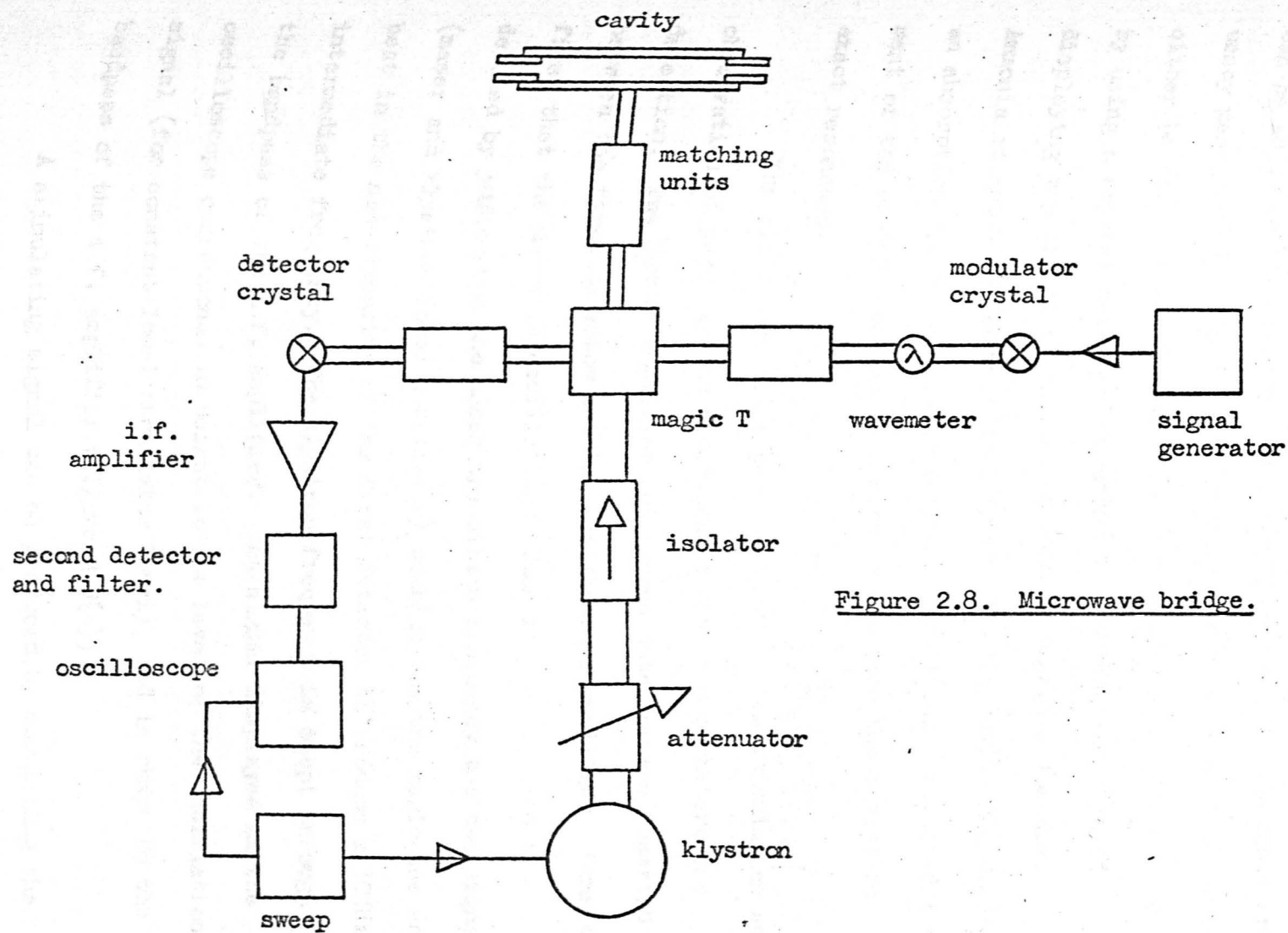


Figure 2.8. Microwave bridge.

can be adjusted for maximum cavity absorption and the resonant frequency measured with the cavity wavemeter, the response of which can either be observed as an absorption dip on the klystron mode, or by using a crystal detector connected to the reaction arm and displaying the signal on the second beam of the oscilloscope. Ammonia at about  $10^{-3}$  torr is introduced into the cavity and produces an absorption dip on the cavity response permitting precise adjustment of the cavity temperature controller to tune the cavity to exact resonance.

The microwave bridge permits simultaneous stimulation and observation of maser action under conditions of superheterodyne detection. The 30MHz. amplifier and second detector are inserted between the first detector and the oscilloscope amplifier. Consider first that the maser is oscillating. Then if the klystron is detuned by 30MHz. from the maser transition frequency the two signals (maser and klystron local oscillator) combine via the magic tee and beat in the non-linearity of the first detector to produce a 30MHz. intermediate frequency. The klystron frequency is swept through the bandpass of the i.f. amplifier. The signal displayed on the oscilloscope corresponds in height to the level of the oscillation signal (for constant local oscillator level), and in shape to the bandpass of the i.f. amplifier (Figure 2.9(a)).

A stimulating signal can be produced by modulating the

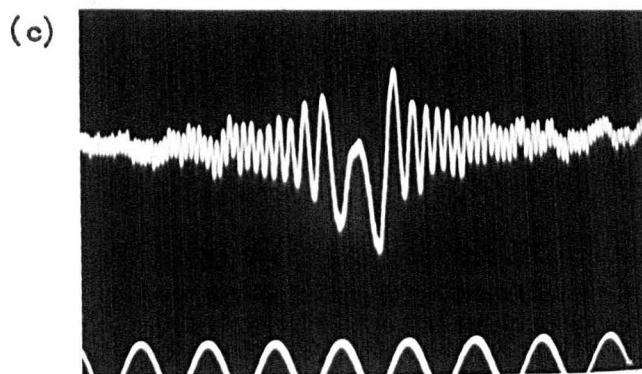
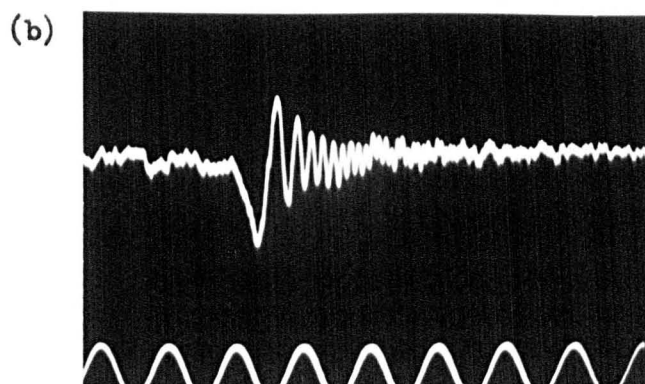
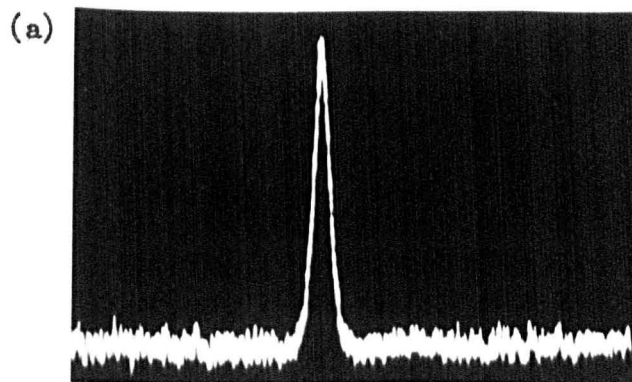


Figure 2.9

impedance of the crystal in the other (collinear) arm of the bridge. If the modulation is made at 30MHz. then the klystron wave reflected from that crystal possesses two sidebands, one of which is at the maser frequency. The appearance of the stimulated signal is registered as a beat signal which appears on the bandpass envelope. It has a high frequency in the wings and passes through a zero beat at the central position, the locus of which may be varied on the bandpass representation by changing the signal generator frequency.

Below oscillation threshold the stimulating signal excites coherent emission from the molecules which beats with the frequency varying stimulating signal to produce a changing beat frequency. Figure 2.9(b) shows this signal. The decaying envelope represents the effect of bandpass restrictions as well as the decay with time of the induced molecular ringing signal. Figure 2.9(c) shows the beat signal that registers the onset of oscillation in the maser.

The stabilised superheterodyne mode differs from the unstabilised mode of operation only in that the klystron is no longer swept in frequency but stabilised with a Micronow stabilisation circuit (some details of which are given in Appendix B). Changes in the oscillation signal are monitored as changes of D.C. level on the oscilloscope, or on a pen recorder.

## 2.5 Electronic equipment

The klystron power supply is an A.P.T. Model K.P. 20.

The klystron filament heater supply is a transistorised d.c. supply designed by Midcentury (private communication). It has been modified by the inclusion of a reed switch in the mains supply to the K.P. 20. The circuit is shown in Figure 2.10. Failure of the filament supply will result in switching off of the high voltages supplied to the klystron. Since the thermal time constant of the filament is larger than the RC time constant for the E.H.T. circuits, this device affords a large measure of protection for the klystron.

Figure 2.11 shows the circuit of the klystron frequency sweep unit. It is a modification of a television frame timebase circuit to give a linear saw-tooth. The output is transformer coupled: the secondary winding being in series with the reflector lead. The saw-tooth is closely linear down to a few millivolts; below, in fact, the level of ripple on the reflector supply from the K.P. 20.

The 30MHz. i.f. amplifier has a gain of 66 dB and a bandwidth of 2MHz.. The circuit is described by A. L. S. Smith (1966), who also reviews considerations of noise for superheterodyne systems such as the one employed here.

Two 30kV. supplies have been used to charge the state focusers: one, a Brandenburg S 0530 (positive polarity) with a stability of better than 0.25%; the other, a Brandenburg 800







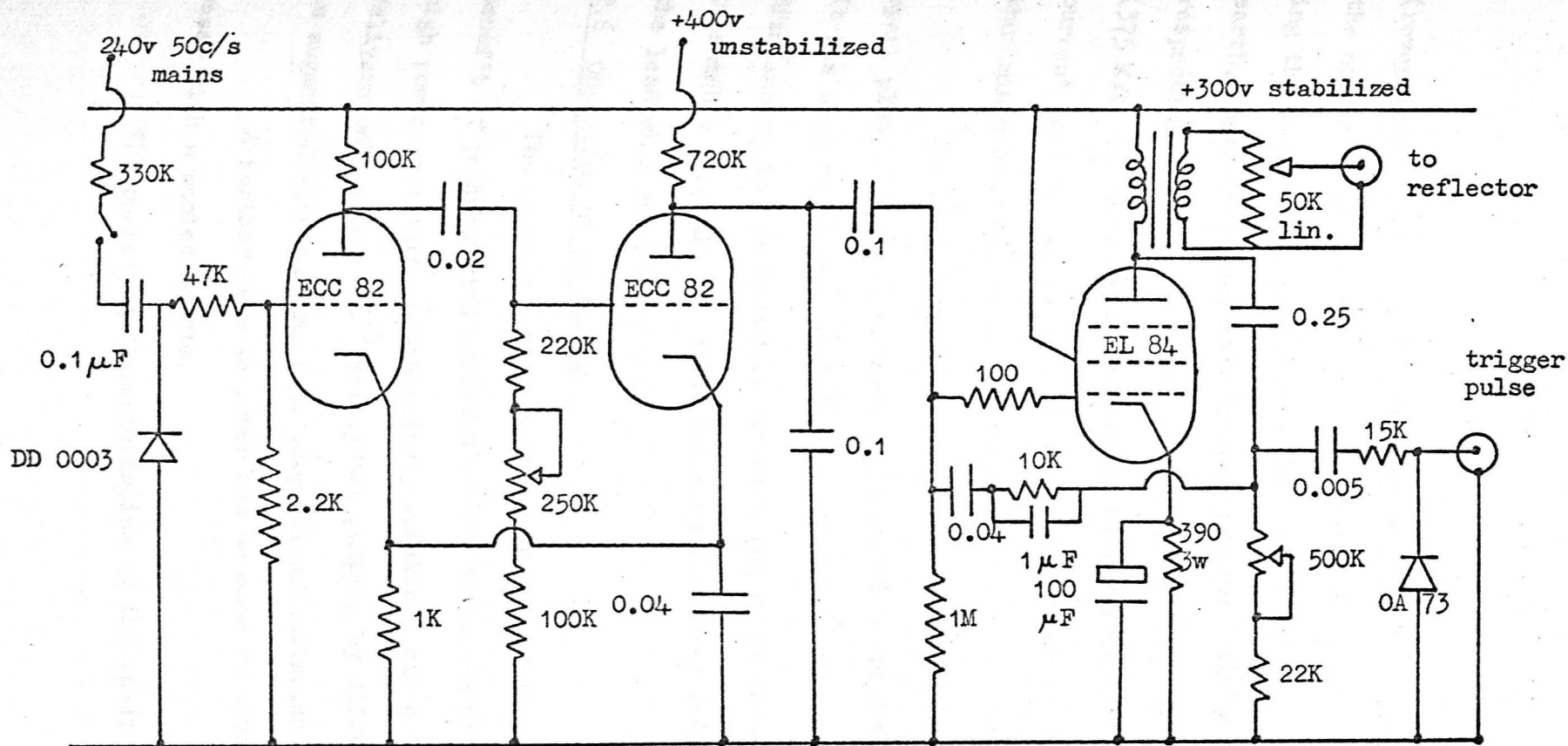


Figure 2.11. Circuit of reflector sweep unit.

(reversible polarity). The feature of reversible polarity permits the operation of the focuser at a potential up to 60kV., by connecting the two focuser plates at +30kV. and -30kV. with respect to earth. Both units are radiofrequency units (100kHz. and 12kHz. respectively), and an RC smoothing is required. The high resistance ( $375\text{ M}\Omega$ ) in series with the supply also serves to reduce the current that can be drawn when breakdown occurs in the focuser, thus minimising damage to the focuser.

The lead-through to the state focuser is a long-reach spark plug, suitably machined, and mounted in an Araldite casting. It has been found that sparking is reduced if the lead from the Brandenburg is terminated by  $125\text{ M}\Omega$  in the spark plug. This is presumably a result of better matching for waves propagated along the lead when sparking occurs.

## 2.6 Operation of the maser

The maser has been operated as an oscillator without the benefit of pumping with surfaces cooled by liquid nitrogen. For high power operation (comparatively speaking, since the oscillator delivers only about  $10^{-10}$  watt.) the pumping by diffusion pumps is augmented with pumping from three liquid nitrogen traps.

A further gain in power can be made by operating the maser with a cooled nozzle.

The operating characteristics of the maser under these

varying conditions are detailed below. Since the characteristics of maser operation have been examined in detail by previous workers, attention is focused only on those features which are comparatively novel (the thesis by A. L. S. Smith (1966) details investigations of velocity effects and also reviews previous investigations of maser parameters). It emerges that the design feature of a remotely controlled variable iris diaphragm is a very desirable one, for it permits an easy transition between optimum conditions for various experiments.

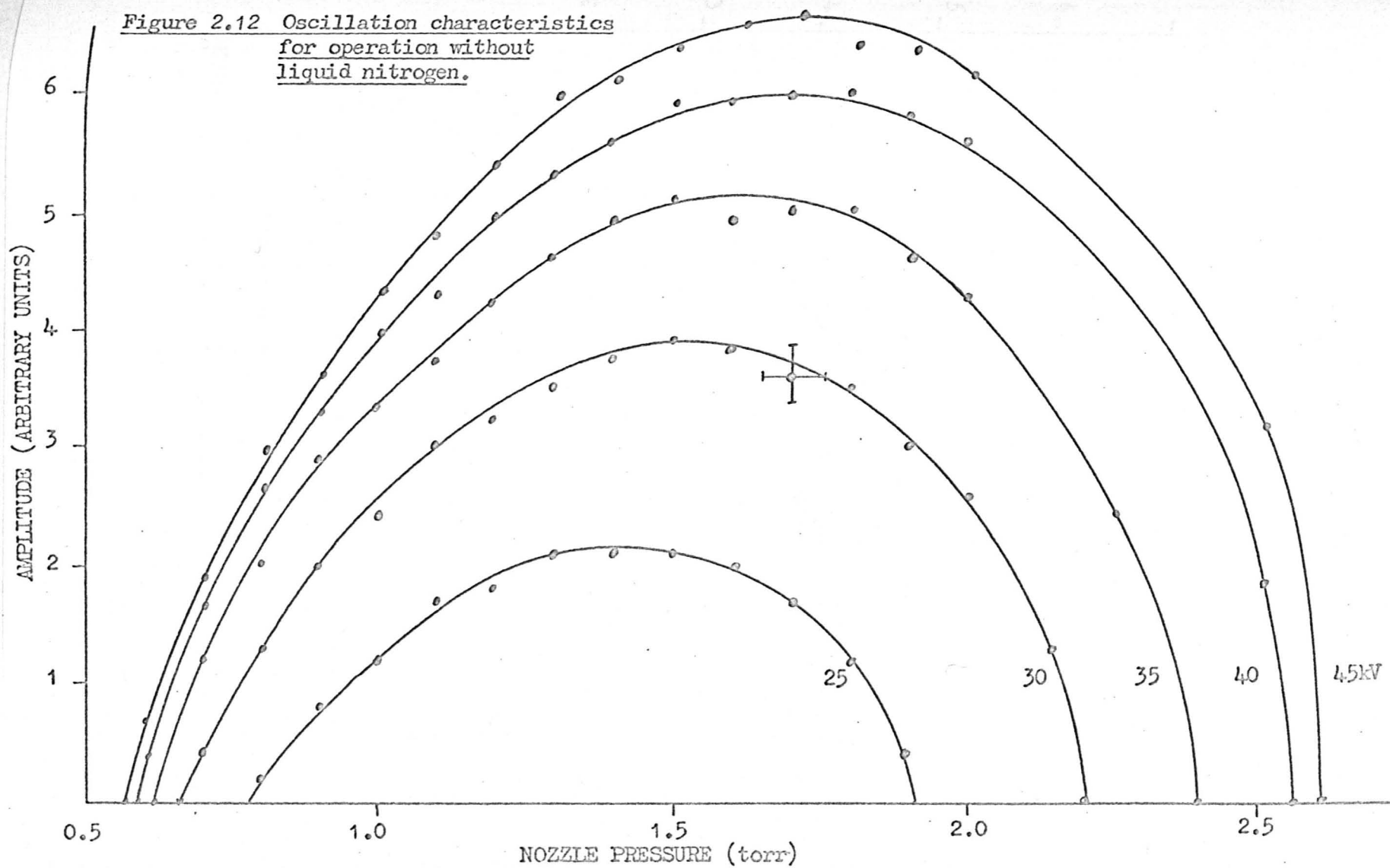
(a) Operation without liquid nitrogen pumping

Operation of the maser without liquid nitrogen is critically sensitive to the iris aperture. It must be stopped down to about 1mm.

Two sets of characteristics are plotted: one of variation of oscillation amplitude with change in nozzle pressure at fixed focuser voltages; the other, the variation of oscillation amplitude with change in focuser voltage at fixed nozzle pressures. (Figures 2.12 and 2.13) These graphs are sections of a three-dimensional function. A model representation of this function is shown in the photograph Figure 2.14.

The oscillation amplitude is plotted in terms of the height of the oscillation signal on the oscilloscope screen. Since the main value of the characteristics is the indication

Figure 2.12 Oscillation characteristics  
for operation without  
liquid nitrogen.



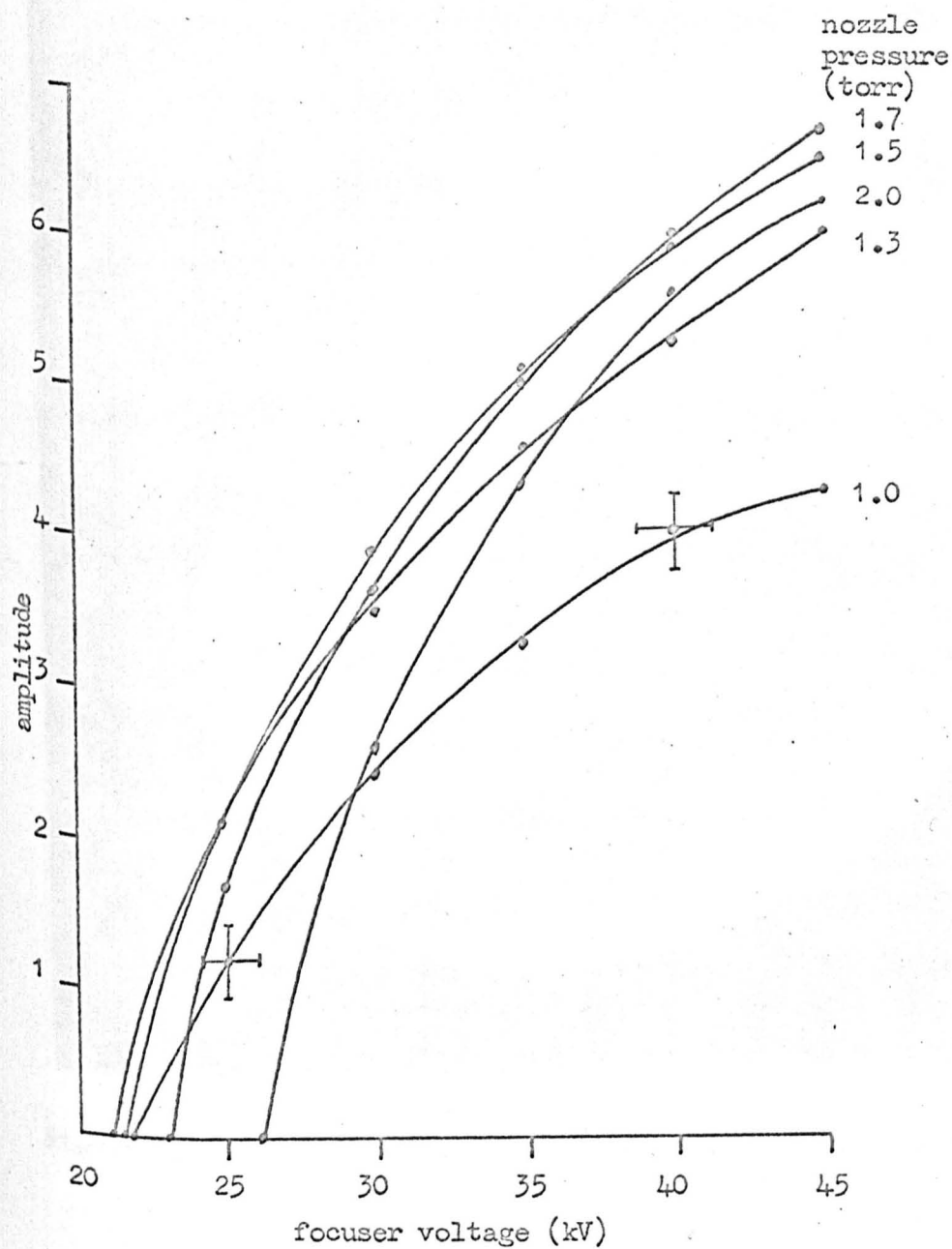


Figure 2.13 Characteristics for operation without liquid nitrogen.

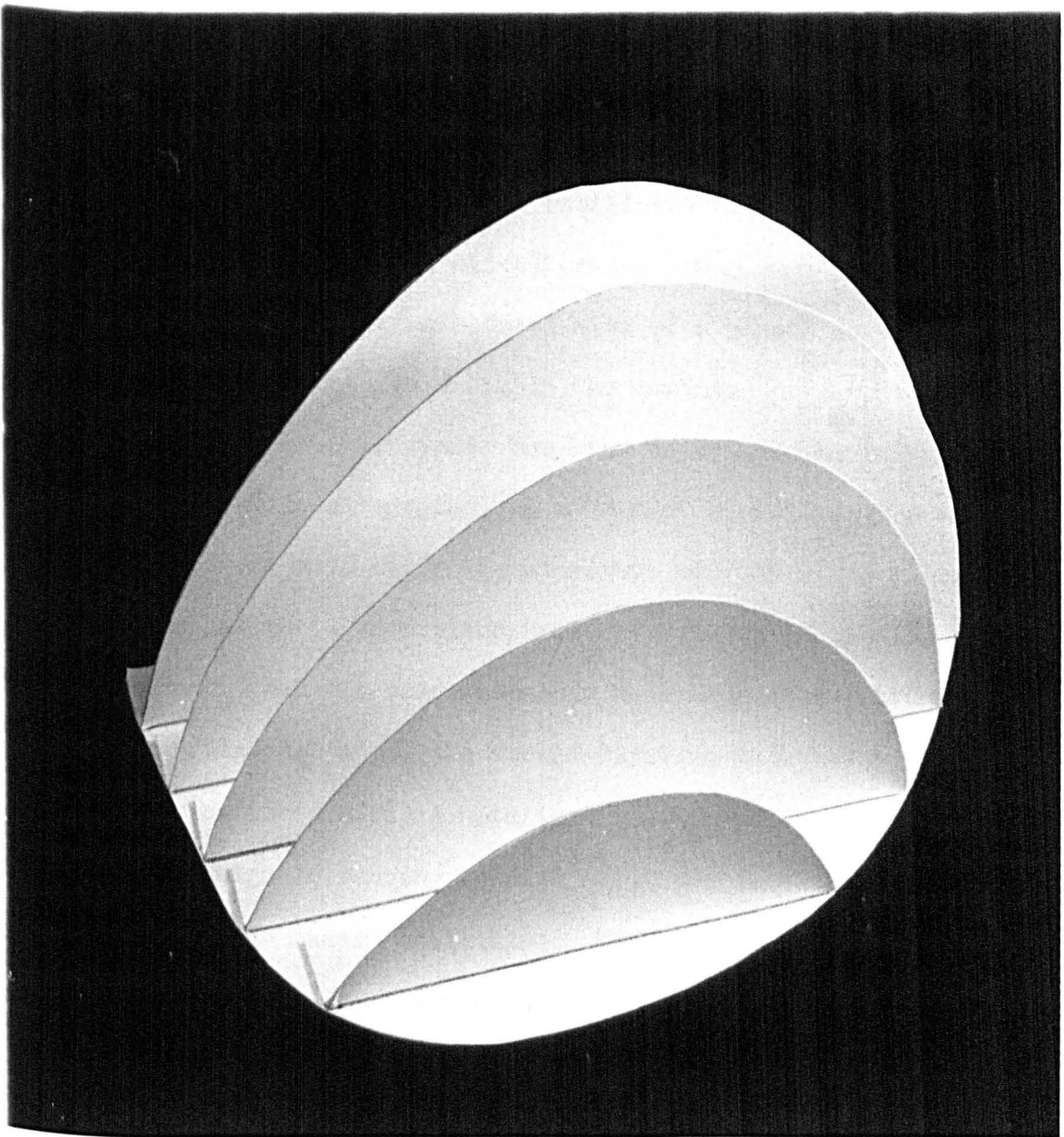


Figure 2.14 Three-dimensional representation of characteristics of the maser operated without liquid nitrogen

they give of trends, and of thresholds and optima, a knowledge of the law of response of the system is not usually required. However, if a quantitative comparison of oscillation amplitudes is required to relate changes to theoretical predictions, then it is necessary to determine the relation between size of a signal on the oscilloscope screen and the field within the cavity.

The law of response has been determined by using a second klystron, heavily attenuated, as a "mimic" signal for the maser output. Figure 2.15 shows the microwave circuit. The microwave bridge is set for a comparison between two sets of oscillation conditions. When the comparison has been made, then without altering the bridge settings, the second klystron is switched on and the maser switched off. A note is taken of the attenuation required to produce signals ranging in size about the level of the signal produced by the maser oscillation. The variation is plotted in graphical form as dB of attenuation versus logarithm (base 10) of response (Figure 2.16) This graph permits evaluation of the law of response (from the slope) and also a relative power comparison for particular oscilloscope signal voltages. The method yields only relative powers since, of course, it does not take cognisance of the attenuation effect of the coupling hole in the cavity. However, it seems reasonable to argue that the coupling attenuation factor ( $Q_L / Q_0$ ) is not likely to vary over a small power range, so

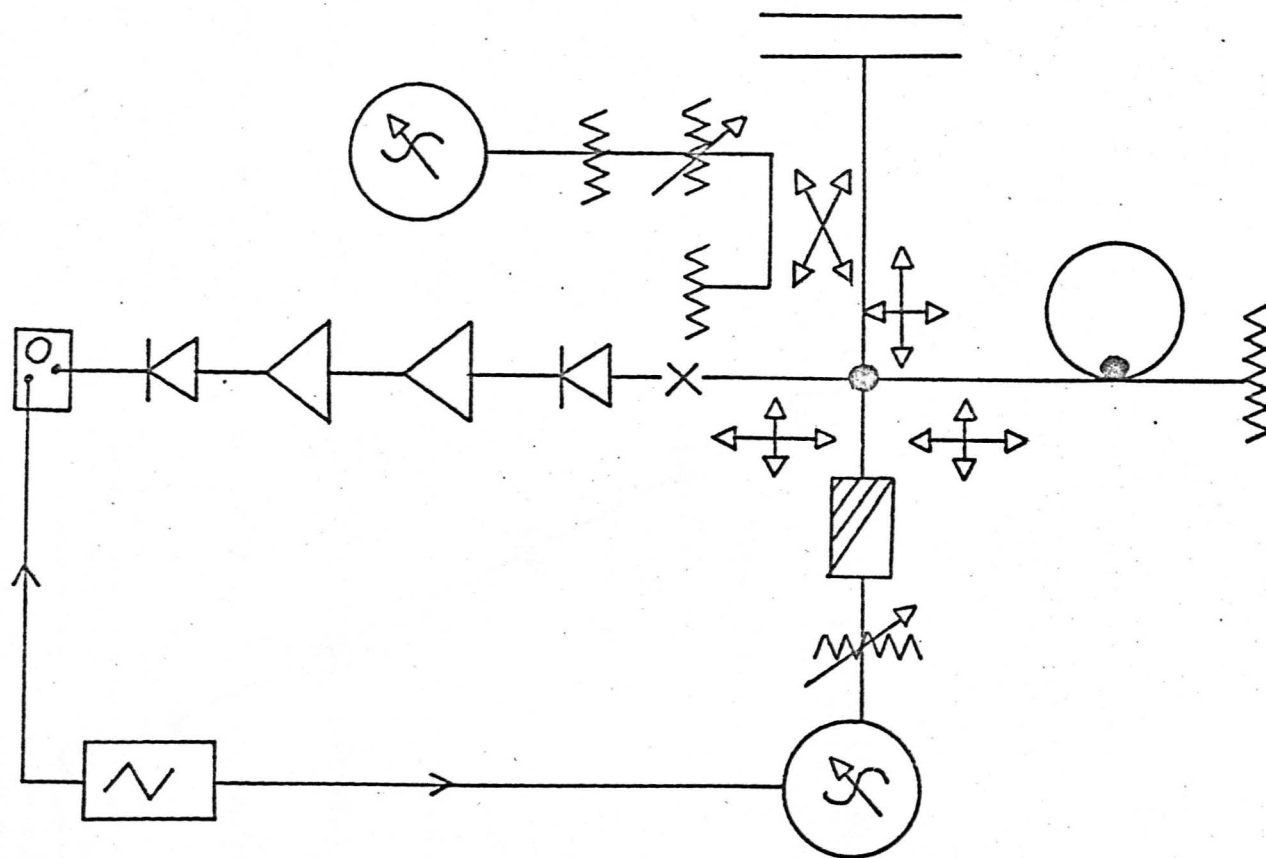


Figure 2.15. Scheme devised for the determination of the law of the response of the detection system.



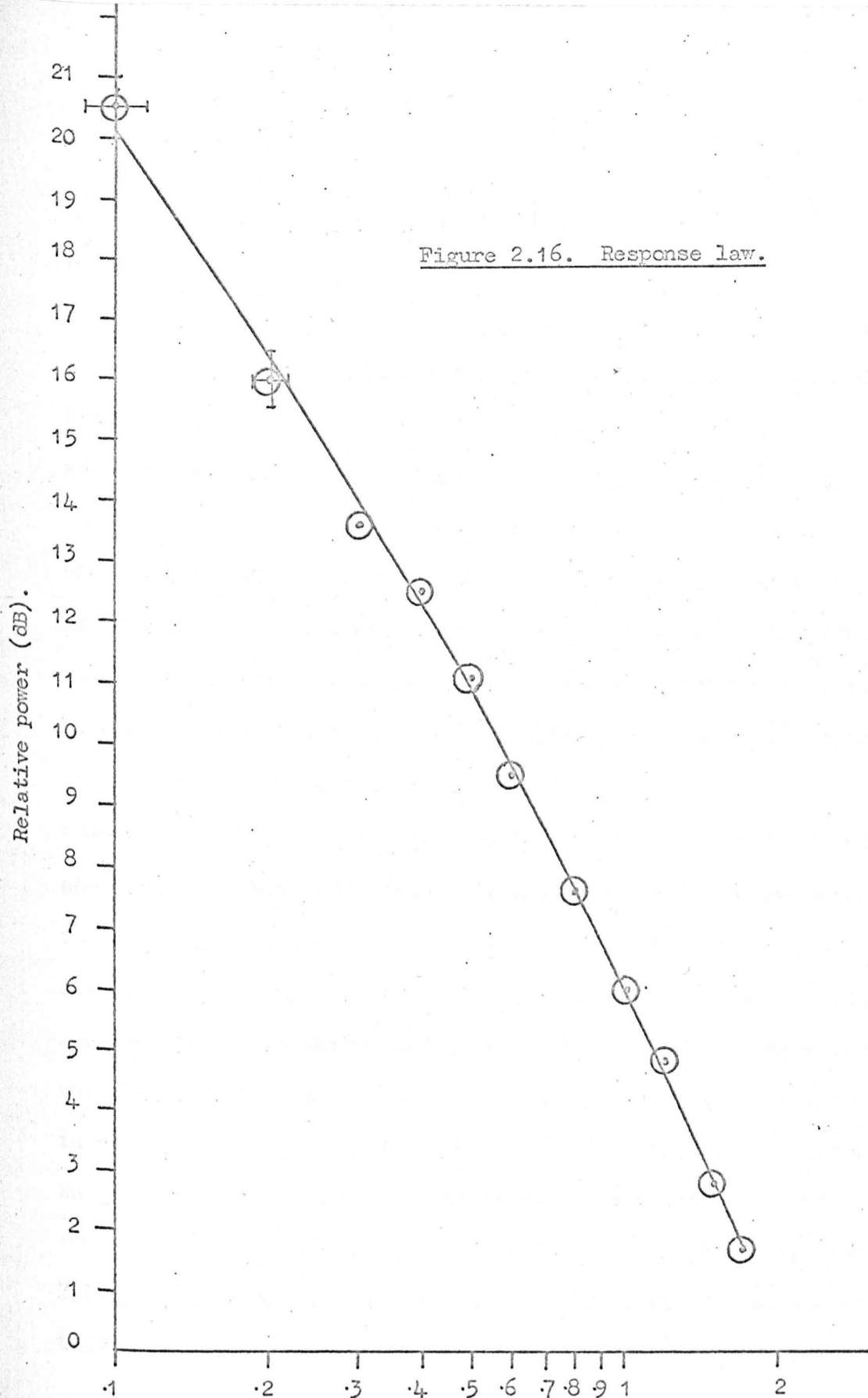


Figure 2.16. Response law.

Response (amplitude of oscilloscope signal).

that the response law is a fairly reliable indication of the change of field in the cavity.

The "mimic" signal is at very low level and thus it is necessary to determine that the signal registered at the detector has been propagated via the waveguide and is not a leakage signal which has bypassed the attenuator. Ideally, choked flange couplings should be used, but since these were not available the leakage was minimised by using aluminium foil shields around the components. The level of leakage coupling was determined by noting the fluctuations in level consequent upon moving metal sheets near the bridge. It was possible to reduce the leakage to an acceptable low level.

Another point to be made about the characteristics is that for the higher voltages the meter indications on the Brandenburg generators are not reliable. If there is a small leakage current in the focuser insulation then there occurs a drop of voltage across the  $500\text{ M}\Omega$  resistance in the leads. The only test equipment available was restricted to the range 0-20kV. Tests with this revealed a small drop in voltage which may assume greater proportions in the higher ranges. The change in field in the cavity with change in focuser voltage at high voltages has been monitored by means of the frequency modulation of the oscillation transient (discussed later) which is a more reliable indication of field than the amplitude on the oscilloscope. It has been observed that non-monotonic

changes in the amplitude with increasing voltage attributable to voltage drop have always been accompanied by sparking (which shows as spikes on the oscilloscope trace). It is therefore felt that the characteristics are not subject to a marked non-linearity attributable to leakage currents.

The total molecular flux at the optimum nozzle pressure at 30kV. (1.5 torr) has been determined by noting the change in pressure of the gas in the reservoir for a steady flow with constant pressure in the source chamber. This yields a value for the flux of  $8.7 (\pm 0.4) \times 10^{17}$  molecules per second. For this flux the pressures in the main chamber and forechamber are respectively  $1 \times 10^{-5}$  torr and  $5 \times 10^{-4}$  torr.

(b) Operation of the maser with liquid nitrogen pumping and a cooled surface

Figures 2.17 and 2.18 show the maser characteristics for operation with full liquid nitrogen pumping and cooling of the nozzle to  $-60^{\circ}\text{C}$ . Figure 2.19 shows a typical characteristic in terms of the amplitude of the oscilloscope trace and in relative power.

Cooling of the nozzle can be expected to yield an increase in maser oscillation power for two reasons: it increases the population in the  $J = 3, K = 3$  state (about 6% of the total population at room temperature), and it reduces the average molecular

Figure 2.17 Oscillation characteristics for operation with liquid nitrogen

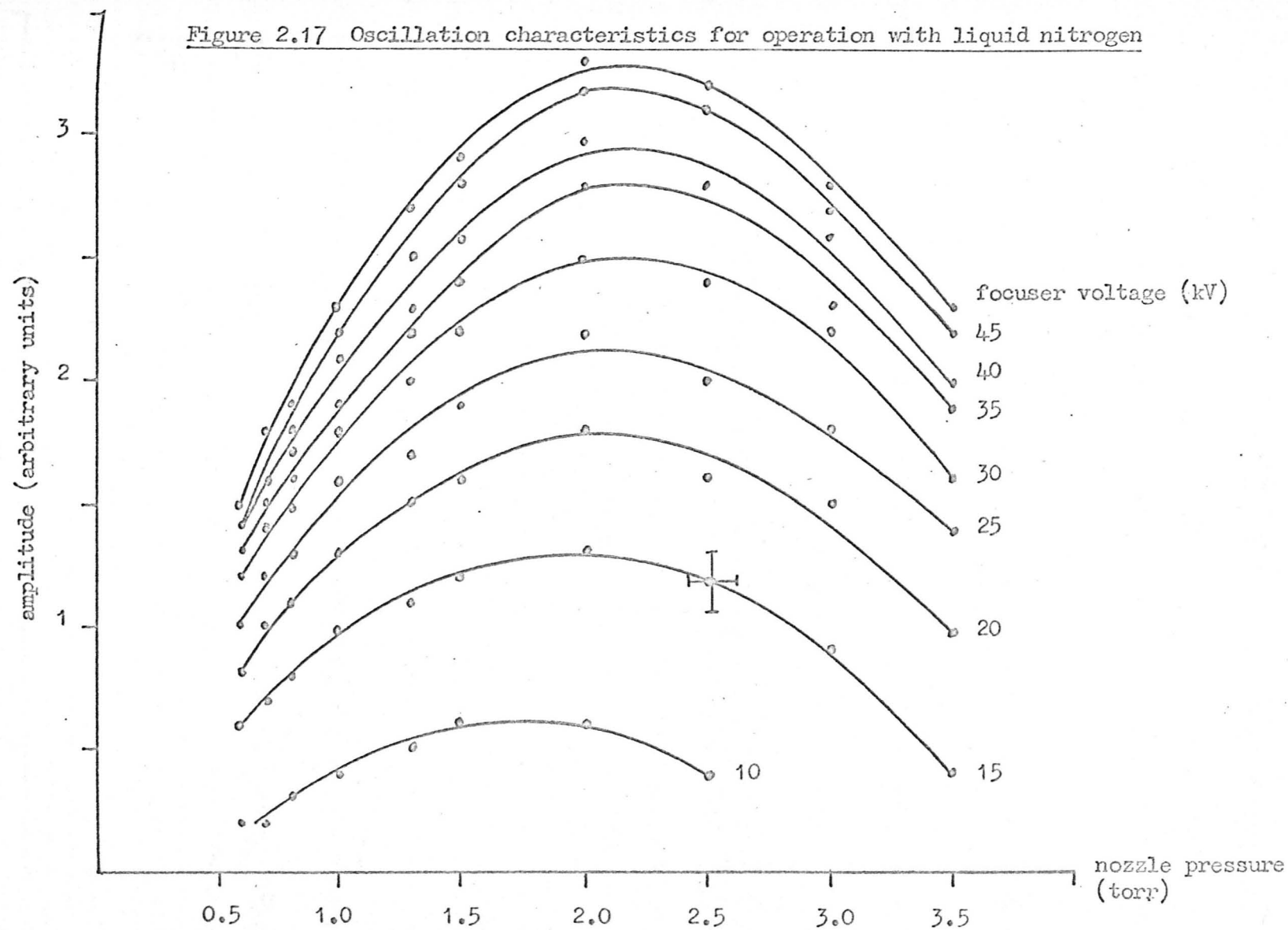
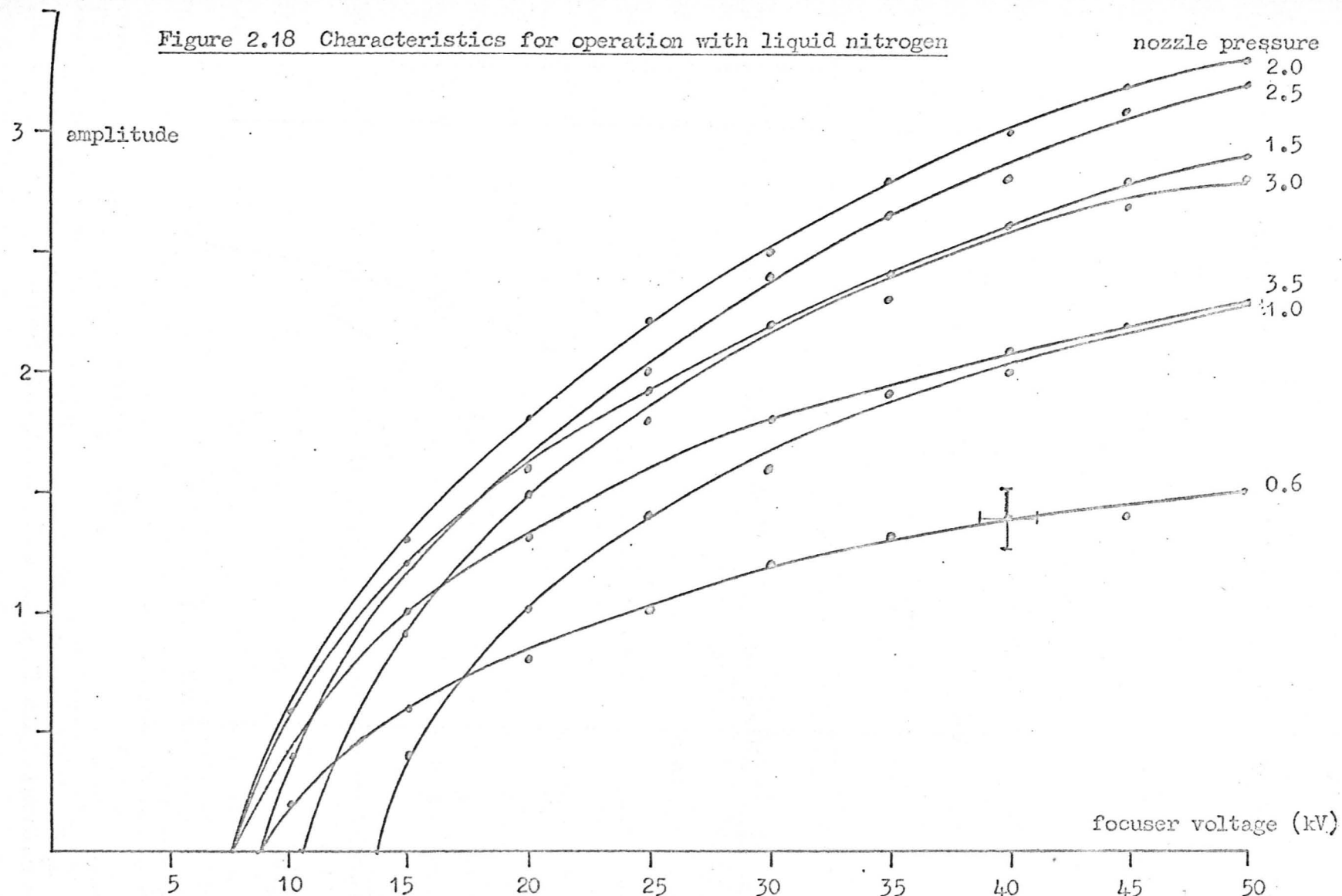


Figure 2.18 Characteristics for operation with liquid nitrogen



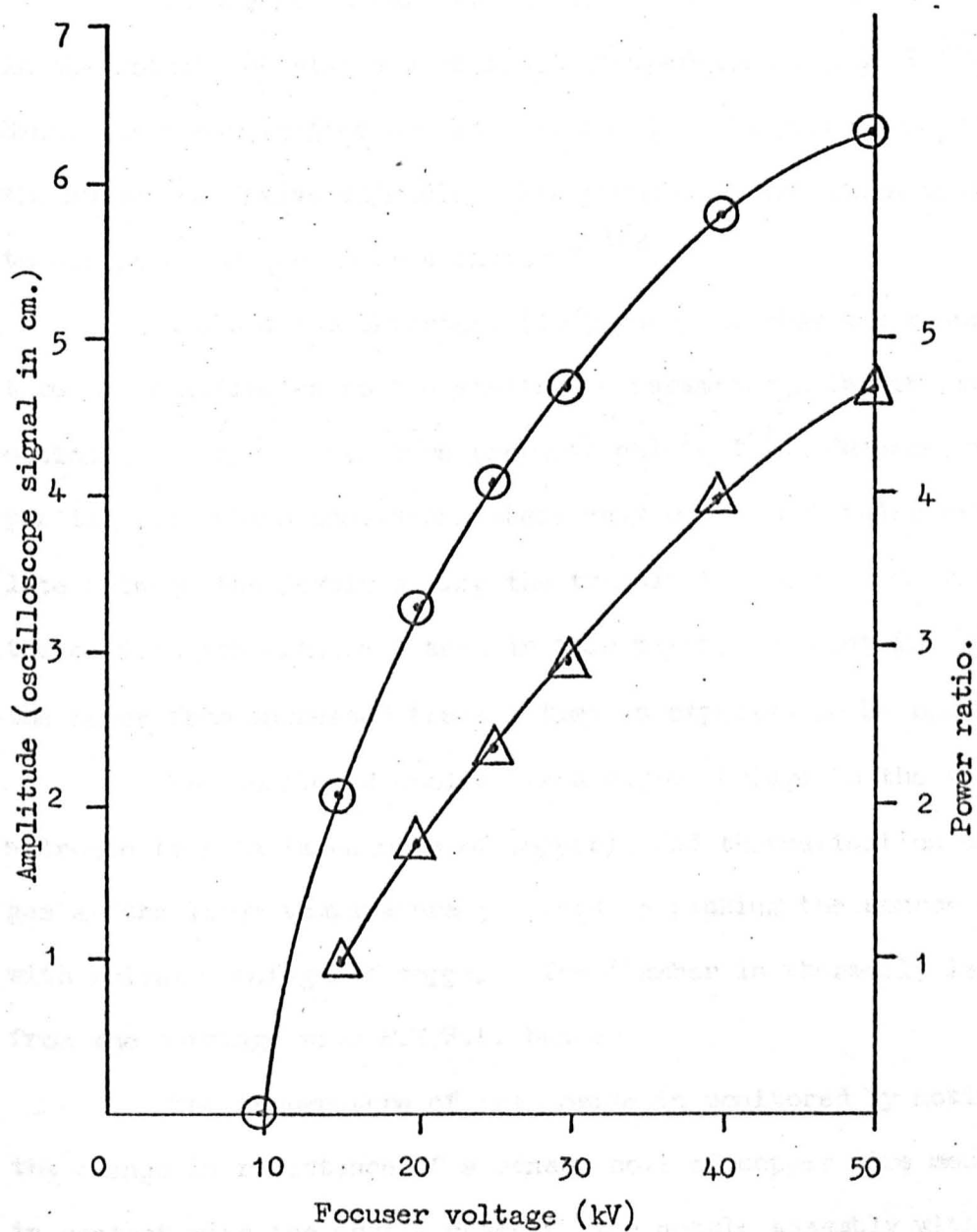


Figure 2.19. Characteristics in terms of oscilloscope signal amplitude ○ and in terms of relative power △ .

velocity, thus increasing the interaction time which, in turn, increases the transition probability.

It was noted earlier in the chapter that the population in the rotational states varies with temperature  $T^{\circ}\text{K}$  as  $T^{-3/2}$ . Since the power emitted by the beam is directly proportional to the number of active molecules this population variation contributes to the power of the maser a factor  $T^{-3/2}$ .

Krupnov and Skvortsov (1965) suggest that the transit time  $\tau$  contributes to the excitation parameter a factor proportional to  $\tau^2$ , in turn proportional to  $T^{-1}$ . However, under partial saturation conditions where many of the molecules oscillate between the levels during the transit time (as evidenced by the oscillation transient seen in this maser) the contribution to the power from increased transit time is expected to be small.

The nozzle is cooled via a copper bridge to the liquid nitrogen trap (a large mass of copper), and thermalisation of the gas at the lower temperature is aided by packing the source chamber with spiral turnings of copper. The chamber is thermally isolated from the carriage with P.T.F.E. bushes.

The temperature of the nozzle is monitored by noting the change in resistance of a sensor coil of copper wire mounted in contact with the nozzle chamber (the nozzle assembly with sensor and heating windings can be seen in Figure 2.3) This has

been calibrated in the range  $-150^{\circ}\text{C}$  to  $+20^{\circ}\text{C}$  by A. Codling in a cold gas flow system devised for an E.S.R. spectrometer. The resistance of the wire changes from 13.3 ohms at room temperature to 7.5 ohms at  $170^{\circ}\text{K}$ , the minimum operating temperature possible with the present scheme. The critical point for ammonia occurs at about  $195^{\circ}\text{K}$  and 45 torr. The nozzle has been stabilised somewhat above the minimum temperature, at  $210^{\circ}\text{K}$ , with an Airmec N.299 Temperature Controller.

Comparison between the oscillation powers for the two cases of liquid nitrogen pumping plus cooling of the nozzle, and liquid nitrogen pumping only, is made by operating the maser with the nozzle cooled and then heating it to room temperature, and noting the change in amplitude of the oscilloscope signal. The corresponding change in power is then obtained from the response calibration graph.

The oscillation threshold changes from 23kV. (1.7 torr) for operation without liquid nitrogen pumping, to 13kV. (2.5 torr) for liquid nitrogen pumping only, and then to 10.5kV. (2.5 torr) on cooling the nozzle. These thresholds are for nozzle pressures which give high output. The absolute thresholds, with minimum nozzle pressure, are somewhat lower (21, 10, 7.5kV. respectively).

The power ratios for the various modes of operation are approximately:



- (a) without liquid nitrogen pumping, at the optimum  
1.5 torr nozzle pressure and 40kV, power unity;
- (b) with liquid nitrogen pumping in the main chamber  
only,
  - (i) at 1.5 torr and 40kV.,  
power 2 ,
  - (ii) at the new optimum 2.8 torr and 40kV.,  
power 2.7;
- (c) with liquid nitrogen pumping in both chambers,
  - (i) 1.5 torr, 40kV, power 2 ,
  - (ii) 2.8 torr, 40kV, power 3.

The power ratio for the change in nozzle temperature from  $293^{\circ}\text{K}$  to  $213^{\circ}\text{K} \pm 5^{\circ}\text{K}$  (at 50kV. and 2.5 torr nozzle pressure) is  $1.6 \pm 0.2$ , which is close to the ratio of  $(213)^{-3/2} / (293)^{-3/2}$  of  $1.61 \pm 0.05$ . The  $T^{-5/2}$  dependence yields a ratio of 2.2. It may thus be reasonable to argue that the contribution to the power afforded by cooling the nozzle consists mainly of the change wrought in the population of the 3,3 level. However, it can be argued (Chapter IV) that conditions for observation of the oscillation transient are favoured by increasing the transit time.

## REFERENCES

- Gordon, J. P. (1955), Phys. Rev. 99, 1253.
- Vuylsteke, A. A. (1960), Elements of Maser Theory, Princeton,  
van Nostrand.
- Townes, C. H., Schawlow, A. L. (1955), Microwave Spectroscopy,  
New York, McGraw-Hill.
- White, L. D. (1959), Proc. 13th. Ann. Freq. Control Symp.
- Grigor'yants, V. V., Zhabotinskii, M. E., (1961), Radio Eng. and  
Electron. Phys., 6, 260-3.
- Skvortsov, V. A., Krupnov, A. F., and Naumov, A. I. (1960).  
Izv. VUZ. Radiofiz., 3, 1128-9.
- Basov, N. G., Borisenko, M. I., Vlasov, V. P., Dubonosov, S. P.,  
Ivanov, N. E., Strakhovskii, G. M., Fedorenko, G. M., Chikhakhev, B. M.,  
Kosmicheskii Issledovaniya, 5, 608-616 (1967); translated in Cosmic  
Research (Consultants Bureau), 5, 526-532 (1967).
- Vonbun, F. O., (1958), J. App. Phys., 29, 632-6.
- Mednikov, O. I., Parygin, V. H. (1963), Radio Eng. and Electron.  
Phys., 8, 685-90.
- Krupnov, A. F., Skvortsov, V. A. (1965), Radio Eng. and Electron.  
Phys., 10, 320-2.
- Krupnov, A. F. (1959) Izv. VUZ. Radiofiz., 2, 658-9.
- Becker, G. (1961), Z. angew. Phys., 13, 59.
- Becker, G. (1963), Z. angew. Phys., 15, 281-5.

Shcheglov, V. A. (1961), Izv, VUZ., Radiofiz., 4, 648-55.

Soviet Maser Research, (1964), ed. by Acad. D. V. Skobel'tsyn, Consultants Bureau, New York., translation from Transactions of P. N. Lebedev Physics Institute, Volume XXI, 1963. U.S.S.R. Academy of Sciences, Moscow.

Strakhovskii, G. M., Tatarenkov, V. M. (1965), Izv. VUZ. Radiofiz., 7, 994-5.

Kazachok, V. S. (1965), Sov. Phys. - Tech. Phys., 10, 882-5.

Gordon, J. P., Zeiger, H. J., and Townes, C. H. (1955), Phys. Rev., 99, 1264.

Herrmann, J., Bonanomi, J. (1956), Hel. Phys. Acta, 29, 448-51.

Shimoda, K., Wang, T. C., and Townes, C. H. (1956), Phys. Rev., 102, 1308-1321.

Smith, A. L. S. (1966), doctoral thesis, University of Keele.

Krupnov, A. F., Skvortsov, V. A. (1965), Izv. VUZ. Radiofiz., 8, 200-3.

## CHAPTER III

### THEORIES OF MASER BEHAVIOUR

#### 3.1 Introduction

The analogies established in recent years between maser behaviour and macroscopic devices have proved a fruitful source of understanding and prediction, and have stimulated the search for principles underlying phenomena in diverse fields.

The most important one has been the analogy between electric dipole systems and magnetic dipole systems. Much of the formalism of nuclear magnetic resonance theory can be interpreted to clarify behaviour of electric dipole systems. This involves utilising a macroscopic analogue since,

- (a) the behaviour of a two-level system coupled by an electric dipole transition is equivalent to the motion of a spin  $1/2$  magnetic dipole precessing in a static magnetic field and subject to the influence of a time varying magnetic field,
- (b) this in turn is equivalent to the motion of a macroscopic magnetized gyroscope in the magnetic field.

Much of this chapter is devoted to discussions of various facets of the interaction of radiation with two-level electric dipole systems, where the behaviour can be interpreted in terms of the analogous effect in a magnetic resonance system.

Consider first however another macroscopic maser device.

### 3.2 Dehmelt's macroscopic embodiment of the maser principle

Dehmelt (1968) proposes a gravitational analogue for the simulation of the interaction between excited molecules and a resonant circuit. For the analogue of the cavity he suggests a rigid pendulum which oscillates in the plane of the diagram (Figure 3.1). For the atom he chooses a loaded gyroscope of which the precession frequency due to the gravitational pull on the loaded M is the same as the oscillation frequency of the pendulum. In the excited state the vector  $\vec{A}$  pointing from the centre point of the suspension to M is directed upwards, and in the de-excited state, down. The choice of the gyroscope is governed by the considerations of the correspondences discussed above, only here the magnetic field is replaced by a gravitational field.

The two oscillators are coupled by means of a light, soft spring connecting a point on the rod of the pendulum close to the fulcrum to one on the axis of the gyroscope. Then the excitation of the pendulum is nearly proportional to the rotating component of the vector  $\vec{A}$ , simulating the excitation of the cavity by the fluctuating atomic dipole moment which appears during transition. The flow of excited atoms into the cavity is imitated by forcing  $\vec{A}$  into the upwards position at a random rate (since the phase of the rotating component of  $\vec{A}$  is determined only by the phase of the oscillating pendulum). The macroscopic maser then behaves like an atomic one.

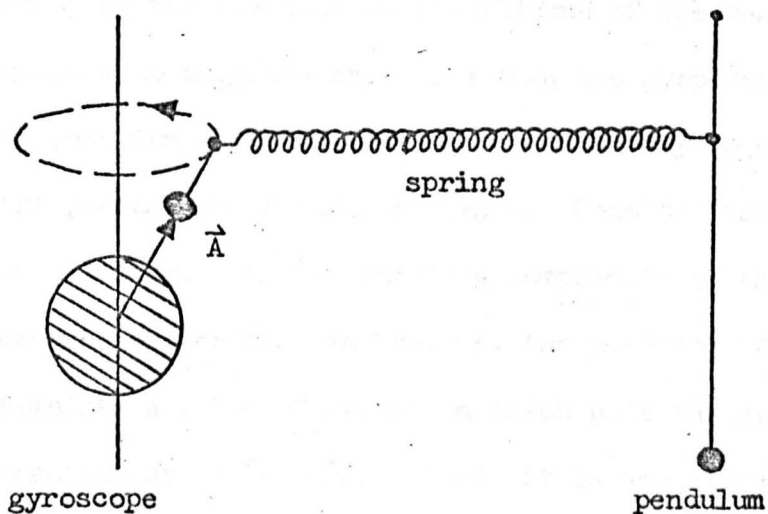


Figure 3.1 Macroscopic maser (after Dehmelt, 1968).

Assuming sufficiently weak damping of the pendulum, any random (thermal) disturbance of the system will result in the oscillation of the pendulum growing exponentially, as energy is transferred to it from the gyroscope. During this process  $\vec{A}$  gradually tilts towards its equilibrium position of lowest energy. The amplitude of oscillation of the pendulum is limited by the non-linearities of the system. The rate at which  $\vec{A}$  tilts (radiation damping) is determined mainly by the friction at the fulcrum of the pendulum.

Dehmelt also suggests that more than one gyroscope may be coupled to the pendulum simultaneously. This idea may be utilised to describe the phenomenon of super-radiance. Consider that the pendulum is oscillating, then the rotating components of the vectors  $\vec{A}$  of the gyroscopes are ordered in phase by the pendulum (field). In order to simulate a pulse of radiation which puts the gyroscopes into a super-radiant state ( $\sim \pi/2$  pulse), it is necessary to imagine that the pendulum is at first still then made to oscillate, and then stilled again. The gyroscopes are coherently excited and subsequently cooperatively "radiate" their energy to the pendulum. The time taken for the system to "radiate" spontaneously and coherently can be very much shorter than that for an incoherent de-excitation of the gyroscopes. If the gravitational field in which the gyroscopes are placed is very inhomogeneous then the rotating components of the vectors  $A$  can move out of phase quite rapidly (in a time  $\sim T_2^*$ ) and the coherence be lost.

### 3.3 Eberly's pendulum analogue

The phenomenon of coherent self-induced transparency (discussed later) has been described in terms of the motion of a classical pendulum. Eberly (1968) has shown that such a picture has quantitative validity.

He considers just one atom interacting without loss with a single mode of the radiation field. The semiclassical Hamiltonian is

$$\mathcal{H} = \mathcal{H}_0 - ME(t).$$

where  $\mathcal{H}_0$  is the unperturbed Hamiltonian,  $M$  is the component of the electric dipole moment operator in the direction of the electric field, and  $E(t)$  is the electric field strength. The equation of motion

$$i\hbar(\partial/\partial t)\langle \rangle = \langle [ \cdot, \mathcal{H} ] \rangle,$$

in conjunction with Maxwell's equations for the single mode, leads to a set of coupled non-linear equations:

$$\langle \dot{\mathcal{H}}_0 \rangle = \langle \dot{M} \rangle E(t), \quad (1)$$

$$\langle \ddot{M} \rangle + \Omega^2 \langle M \rangle = -\lambda \langle \mathcal{H}_0 \rangle E(t), \quad (2)$$

$$\ddot{E} + \Omega^2 E = \sigma \Omega^2 \langle M \rangle, \quad (3)$$

where  $\lambda = (2\mu/\hbar)^2$ ,  $\mu$  is the atomic dipole moment, and  $\sigma$  is practically a constant.

Two exact integrals of motion exist for equations (1) - (3) -

These are:



$$\langle \dot{M} \rangle^2 + \Omega^2 \langle M \rangle^2 + \lambda \langle \mathcal{H}_0 \rangle^2 = \mu^2 \Omega^2 \quad (4)$$

$$(2\sigma)^{-1} (E^2 + \Omega^{-2} \dot{E}^2) + \langle \mathcal{H}_0 \rangle - \langle M \rangle E(t) = W, \quad (5)$$

where the constant  $W$  is the total of field + atom + interaction energies.

Transferring to a rotating frame of reference serves to eliminate variables other than  $\langle \mathcal{H}_0 \rangle$ . By differentiating again the  $\langle \mathcal{H}_0 \rangle$  equation and using the conservation laws (4) and (5), Eberly derives a non-linear equation for the time variation of  $\langle \mathcal{H}_0 \rangle$  alone:

$$(4/\sigma\lambda) \langle \ddot{\mathcal{H}}_0 \rangle = 3 \langle \mathcal{H}_0 \rangle^2 - 2W \langle \mathcal{H}_0 \rangle - (\frac{1}{2} \hbar \Omega)^2 \quad (6)$$

Equation (6) is in the form of the equation of motion of a classical particle in a potential well. Multiplying both sides by  $\dot{\mathcal{H}}_0$  and integrating once, then making the change of variables

$$\langle \mathcal{H}_0 \rangle = (\frac{1}{2} \hbar \Omega) \cos \theta,$$

the transformed equation becomes

$$\frac{2}{\sigma\lambda} \dot{\theta}^2 + \frac{D^2}{\sin^2 \theta} + \frac{\hbar}{2} \Omega \cos \theta = W, \quad (7)$$

where  $D^2$  is a constant. This bears a quantitative correspondence with the equation for a spherical pendulum of mass  $m$ , length  $l$ , and moment of inertia  $I = ml^2$ :

$$\frac{1}{2} I \dot{\theta}^2 + L^2 / 2I \sin^2 \theta + mgl \cos \theta = W. \quad (8)$$

This establishes the quantitative validity of the pendulum picture of the change with time of the atom's energy.

Similar considerations of super-radiance phenomena given in the previous analogy apply here.

### 3.4 The theorem of Feynman, Vernon and Hellwarth (1957)

Feynman et al propounded a theorem which establishes a rigorous analogy between the behaviour of any non-interacting two quantum-level systems subject to a perturbation, and the behaviour of spin 1/2 systems in a magnetic field (the systems do interact via the common radiation field, but are non-interacting in the sense that the spatial wavefunctions do not overlap). The Schrödinger equation is transformed to the formalism of a three-dimensional vector equation

$$\frac{d \underline{r}}{dt} = \underline{\omega} \wedge \underline{r} ,$$

where the components of  $\underline{r}$  uniquely determine the wavefunction  $\psi$  of the system, and the components of  $\underline{\omega}$  represent the perturbation. " $\underline{r}$ " space reduces to physical space when the magnetic interaction with a spin 1/2 system is considered. By this means the technique and formalism of the theoretical techniques of magnetic resonance may be brought to bear on problems of the behaviour of a pseudo-electric dipole moment in an abstract space. The precession model renders possible intuitive solutions of many problems.

Before considering the theorem it is worthwhile reviewing some aspects of the precession model.

(a) The magnetic precession model

The time variation of the expectation value of the magnetic moment of an atom is given by

$$\frac{d \langle \underline{\mu} \rangle}{dt} = \frac{i}{\hbar} \langle [\mathcal{H}, \underline{\mu}] \rangle$$

where  $\mathcal{H}$  is the Hamiltonian and  $\underline{\mu}$ , the magnetic moment operator, does not depend explicitly on time. This may be transformed (Yariv, 1967) into

$$\frac{d \langle \underline{\mu} \rangle}{dt} = \gamma \langle \underline{\mu} \rangle \wedge \underline{H}$$

where  $\underline{H}$  is the magnetic field and  $\gamma = g_J \beta / \hbar$  ( $g_J$  the "g factor",  $\beta = e\hbar/2mc$  is the Bohr magneton). Compare this with the classical equation of motion of a spinning magnetic moment  $\underline{\mu}$  having angular momentum  $\underline{J}$ :

$$\frac{d \underline{J}}{dt} = \text{torque} = \underline{\mu} \wedge \underline{H},$$

which for  $\underline{\mu} = \gamma \underline{J}$  becomes

$$\frac{d \underline{\mu}}{dt} = \gamma \underline{\mu} \wedge \underline{H}.$$

(In what follows the expectation value  $\langle \underline{\mu} \rangle$  is denoted simply by  $\underline{\mu}$ ).

Consider the behaviour of the magnetic moment  $\underline{\mu}$  in a static magnetic field  $\underline{H} = (0, 0, H_0)$ . The equation of motion

$$\frac{d \underline{\mu}}{dt} = \gamma \underline{\mu} \wedge \underline{H},$$

has the steady state solution

$$\begin{aligned}\mu_z &= \text{constant} = |\mu| \cos \theta, \\ \mu_x &= |\mu| \sin \theta \cos (\gamma H_0 t), \\ \mu_y &= -|\mu| \sin \theta \sin (\gamma H_0 t), \\ &= |\mu| \sin \theta \sin (|\gamma| H_0 t).\end{aligned}$$

This corresponds to a precession of  $\underline{\mu}$  about the  $+z$  direction at a radian rate  $\omega = |\gamma| H_0$  with an inclination angle  $\theta$  that depends upon the initial conditions (Figure 3.2(a)).

It can be seen that a time-varying magnetic field with transverse (x - y) components varying at a radian frequency  $\omega \sim \gamma H_0$  will "keep in step" with the precession of  $\underline{\mu}$  and exert a steady torque which will tilt the magnetization vector.

It is convenient to transfer to a rotating frame of reference in which the observer moves round  $H_0$  with the magnetic dipole at the precession frequency.

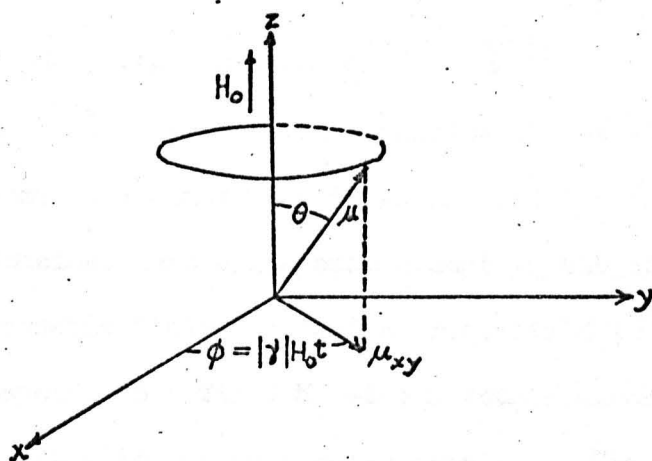
The equation of motion in the rotating frame is

$$\begin{aligned}\frac{\partial \underline{\mu}}{\partial t} &= \gamma \underline{\mu} \wedge \underline{H} - \underline{\omega} \wedge \underline{\mu} \\ &= \gamma \underline{\mu} \wedge \left( \underline{H} + \frac{\underline{\omega}}{\gamma} \right).\end{aligned}$$

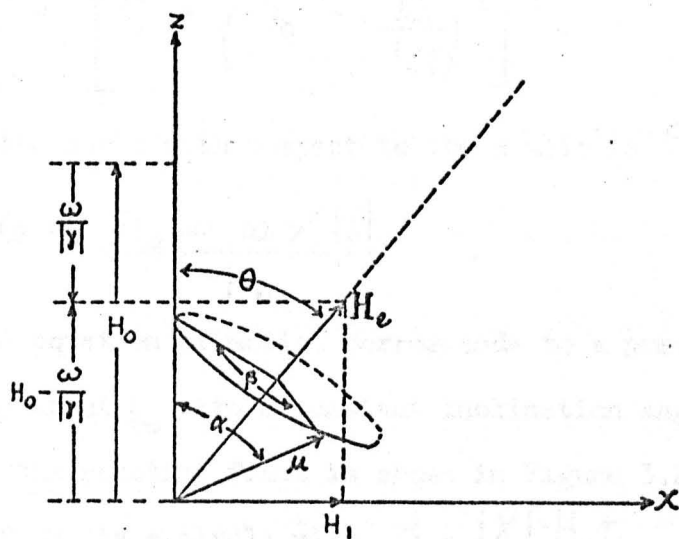
Thus it is possible to view the motion of  $\underline{\mu}$  in the rotating frame using the equation of motion with an effective magnetic field

$$\underline{H}_e = \underline{H} + \frac{\underline{\omega}}{\gamma}.$$

If the motion is one of precession about the steady magnetic



(a) precession of magnetization vector about a steady magnetic field



(b) the rotating coordinate system

Figure 3.2 Magnetic resonance (after Yariv, 1967)

field  $\underline{H} = \underline{k}H_0$ , then choosing  $\underline{\omega} = -\gamma \underline{H} = -\underline{k}\gamma H_0$ ,  $\underline{H}_e = 0$ , and so  $\partial \underline{\mu} / \partial t = 0$ . The magnetization as viewed in the rotating frame is a constant with an inclination  $\theta$  about the z axis.

Consider next a magnetic moment  $\underline{\mu}$  subjected simultaneously to a d.c. magnetic field  $\underline{k}H_0$  and an r.f. field  $\underline{i}H_1 \cos \omega t + \underline{j}H_1 \sin \omega t$  which corresponds to a field  $H_1$  with a counterclockwise (positive) circular polarisation at an angular rate  $\omega$ . The effective field in the rotating frame is then

$$\underline{H}_e = \underline{i}H_1 + \underline{k}\left(H_0 - \frac{\omega}{|\gamma|}\right)$$

which is time independent. It has the magnitude

$$H_e = \left[ H_1^2 + \left( H_0 - \frac{\omega}{|\gamma|} \right)^2 \right]^{\frac{1}{2}}$$

The inclination angle with respect to the z axis is  $\theta$  where

$$\cos \theta = \frac{H_0 - \omega / |\gamma|}{H_e}$$

The equation of motion corresponds to a precession at a rate  $|\gamma|H_e$  about  $\underline{H}_e$  with a constant inclination angle. The precession seen in the rotating frame is shown in Figure 3.2(b). The locus of the tip of  $\underline{\mu}$  is a circle with  $\beta = |\gamma|H_e t$ . For  $\underline{\mu}$  parallel to the z axis at  $t = 0$

$$\begin{aligned} \cos \alpha &= \cos^2 \theta + \sin^2 \theta \cos(|\gamma|H_e t), \\ &= 1 - 2 \sin^2 \theta \sin^2 \frac{1}{2}(|\gamma|H_e t), \end{aligned}$$

where  $\alpha$  is the instantaneous angle between  $\underline{\mu}$  and the z axis. The z component of the magnetization is

$$\langle \mu_z \rangle = (\mu_z)_{\max} \cos \alpha.$$

At resonance,  $\omega = \gamma H_0 = \omega_0$ ,  $H_e = H_1$ ,  $\theta = \pi/2$ ,

and the precession cone degenerates into a plane.

It is possible to remove the remaining time dependence by transforming to a doubly-rotating frame rotating about  $H_e$ .

$\partial \mu / \partial t = 0$  in this frame as long as  $H_e$  is constant.

(b) the geometrical representation of the Schrödinger Equation.

Feynman, Vernon and Hellwarth transform the Schrödinger equation in the following manner.

The wavefunction for an individual molecule is

$$\psi(t) = a(t) \psi_a + b(t) \psi_b.$$

$\psi_a$  and  $\psi_b$  are the two eigenstates of the Hamiltonian for the single system corresponding to the energies  $W + \hbar \omega_0/2$  and  $W - \hbar \omega_0/2$  respectively.  $W$  is the mean energy of the two levels determined by velocities and internal interactions.  $W$  is taken as the zero of energy for each system.  $\omega_0$  is the resonant angular frequency for the transition between the two levels.

A three dimensional vector  $\underline{r}$  is constructed with real components

$$r_1 \equiv ab^* + ba^*,$$

$$r_2 \equiv i(ab^* - ba^*),$$

$$r_3 \equiv aa^* - bb^*.$$

The time dependence is given by Schrödinger's equation

$$i \hbar \frac{da}{dt} = a \left[ (\hbar \omega_0 / 2) + V_{aa} \right] + b V_{ab},$$

and similar equations for the other coefficients. The matrix elements

$V_{aa} = V_{bb} = 0$  for the case of interest. Solution of the two sets of equations gives

$$\frac{d\mathbf{r}}{dt} = \underline{\omega} \wedge \mathbf{r}$$

where  $\underline{\omega}$  is a three-vector in  $\mathbf{r}$  space defined by three real components

$$\omega_1 \equiv (V_{ab} + V_{ba}) / \hbar,$$

$$\omega_2 \equiv i(V_{ab} - V_{ba}) / \hbar,$$

$$\omega_3 \equiv \omega_0.$$

The remaining real combination  $aa^* + bb^*$  is equal to the length of the  $\mathbf{r}$  vector, and is constant in time. It is equal to unity when  $\psi$  is normalised.

For transitions between the two levels of a spin  $1/2$  particle,  $\mathbf{r}$  space reduces to physical space with  $r_1, r_2$ , and  $r_3$  proportional to the expectation values of  $\mu_x, \mu_y$  and  $\mu_z$ , and  $\omega_1, \omega_2, \omega_3$  proportional to the components of the magnetic field  $H_x, H_y$ , and  $H_z$ .

Feynman et al analyse a beam maser oscillator in terms of their formalism. They consider a beam of molecules which enters a microwave cavity which is near resonance with a  $\Delta m = 0$  transition of the molecule. Only those molecules in the upper energy state enter the cavity. It is assumed that the cavity mode shape



permits the molecules to see an oscillating field of constant amplitude and phase.  $\omega_1$  is separated into two counter-rotating components in the 1-2 plane, and then the perturbation is viewed in the rotating frame in which the appropriate component of  $\omega_1$  appears stationary. The other component rotating at  $2\omega_1$  relative to the rotating frame is neglected. The rotating axes are designated the I, II and III axes. The I axis is taken in the plane of the stationary driving torque which has the constant components

$$\begin{aligned}\omega_I &= |\omega_1| / 2 \\ \omega_{II} &= 0 \\ \omega_{III} &= \omega_0 - \omega ,\end{aligned}$$

where  $\omega$  is the frequency of the perturbation. The molecules enter the cavity with  $\underline{r} = \underline{III}$  and at a time  $t$  later the components  $r_I$  and  $r_{II}$  are

$$\begin{aligned}r_I &= \frac{\omega_I (\omega_0 - \omega)}{\Omega^2} [1 - \cos(\Omega t)] , \\ r_{II} &= -\frac{\omega_I}{\Omega} \sin(\Omega t) .\end{aligned}$$

$\Omega$  is the magnitude  $[\omega_I^2 + (\omega_0 - \omega)^2]^{\frac{1}{2}}$  of the driving torque as seen in the rotating frame.

These results are transferred to the stationary frame by choosing the time reference so that

$$\omega_1 = 2 \omega_I \cos(\omega t) .$$

Then

$$r_1 = r(t) \cos[\omega t + \delta(t)]$$

where  $r(t)$  is the magnitude of the projection of  $\underline{r}$  on the 1-2 plane,

$$\delta(t) = \tan^{-1} r_{II} / r_I. \quad r_1 \text{ is represented by } (r_I + 2r_{II}).$$

Assuming a thin beam the complex polarization per unit length  $P_z$  is

$$(n/v)\mu_{ab} (r_I + ir_{II}). \quad n \text{ is the number of molecules entering}$$

the cavity per second, with a velocity  $v$ .

The electric field is written

$$\underline{E} = \underline{E}_c(x, y, z) \mathcal{E}(t) e^{i\omega t}$$

where  $\mathcal{E}$  is a real amplitude, constant in the steady state of oscillation, and  $\underline{E}_c$  describes the normal mode configuration. Then Maxwell's equations in complex form give

$$-\omega^2 [\mathcal{E} \underline{E}_c + (4\pi \underline{E}_c / |\underline{E}_c|) P] + i(\omega\omega_c/Q) \underline{E}_c \mathcal{E} + \omega_c^2 \underline{E}_c \mathcal{E} = 0.$$

$\omega_c$  is the resonant frequency of the cavity and  $Q$  is the quality factor of the cavity. Integrating this equation by  $\underline{E}_c$  over the cavity volume  $V$  gives in the case of a very thin beam

$$-\omega^2 [\mathcal{E} + (4\pi n/v)\mu_{ab} \int_0^L f V^{-1/2} (r_I + ir_{II}) dz] + i(\omega\omega_c/Q) \mathcal{E} + \omega_c^2 \mathcal{E} = 0,$$

where  $V$  is the volume of the cavity, and  $f$  is the cavity form factor.

The imaginary part of this equation gives  $\frac{n}{n_{th}} = \frac{\theta^2}{2(1-\cos \theta)}$ .

$$n_{th} \equiv \hbar V v^2 / 2\pi f^2 \mu_{ab}^2 L^2 Q$$

is the threshold number of molecules per second required to sustain oscillation.  $\theta$  is the total angle  $\Omega L / v$  through which each  $r$

precesses about the effective  $\omega$ . This determines the spread of frequency over which oscillations can occur.

The real part of the equation yields

$$\frac{\omega_0 - \omega}{\omega - \omega_c} = \frac{Q}{\pi Q_B} \frac{1 - \cos \theta}{1 - (\sin \theta)/\theta} \approx \frac{\omega_0 - \omega}{\omega_0 - \omega_c}$$

where  $Q_B \equiv 2\pi \omega_0 L/v \approx \omega_0 / \Delta \omega$

describes the natural molecular resonance linewidth. These are the results of Shimoda, Wang and Townes (1956).

It is seen that the analogue can yield quantitative results in agreement with results derived by other methods endowed with less transparency.

### 3.5 Two-level transition probabilities.

Consider the changing probability of a transition during a spin resonance experiment. The treatment given below follows that of Baym (1969).

Using a Schrödinger representation the spin state obeys the relation

$$i\hbar \frac{d}{dt} |\Psi(t)\rangle = -\frac{e\hbar}{2mc} \frac{g}{2} (H_0 \sigma_z + H_1 \cos \omega t \sigma_x) |\Psi(t)\rangle$$

$\sigma_z$  is the Pauli spin matrix.

The transformation to the rotating frame can be achieved without explicit calculation by writing

$$|\Psi(t)\rangle = e^{i\omega t \sigma_z / 2} |\Psi'(t)\rangle.$$

Substituting this into the above equation and multiplying on the left by  $e^{-i\omega\sigma_z t/2}$  gives

$$i \frac{d}{dt} |\Psi'(t)\rangle = \left[ \frac{\omega - \omega_0}{2} \sigma_z - \omega_1 \cos \omega t (e^{-i\omega\sigma_z t/2} \sigma_x e^{i\omega\sigma_z t/2}) \right] |\Psi'(t)\rangle,$$

where  $\omega_1 = g e H_1 / 4mc$ . The  $H_1$  field is a linear one of which only one rotating component is effective.

Now

$$\begin{aligned} & \cos \omega t (e^{-i\omega\sigma_z t/2} \sigma_x e^{i\omega\sigma_z t/2}), \\ &= \cos \omega t \sigma_x e^{i\omega\sigma_z t}, \\ &= \sigma_x (\cos^2 \omega t + i \sigma_z \cos \omega t \sin \omega t), \\ &= \frac{\sigma_x}{2} + \frac{1}{2} (\sigma_x \cos 2\omega t + \sigma_y \sin 2\omega t). \end{aligned}$$

The two high frequency terms result from the counter-rotation component of the r.f. field; they produce high frequency wiggles in  $|\Psi'(t)\rangle$  and may be neglected in considerations of the average motion of the spin. Thus

$$|\Psi'(t)\rangle = e^{-i\Omega t \hat{\sigma}/2} |\Psi'(0)\rangle,$$

where

$$\Omega = [(\omega - \omega_0)^2 + \omega_1^2]^{1/2}$$

and

$$\hat{\sigma} = \frac{\omega - \omega_0}{\Omega} \sigma_z - \frac{\omega_1}{\Omega} \sigma_x,$$

with

$$\hat{\sigma}^2 = 1.$$

Thus

$$|\Psi(t)\rangle = e^{i\omega t \sigma_z / 2} e^{-i\Omega t \hat{\sigma} / 2} |\Psi(0)\rangle.$$

This result may now be used to compute the transition probabilities.

Suppose that the initial state of the spin is along  $z$ :

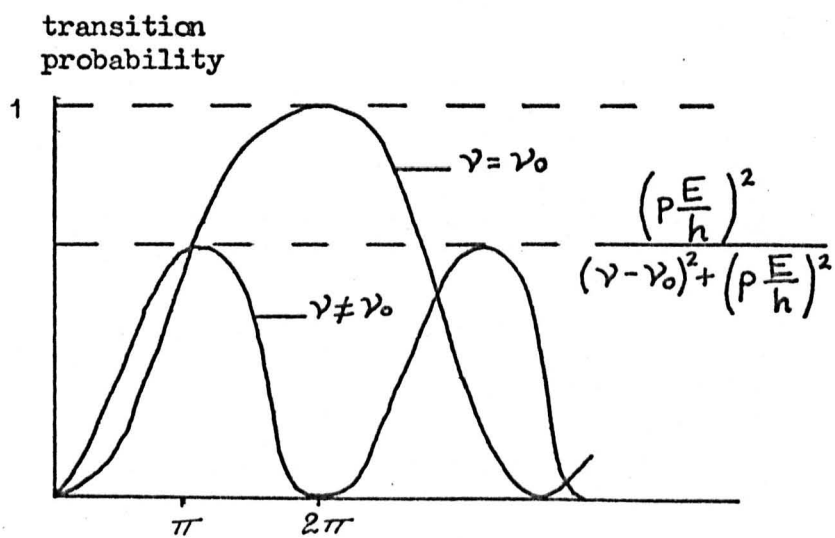


Figure 3.3 Transition probabilities

$$|\bar{\Psi}(0)\rangle = |z \uparrow\rangle.$$

The amplitude for the spin having flipped over to the state  $|z \downarrow\rangle$  at time  $t$  is then

$$\begin{aligned} \langle z \downarrow | \bar{\Psi}(t) \rangle &= e^{-i\omega t/2} \langle z \downarrow | \left( \cos \frac{\Omega t}{2} - i\hat{\sigma} \sin \frac{\Omega t}{2} \right) | z \uparrow \rangle \\ &= -ie^{-i\omega t/2} \langle z \downarrow | \hat{\sigma} | z \uparrow \rangle \sin \frac{\Omega t}{2}, \end{aligned}$$

and the probability that the spin has flipped by time  $t$  is

$$\begin{aligned} P_{\downarrow}(t) &= |\langle z \downarrow | \bar{\Psi}(t) \rangle|^2 \\ &= \frac{\omega_1^2}{2\Omega^2} (1 - \cos \Omega t). \end{aligned}$$

The maximum value of  $P_{\downarrow}(t)$  is

$$\frac{\omega_1^2}{\Omega^2} = \frac{\omega_1^2}{(\omega - \omega_0)^2 + \omega_1^2}$$

and occurs after a  $\pi$  pulse, i.e.  $\Omega t = \pi$ .

The dependence is shown in Figure 3.3. For  $\omega - \omega_0 \gg \omega_1$ , this maximum probability is very small, but for resonance,  $\omega = \omega_0$ , the maximum probability is unity; the spin has flipped with certainty.

### 3.6 Transient aspects of two-level behaviour

In this section a number of transient effects are considered.

Most were originally observed in magnetic dipole systems, but some have recently been produced in electric-dipole, laser systems.

#### (a) "wiggles"

Figure 2.9(b) displays the electric dipole analogue of the well known magnetic resonance "wiggles". They arise when the

system is excited into a superposition state by means of a rapid sweep in frequency through the molecular resonance. The coherent emission from the system beats with the receding stimulating signal. The different forms the wiggles may assume are discussed by Andrew (1958).

The sweep must occur in a time short compared with  $T_1$ ,  $T_2$  and  $(\gamma \delta H_0)^{-1}$ , where  $\delta H_0$  is the inhomogeneity of the steady field  $H_0$  over the specimen. The beats have the form

$$(\exp - t/T_2) \cos (1/2 \gamma \dot{H}_0 t^2),$$

and so their persistence is a measure of the degree of phase coherence permitted by relaxation processes.

The electric dipole analogue has been observed in molecular beams in emission (Lainé, 1966), and absorption (Lainé and Kakati, 1969). Recently Lainé et al (1969) have shown that the effect may be obtained in the bulk gas and used to measure relaxation times. It is interesting to note that an accurate measurement is precluded in the case of  $N^{14}H_3$ , because the sweep signal causes excitation of the quadrupole lines during the decay time of the main line polarisation. The coupling of the two lines via common energy levels is manifested as a perturbation upon the decaying wiggles.

#### (b) oscillation transient

Singer and Wang (1961) have shown that, in general, an amplitude modulation of the output of a maser oscillator will be observed, provided that the rate at which excited atoms is supplied

does not much exceed the depopulation rate due to coherent emission.

The outline of their analysis is reproduced below.

They consider a two-level system with level separation  $\hbar \omega_0$ . The two eigenstates are  $u_2$  (upper) and  $u_1$  (lower) with time dependent probability coefficients  $a_2(t)$  and  $a_1(t)$ . The population difference is  $N_e$ .

The coherent induced radiation rate of the excited molecules (neglecting collisional relaxation processes and spontaneous emission) is given by

$$\frac{d}{dt} \left[ \hbar \omega_0 N_e |a_2(t)|^2 \right].$$

For resonance, the values of  $a_1$  and  $a_2$  are

$$|a_1(t)|^2 = \sin^2 \left( \int_0^t \frac{p E_1(t)}{\hbar} dt \right)$$

$$|a_2(t)|^2 = \cos^2 \left( \int_0^t \frac{p E_1(t)}{\hbar} dt \right),$$

where  $E_1$  is the oscillating electric field, and  $p$  is the effective dipole moment (suitably averaged over all directions - a factor of  $1/3$ ). The integral takes into account the variation of  $E_1$  with the emission.

Next consider the equation describing the growth and decay of the radiation field. The change in stored energy is

$$\frac{d}{dt} \left[ \frac{\epsilon E_1^2}{4\pi} \right] + \frac{\omega_0 \epsilon E_1^2}{4\pi \times 2Q},$$



where  $Q$  is the quality factor of the cavity. The exchange of energy between the molecules and the radiation is described by the equation,

$$\frac{d}{dt} (E_1^2) + \frac{\omega_0 E_1^2}{2Q} = 4\pi N_e F h \nu_0 \frac{d}{dt} \left[ \cos^2 \left( \int_0^t \frac{p E_1(t)}{\hbar} dt \right) \right]$$

$F$  is a filling factor for the cavity. For an ammonia maser, which is excited and then allowed to radiate  $N_e$  is assumed to be constant. For pumped masers an additional term must be added.

The solution of this non-linear equation gives the line shape of the emitted radiation. An approximate result of the solution is that the oscillation amplitude will be modulated at a frequency

$$\omega_1 \sim \left( \frac{p}{\hbar} \right) (F N_e h \nu_0)^{1/2} \sim \frac{p E_1}{\hbar}.$$

The results of Singer and Wang can be interpreted in a simple fashion.  $\omega_1$  is the angular frequency at which particles oscillate between the two levels, alternately emitting and absorbing radiation. In other words, the modulation frequency is a measure of the rate at which energy is transferred back and forth between the molecules and the field. The mechanism of the process may be viewed in the following manner (Uspenskii, 1963).

When the number of particles in the cavity is sufficiently large, the energy output is greater than the energy losses and the total energy in the cavity increases. This, in turn, increases the probability of downward transitions, and thus results in an even

greater increase in the field. In this process, however, the number of particles decreases and finally the energy gained becomes equal to or even less than the energy lost. The cavity now contains a field and a proportion of the particles at the lower energy level. The energy in the field can either be absorbed by the walls of the cavity, or it may leave the cavity, or it may contribute to raising some of the particles to the higher level. For a high  $Q$  cavity and a long transit time, this latter process has the greatest probability of the three. Thus in a large field the particles will be raised to the higher energy level, and the field will decrease. This corresponds to the trailing edge of the pulse (which may be superimposed on a constant level of oscillation). The cycle is then repeated.

Uspenskii derives a non-linear equation from the equation for the conservation of energy and shows that the onset of the pulsations occurs for the condition

$$\left( \frac{\mu E}{\hbar} \right)^2 > \frac{\omega_0}{4 Q} \cdot \frac{1}{\tau}$$

On the basis of this condition one would not expect an ammonia maser to exhibit such behaviour spontaneously.

Basov et al (1966) have studied the conditions for pulsations in masers and lasers. They show that it is possible to excite oscillations of the radiation intensity below the condition for self-sustained pulsations if the number of active particles entering the

resonator is modulated periodically. They argue that for typical parameters of an ammonia maser a  $Q$  of about 25-30,000 is required, with a 10% modulation. This is for a period of  $5 \cdot 10^{-4}$  seconds. The interval between pulses is  $4 \cdot 10^{-4}$  seconds and the duration of each pulse is  $0.9 \cdot 10^{-4}$  seconds.

Grasyuk and Oraevskii (1964) attempted to induce the amplitude and phase transient in an ammonia beam maser by applying a high voltage pulse to the state focuser. The effect failed to materialise, and they reported that they believed the result was vitiated because the establishment time for the beam of active molecules may have been of the order of the transit time through the focuser and resonator.

The effect has been verified for the atomic hydrogen beam maser (Nikitin and Strakhovskii, 1966, and Audoin, 1966). Conditions in the hydrogen maser are somewhat more favourable than those for the ammonia maser: switching of the discharge that supplies the atomic beam can be achieved in a time very short compared with the time of storage in the bulb ( $\sim 1$  second), also  $Q$  multipliers can be employed.

It has recently been proved possible to induce such a transient in the ammonia beam maser (Lainé and Bardo, 1969). The method of switching does not involve modulation of the number of the particles in the beam; it is better regarded as a kind of "molecular  $Q$  switch". A slight variation of the method has yielded an induced

spiking for a restricted period.

In parenthesis it is interesting to compare the condition for the oscillatory approach to the steady state of oscillation given by Grasyuk and Oraevskii, with that given by Combrisson (1964) for the magnetic dipole case.

For the ammonia maser, Grasyuk and Oraevskii derive the condition (for exact resonance)

$$b > 9/8$$

where b is the excitation parameter defined in Chapter II.

Combrisson gives the condition

$$\frac{Q}{Q_0} > 1 + \frac{1}{8} \frac{T_2}{T_1}$$

for a damped oscillation and with a time constant  $2T_1$  and a frequency

$$\Omega = \frac{1}{2\sqrt{T_1 T_2}} \sqrt{\frac{8Q}{Q_0} - 8 - \frac{T_2}{T_1}} .$$

$Q_0$  is the threshold value of Q for steady state oscillations.  $T_2$  and  $T_1$  are normally regarded as equal in magnitude for the ammonia beam maser.

### (c) Echoes

The observation of the electric dipole analogue of the spin echo in ruby was reported in 1964 by Kurnit, Abella, and Hartmann.

It is interesting to note their analysis.

They consider a volume small compared to  $\lambda^3$ . The

Hamiltonian for each of the two-level systems is written as

$$\mathcal{H} = -\underline{p} \cdot \underline{\mathcal{E}},$$

where the pseudo-dipole moment is defined by

$$\underline{p} = \sqrt{2} P (R_1 \hat{x} + R_2 \hat{y} + R_3 \hat{z}),$$

and a pseudo-electric field is defined as

$$\underline{\mathcal{E}} = [E_x \hat{x} + E_y \hat{y} - (\hbar \Omega / \sqrt{2} P) \hat{z}].$$

Only excitations of the form  $E_x = E \cos(\Omega t + \Theta)$ ,

$E_y = E \sin(\Omega t + \Theta)$  cause transitions.

The operators  $R$  are those defined by Dicke (Chapter I).

$P$  is given by  $|\langle + | \underline{p} | - \rangle|$ , where  $\underline{p}$  is the electric dipole moment operator.  $\Omega$  is the frequency separation of the two-level system. Only the transverse components of  $\underline{p}$  represent the actual dipole moment.  $\underline{p}$  behaves in an analogous fashion with a magnetic dipole moment, thus,

$$\frac{d\langle \underline{p} \rangle}{dt} = \gamma \langle \underline{p} \rangle \wedge \underline{\mathcal{E}},$$

which follows from the quantum mechanical formulation,

$$\langle \underline{p} \rangle = \text{trace } \rho \underline{p}, \quad \frac{d\rho}{dt} = \frac{-i}{\hbar} [\mathcal{H}, \rho],$$

together with the definitions of  $\mathcal{H}$  and  $\underline{p}$ . The analogue of Bloch's equation is reached by adding the phenomenological relaxation terms,

$$\begin{aligned} \frac{d\langle \underline{p} \rangle}{dt} = & \gamma \langle \underline{p} \rangle \wedge \underline{\mathcal{E}} - \frac{\langle p_x \rangle \hat{x} + \langle p_y \rangle \hat{y}}{T_2} \\ & - \frac{\langle p_z \rangle - \langle p_z \rangle_0}{T_1} \hat{z}. \end{aligned}$$

To explain the formation of the echo it is considered that the resonance line is inhomogeneously broadened, and this is taken into account by writing

$$\frac{d}{dt} \langle p \rangle_j = \gamma \langle p \rangle_j \wedge \underline{E}_j,$$

which in turn implies that  $\Omega$  varies from place to place. The analysis is simplified by transforming to the rotating frame,

$$\rho = e^{-i \Omega R_3 t} \rho^* e^{+i \Omega R_3 t},$$

so that the equation of motion becomes

$$\frac{d}{dt} \langle p \rangle_j^* = \gamma \langle p \rangle_j^* \wedge \underline{E}_j^*,$$

where  $\langle p \rangle^* = \text{trace } p \rho^*$ ,

$$\underline{E}_j^* = \left( \frac{\hbar}{\sqrt{2} \rho} \right) (\Omega_j - \Omega) \hat{z} + E \cos \theta \hat{x} + E \sin \theta \hat{y}.$$

$$\frac{d\rho^*}{dt} = - \left( \frac{i}{\hbar} \right) [\mathcal{H}^*, \rho^*],$$

$$\mathcal{H}^* = - \sum_j p_j \cdot \underline{E}_j^*.$$

The Hamiltonian is now time independent. The pseudo-dipole moment just precesses about the static effective field  $\underline{E}_j^*$ .

At time  $t = 0$  all the atoms are in the ground state so  $\langle p \rangle^*$  points along the  $-\hat{z}$  axis. This state is equivalent to that given by the density matrix

$$\rho^* = \prod_j (1/2 - R_{j3}).$$

When the excitation pulse is applied the fields are intense,

$$\text{i.e. } E \gg \left( \frac{\hbar}{\sqrt{2} P} \right) (\Omega_j - \Omega),$$

and therefore in the rotating frame  $\langle p \rangle$  just precesses about

$$E_1 = E(\cos \theta \hat{x} + \sin \theta \hat{y})$$

at the frequency  $\gamma E$ .

The excitation pulse is applied for a time  $\tau$ , where

$$\gamma E_1 \tau = \pi/2, \text{ so that } \langle p \rangle^* \text{ is rotated into the } x\text{-}y \text{ plane.}$$

Once the excitation pulse is over, the effective field is in the  $\hat{z}$  direction and varies from site to site. The individual  $\langle p \rangle_j^*$  vectors begin to fan out in the  $x\text{-}y$  plane. The macroscopic transverse electric dipole moment formed immediately after the first pulse is rapidly dephased. A second excitation pulse is applied a little later. This pulse is twice as intense as the first, and causes a rotation of  $\pi$  about the effective field. Once the excitation pulse is turned off, the vectors rotate about the effective field given by

$$\underline{E}_j^* = (\hbar/\sqrt{2} P)(\Omega_j - \Omega).$$

This precession is in the same sense as before the excitation pulse,

and so the  $\langle \underline{p} \rangle_j^*$  vectors come back into phase in just the same time that it took them to dephase.

The latitude of timing permitted for the excitation pulses is governed by the  $T_1$  and  $T_2$  relaxation times. The loss of coherence occurs in a time  $\sim T_2^*$  and is reversible: it occurs as a result of inhomogeneous broadening. There are also irreversible processes with relaxation times  $T_1$  and  $T_2$  governing the decay of the longitudinal (population) and the transverse (polarisation) components of the dipole moment.

Oraevskii (1967) has proposed that echoes could be observed in a molecular beam maser. The dephasing and rephasing occurs as a result of Doppler broadening. The inverse Doppler width of the line ( $T_2^*$ ) is much less than  $T_1$  (the time of flight through the resonator).

Oraevskii proposes the use of a  $E_{0lm}$  mode in a cylindrical resonator. The Doppler width of the line is then of the order of  $\pi (V / L)_m$ , where  $L$  is the length of the resonator,  $V$  is the mean speed of the molecules, and  $m$  is the number of half-waves along the resonator. Since the time of flight is  $L / V$  the condition on relaxation time becomes,  $\pi m \gg 1$ .  $m$  must also be odd because the resonator is poorly excited by the molecular beam for even  $m$  (Klimontovich and Khoklov, 1957).

The inhomogeneity could also be furnished by a small magnetic or electric field.



Echoes have been observed (Jenkins and Wagner, 1968) in gaseous ammonia contained in a waveguide cell (that is, the initial state is a thermal one). The gas was excited by pulses of  $0.1\mu$  second duration and peak power levels of  $\sim 100\text{mw}$ . The echo corresponded to the  $J = 3, K = 3$  inversion transition at 24 GHz. The echo formation depended upon the inhomogeneity provided by Doppler broadening.

(d) The transient nutation effect

The electric dipole analogue of the magnetic resonance effect has recently been seen (Hocker and Tang, 1968) by illuminating gaseous  $\text{SF}_6$  with a pulse from a Q-switched  $\text{CO}_2$  laser. The effect shows up in the form of a damped amplitude modulation near the leading edge of the light pulse.

The physical explanation of the effect is that the intense coherent light pulse can successively drive the molecules between the two levels, through  $\pi/2, \pi, 3\pi/2, 2\pi$  positions and so on until the cycle is damped by relaxation processes to a steady state corresponding to absorption by a partially saturated system. The process produces a sinusoidal modulation of the population and coherent polarisation. The oscillation in the population difference reacts on the field and amplitude modulates the light wave.

The effect is described as transient nutation because the precession of the transition dipoles about the field in the rotating frame appears in the laboratory frame as the slow nutation (modulation)

superimposed on the rapid oscillation of the coherent polarisation at the transition frequency.

It should be noted that the oscillation transient corresponds to a transient nutation; one which is self driven, and not initiated by an external pulse of illumination.

Macomber (1968) has pointed out that the Fourier transform of a saturated slow passage spectrum is the transient nutation signal. He proposes that separate fields be employed for the saturation and slow passage.

#### (e) Other analogues

Another phenomenon of interest is that of self-induced transparency in gases (McCall and Hahn, 1967) in which a pulse propagates without absorption. This may be termed a  $2\pi$  pulse.

Lefrère (1969) has recently observed some transients, notably "wiggles", in an optically pumped system.

#### 3.7 The detuning effect observed with cascaded cavities

Higa (1957) was the first to conduct an experiment on an ammonia beam maser with cascaded cavities through which the beam passes in succession. The two cavities are coupled only by the beam; microwave leakage from one to another is prevented by fitting each cavity with end-caps of a diameter below cut-off for the mode.

It was found that if (a) the second cavity is tuned near to the molecular resonance and there is sufficient flux to permit it

to oscillate, but (b) the first cavity is detuned so far that it will not support oscillation, then the frequency of the oscillation in the second cavity is governed by the usual "pulling factor" appropriate to that cavity. However, if the first cavity is successively tuned closer to the molecular resonance it will at some stage break into oscillation. An amplitude modulation of the oscillation is then perceived for a time in the second cavity. With a little more change of tuning these "Higa beats" cease. It is then found that the frequency of oscillation in the second cavity follows precisely that of the first. It is determined by the "molecular ringing" from the first cavity. In this mode of operation it is observed that the intensity of the oscillation in the second cavity displays a series of maxima and minima with change in detuning. (Strakhovskii and Tatarenkov, 1962, and Laine and Srivastava 1963) These "S - T" curves are symmetrical about the molecular resonance frequency  $\omega_0$ , if the second cavity is tuned to  $\omega_0$  (and if the matching for the first cavity is constant - Smith and Laine, 1968). A series of such curves are reproduced in Figure 3.4 (a) and (b) (Laine and Smith, 1966).

For low flux of active molecules it is found that the second cavity will not oscillate independently of the first.

These successive effects have been interpreted as indicating that the "ringing" signal from the first cavity at first beats with the oscillation of the second cavity to produce the Higa beats (regions

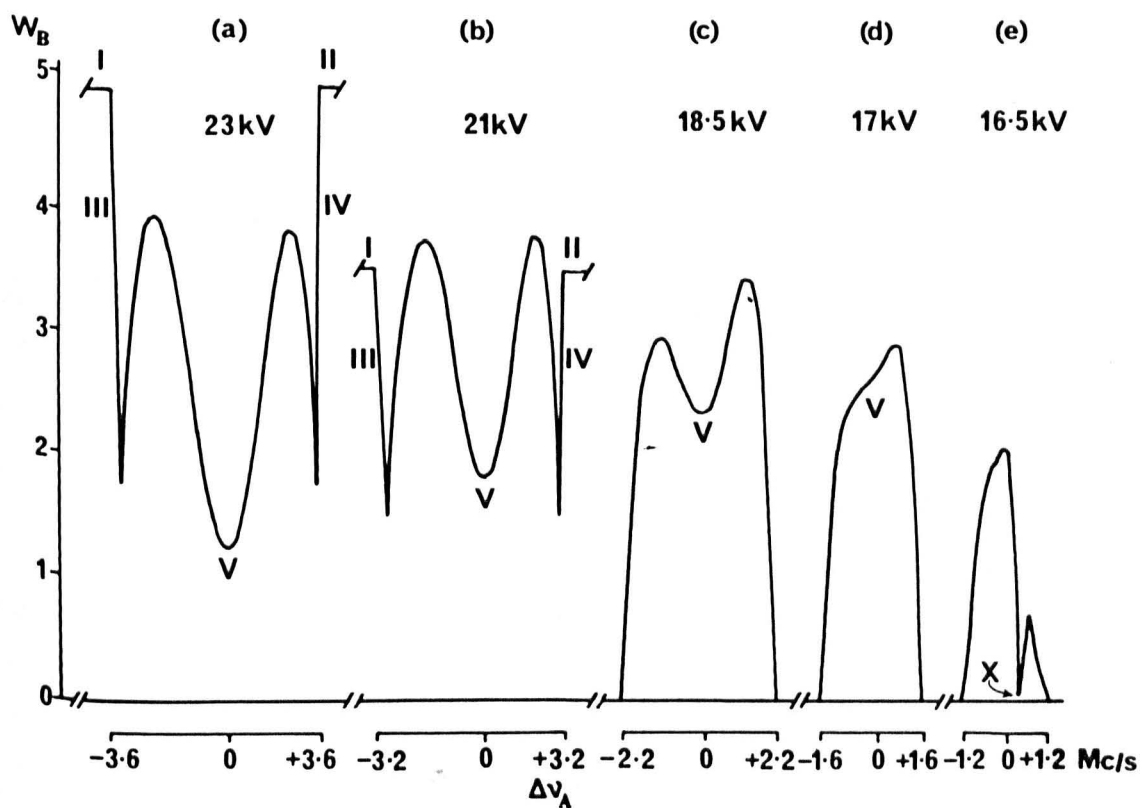


Figure 3.4 Detuning curves (after Lainé and Smith, 1966)

III and IV in Figure 3.4). But then with less detuning the first cavity dominates the second and the polarisation impressed upon the beam by the first cavity synchronizes the oscillation of the second (region V). For conditions where the second cavity would not oscillate independently of the first, the phase-locked conditions give way to one in which the second cavity is solely dependent upon the coherent excitation from the first.

A number of theoretical explanations have been proffered to explain the shape of the S - T curves. However, none has provided a convincing explanation of the shape exhibited in the various S - T curves. Basov et al (1964) were able to show that the frequency of excitation in the second cavity should be that of the first cavity, and that for zero detuning of the first cavity and a large electric field amplitude, the radiation intensity could become zero. Spectroscopic examination of the beam in the second cavity revealed it to be strongly absorbing (Basov et al, 1963).

Basov et al (1964) used a semiclassical approach in which a classical field was assumed to arise from a polarisation of the beam which was calculated quantum mechanically. In contrast Li Tie-Cheng and Fang Li-Zhi (1964) adopted a more rigorous approach in which the radiation field was quantized. They employed a perturbation treatment due to Senitzky (1958). Their treatment predicted sectors in the frequency detuning which would permit oscillation, and others that

would not sustain oscillation. This sectional behaviour was argued to be in qualitative agreement with the double maximum S - T curves. They were not able to offer an explanation for the single maximum curves seen at low focuser voltages.

A more recent explanation offered by Basov, Oraevskii and Uspenskii (1967) attempts to explain the gap in the S - T curves at zero detuning in terms of interference effects arising from emission by molecules moving with different velocities and radiating fields with different phases.

It is interesting to note that Wells (1958) gave an explanation of the Higa beats in terms of the orbits described by the  $\mathbf{r}$  vectors in a Feynman diagram.

It has recently proved possible to offer a reasonably cogent explanation for much of two cavity behaviour. The reasoning was based on the consideration that in passing through the first cavity the molecules experience a pulse of radiation (Laine 1966). The polarisation imparted to the beam depends upon the magnitude of the pulse, which in turn depends upon the electric field within the cavity. It is well known that the ringing signal is a maximum for multiples of  $\pi/2$  (Bloem 1956, Smith and Laine, 1968). As the first cavity is detuned then the pulse received by the molecules diminishes. Since the behaviour of the second cavity is governed by the ringing from the first, it should prove possible to derive, at least qualitatively,

the form of the S - T curves from considerations of the transition probabilities appropriate to the two cavities. A simple quantum-mechanical derivation is reproduced below. Acting on this idea Krause (1968) independently produced an equivalent treatment in a different form of simple quantum mechanics. However, the treatment given here is more general and the assumptions made for simplifying the equations may be more obvious. Moreover, Krause did not consider pulses greater than  $\pi$  (which correspond to the S - T curves already observed). It is shown in Chapter IV that it is possible to extend the treatment to the case of pulses greater than  $\pi$  (corresponding to absorption of radiation by molecules during part of their transit through a resonator). It is seen that it is possible to devise a modified Feynman diagram appropriate to the electric dipole case, from which S - T curves corresponding to various levels of excitation may be constructed. By this means S - T curves having shapes not seen previously are predicted. A spectroscopic examination of the beam permits an approximate scale in terms of focuser voltage to be assigned to the Feynman graph. This latter diagram is obtained by transforming into a rotating frame for which the phase is chosen so that the motion of the pseudo-dipole vector occurs in one plane.

The maser described in Chapter II is shown to be capable of providing an approximately  $2\pi$  pulse. An S - T curve having the form of one of the predicted S - T curves has been obtained.

The quantum mechanical treatment for the two-cavity detuning effect is given in a matrix formulation employing spinors. The initial formulation is similar to that given by Kukolich (1965) for the two cavity problem of the resonance pattern produced by a Ramsey separated fields configuration. In formulating the problem relaxation processes are ignored.

A superposition state for the two level system is given as a linear combination of the upper and lower state eigenfunctions  $u_a$  and  $u_b$

where 
$$\psi = a u_a + b u_b ,$$

and 
$$aa^* + bb^* = 1.$$

$\psi$  is written as a spinor  $\begin{pmatrix} a \\ b \end{pmatrix}$  in analogy with the magnetic spin 1/2 system.

The Hamiltonian for the system when no external fields are present is

and 
$$\mathcal{H}_0 = \frac{1}{2} (\hbar \omega_0) \sigma_z$$

$$\psi^* \mathcal{H}_0 \psi = \frac{1}{2} (\hbar \omega_0) (a^* a - b^* b);$$

$\hbar \omega_0$  is the energy separation between the levels, and  $\sigma_z$  is a Pauli spin matrix. The r.f. field provided by the auto-oscillation in the first cavity administers a pulse described by

$$V_I = \begin{pmatrix} 0 & \frac{1}{2} (\hbar \omega_1) e^{-i\omega t} \\ \frac{1}{2} (\hbar \omega_1) e^{i\omega t} & 0 \end{pmatrix} ,$$



and the Schrödinger equation

$$i \hbar (\partial / \partial t) \psi = \mathcal{H} \psi$$

is

$$i \frac{\partial}{\partial t} \begin{pmatrix} a \\ b \end{pmatrix} = \begin{pmatrix} 1/2 \omega_0 & 1/2 \omega_1 e^{-i\omega t} \\ 1/2 \omega_1 e^{i\omega t} & -1/2 \omega_0 \end{pmatrix} \begin{pmatrix} a \\ b \end{pmatrix}$$

where  $\hbar \omega_1 = \mu_{ab} E_1$ ,  $\mu_{ab}$  is the dipole matrix element connecting the two states, and  $E_1$  is the magnitude of the r.f. field,

$$(\mu_{aa} = \mu_{bb} = 0).$$

Making the substitution

$$\begin{pmatrix} a \\ b \end{pmatrix} = \begin{pmatrix} a' e^{-i(\omega/2)t} \\ b' e^{i(\omega/2)t} \end{pmatrix},$$

the Schrödinger equation becomes

$$i \frac{\partial}{\partial t} \begin{pmatrix} a' \\ b' \end{pmatrix} = \begin{pmatrix} 1/2 (\omega_0 - \omega) & 1/2 \omega_1 \\ 1/2 \omega_1 & -1/2 (\omega_0 - \omega) \end{pmatrix} \begin{pmatrix} a' \\ b' \end{pmatrix}.$$

Kukolich writes the solution

$$\begin{pmatrix} a'(t) \\ b'(t) \end{pmatrix} = \Omega \begin{pmatrix} a(0) \\ b(0) \end{pmatrix}$$

$$= \begin{pmatrix} \cos \alpha t - i \left( \frac{\omega_0 - \omega}{2\alpha} \right) \sin \alpha t & -i \left( \frac{\omega_1}{2\alpha} \right) \sin \alpha t \\ -i \left( \frac{\omega_1}{2\alpha} \right) \sin \alpha t & \cos \alpha t + i \left( \frac{\omega_0 - \omega}{2\alpha} \right) \sin \alpha t \end{pmatrix} \begin{pmatrix} a(0) \\ b(0) \end{pmatrix},$$

where  $\alpha^2 = (1/2 (\omega_0 - \omega))^2 + (1/2 \omega_1)^2$ .

The state of the beam entering the first cavity is  $\psi_0 = \begin{pmatrix} 1 \\ 0 \end{pmatrix}$ .

The state produced by an r.f. field on for a time  $\tau$  is (a uni-velocity beam is assumed)

$$\begin{pmatrix} a' \\ b' \end{pmatrix} = \begin{pmatrix} \cos \alpha \tau - i \left( \frac{\omega_0 - \omega}{2\alpha} \right) \sin \alpha \tau & -i \frac{\omega_1}{2\alpha} \sin \alpha \tau \\ -i \frac{\omega_1}{2\alpha} \sin \alpha \tau & \cos \alpha \tau + i \left( \frac{\omega_0 - \omega}{2\alpha} \right) \sin \alpha \tau \end{pmatrix} \begin{pmatrix} a(0) \\ b(0) \end{pmatrix}.$$

The average energy is

$$\begin{aligned} E_1 &= \frac{1}{2} (\hbar \omega_0) \langle \sigma_z \rangle, \\ &= \frac{1}{2} (\hbar \omega_0) (a^* a - b^* b). \end{aligned}$$

and the oscillating polarisation is

$$\rho = \rho_0 \langle \sigma_x \rangle = \rho_0 (a^* b + b^* a).$$

In the region between the cavities the r.f. fields are very small, and the matrix is

$$\Omega_S = \begin{pmatrix} e^{-i \frac{1}{2} (\omega_0 - \omega) T} & 0 \\ 0 & e^{i \frac{1}{2} (\omega_0 - \omega) T} \end{pmatrix},$$

corresponding to free precession, where T is the time spent by the molecules in the region between the cavities.

The final wavefunction, after the molecules have passed through the two-cavity system, is

$$\begin{pmatrix} a' \\ b' \end{pmatrix}_2 = \Omega_2 \Omega_S \Omega_1 \begin{pmatrix} a(0) \\ b(0) \end{pmatrix},$$

where  $\Omega_1$  represents the effect of the first cavity,  $\Omega_S$  the drift-space, and  $\Omega_2$  the effect of the second cavity.

For  $\omega$  close to  $\omega_0$

$$\cos \alpha \tau - i \left( (\omega_0 - \omega) / 2\alpha \right) \sin \alpha \tau \quad \text{becomes} \quad \cos \frac{1}{2} \omega_1 \tau$$

and

$$-i (\omega_1 / 2\alpha) \sin \alpha \tau \quad \text{becomes} \quad -i \sin \frac{1}{2} (\omega_1 \tau).$$

Since the phase within the pulse envelope is not important for the present considerations the drift-space matrix may be taken as the unit matrix. Therefore,

$$\begin{pmatrix} a' \\ b' \end{pmatrix}_2 = \Omega_2 \Omega_S \Omega_1 \begin{pmatrix} a(0) \\ b(0) \end{pmatrix} = \Omega_2 \begin{pmatrix} 1 & 0 \\ 0 & 1 \end{pmatrix} \Omega_1 \begin{pmatrix} a(0) \\ b(0) \end{pmatrix}$$

$$= \begin{pmatrix} \cos \frac{1}{2} \omega_2 \tau_2 & -i \sin \frac{1}{2} \omega_2 \tau_2 \\ -i \sin \frac{1}{2} \omega_2 \tau_2 & \cos \frac{1}{2} \omega_2 \tau_2 \end{pmatrix} \begin{pmatrix} \cos \frac{1}{2} \omega_1 \tau_1 & -i \sin \frac{1}{2} \omega_1 \tau_1 \\ -i \sin \frac{1}{2} \omega_1 \tau_1 & \cos \frac{1}{2} \omega_1 \tau_1 \end{pmatrix} \begin{pmatrix} a(0) \\ b(0) \end{pmatrix}$$

Now,  $\begin{pmatrix} a(0) \\ b(0) \end{pmatrix} = \begin{pmatrix} 1 \\ 0 \end{pmatrix}$ , since the focuser defocuses lower state molecules.

The probability of a transition occurring in cavity 2 from the state  $u_a$  to state  $u_b$  is given by  $bb^*(\tau_1 + \tau_2)$ .

Performing the matrix multiplication gives

$$b'_{(\tau_1 + \tau_2)} = -i \left[ \sin \frac{1}{2} (\omega_1 \tau_1 + \omega_2 \tau_2) \right],$$

and so (neglecting the phase factor)

$$bb^*_{(\tau_1 + \tau_2)} = \sin^2 \frac{1}{2} (\omega_1 \tau_1 + \omega_2 \tau_2).$$

Usually  $\tau_1 \sim \tau_2$  and the field in cavity 2 is about an order of magnitude smaller than the field in cavity 1, so that

$$\omega_1 = \frac{\mu E_1}{\hbar} \gg \omega_2 = \frac{\mu E_2}{\hbar},$$

and  $\omega_2 \tau_2$  may be neglected; in other words, it may be assumed that the molecules experience a negligible pulse in the second cavity.

The field in cavity 2 is given by

$$E_2 = C_1 [bb^*_{(\tau_1 + \tau_2)}]^{1/2}$$

where  $C_1$  is a constant.

The assumption that  $\omega \sim \omega_0$  can be justified if it is noted that the frequency of oscillation in cavity 1 is governed

by the frequency "pulling factor"

$$\omega_1 - \omega_0 = \frac{Q_{c1}}{Q_M} (\omega_{c1} - \omega_0) f(n),$$

where  $\omega_1$  is the angular frequency of the oscillation in cavity 1,

$\omega_{c1}$  is the resonant frequency of cavity 1,  $Q_{c1}$  is its loaded quality factor,  $Q_M$  is the  $Q$  of the molecular resonance defined by

$$Q_M = \frac{\omega_M}{2\Delta\omega_M} = \frac{\omega_M}{0.89} \cdot \frac{L}{v};$$

$L$  is the length of the cavity, and  $v$  the velocity of the molecules.

$f(n)$  is a complex function of beam flux and amplitude of oscillation,

and is approximately unity. For typical values of these parameters

it is found that a detuning of the cavity by several MHz pulls the

oscillation only a few kHz. The spectral line may be regarded as

flat over this small range of frequencies, and the variation in  $E_1$

with the detuning can be obtained by multiplying the magnitude  $E_{01}$

at  $\omega_0$  with a normalized factor which determines the shape of the

detuning characteristic of the oscillation amplitude in cavity 1.

For a semi-elliptical detuning characteristic (Jaynes and Cummings, 1963)

$$E_2 = C_1 \sin \left( C_2 E_{01} \tau_1 \sqrt{1 - \frac{\beta^2}{\beta_m^2}} \right)$$

where  $C_2 = \frac{\mu}{\hbar}$ ,  $\beta = (\omega_{c1} - \omega_0 / \omega_0)$  is

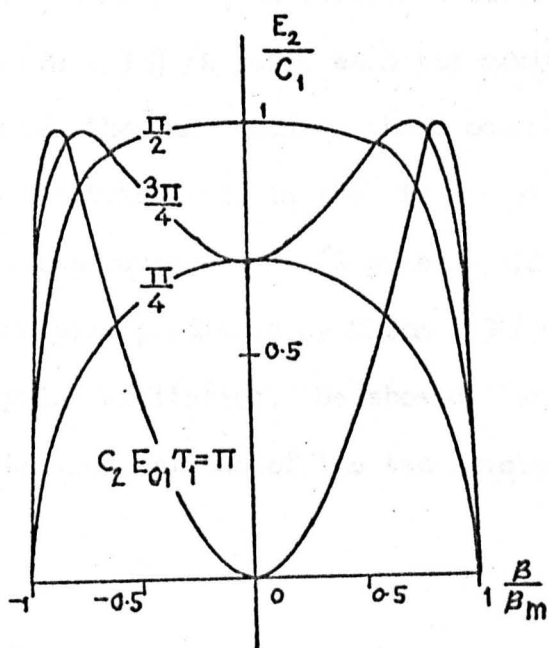
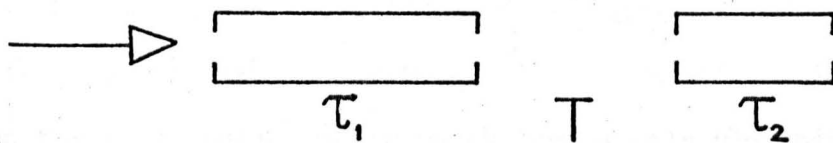


Figure 3.5 Theoretical detuning curves

the detuning of cavity 1, and  $\beta_m$  is the maximum detuning.

Figure 3.5 shows these results graphed for various pulses (up to  $\pi$ ) received in cavity 1. The maximum field in cavity 1 is given for a  $\pi$  pulse, which means that a molecule which enters cavity 1 in state  $u_a$  emerges in state  $u_b$ . Then  $E_2 = 0$ . In all other cases, the molecules emerge from cavity 1 in a mixed energy state. The maxima  $E_2 / C_1$  in the diagram correspond to the situation where the molecules receive a  $\pi/2$  pulse in the first cavity. For example, if the molecules receive a  $3\pi/4$  pulse when the cavity is tuned to the molecular resonance, then on detuning there occurs a point where the magnitude of the electric field in the first cavity drops to the level where the molecules receive a  $\pi/2$  pulse. This is, of course, related to the delayed peak predicted by Bloem (1956) for molecular ringing following a pulse excitation. He showed that the peak occurred at the instant when the populations of the two levels become equal.

## REFERENCES

- Dehmelt, H. G. (1968), Am. J. Phys. 36, 910-11.
- Eberly, J. H. (1968), Phys. Lett. 26A, 499-500.
- Feynman, R. P., Vernon, F. L. and Hellwarth, R. W. (1957), J. App. Phys., 28, 49-52.
- Yariv, A. (1967), Quantum Electronics, New York, Wiley.
- Shimoda, K., Wang, T. C. and Townes, C. H. (1956) Phys. Rev. 102, 1308.
- Baym, G. (1969), Lectures on Quantum Mechanics, New York, Benjamin, Inc.
- Andrew, E. R. (1958), Nuclear Magnetic Resonance, Cambridge University Press.
- Lainé, D. C. (1966), Phys. Lett. 23, 557.
- Lainé, D. C., Kakati, D. (1969), J. Phys. B (Atom. Molec. Phys.) Ser 2, 2, 152.
- Lainé, D. C., Kakati, D., Uppal, G. S., Smart, G. D. S., Bardo, W. S. (1969), Phys. Lett. 29A, 376-7.
- Singer, J. R., Wang, S. (1961), Phys. Rev. Lett. 6, 351-4.
- Uspenskii, A. V. (1963), Radio Engng. Electron. Phys. 8, 1145-8.
- Basov, N. G., Morosov, V. N., Oraevskii, A. N. (1966), I.E.E.E.J.Q.E. QE-2, 542-8. (report of 1966 Quantum Electronics Conference).
- Grasyuk, A. Z., Oraevskii, A. N. (1964), Radio Eng. Electron. Phys. 9, 424-8 and 443-6.
- Nikitin, A. I., Strakhovskii, G. M. (1966) Radio Eng. Electron. Phys. 11, 1650-3.



Audoin, C. (1966), C.R. Acad. Sci., 263, 542-5.

Combrisson, J. (1964), Quantum Electronics I, Paris, Dunod, and New York, Columbia.

Kurnit, N. A., Abella, I. D., Hartmann, S. K. (1964) Phys. Rev. Lett. 13, 567.

Oraevskii, A. N. (1967), Sov Phys. J.E.T.P. 10, 45-51.

Klimontovich, Yu. L., Kokhlov, R. V. (1957), Sov. Phys. J.E.T.P. 5, 937.

Jenkins, J. L., Wagner, P. E. (1968) Appl. Phys. Lett. 13, 308-9.

Hocker, G. B., Tang, C. L. (1968), Phys. Rev. Lett. 21, No. 9.

Macomber, J. D. (1968), Appl. Phys. Lett. 13, 5-6.

McCall, S. L., Hahn, E. L. (1967), Phys. Rev. Lett. 18, 908-11.

Lefrere, P., (1969), M.Sc. Quantum Electronics, Project Report.

Higa, W. H., (1957) Rev. Sci. Instr. 28, 726.

Strakhovskii, G. M., Tatarenkov, V. M., (1962), Sov. Phys. J.E.T.P. 15, 625.

Lainé, D. C., Srivastava, R. C. (1963) J. Brit. I.R.E., 26, 173-180.

Smith, A. L. S., Lainé, D. C. (1968), Brit. J. Appl. Phys. (J. Phys. D.) Ser. 2, 1, 727-732.

Lainé, D. C., Smith, A. L. S. (1966), Phys. Lett. 20, 374-6.

Basov, N. G., Oraevskii, A. N., Strakhovskii, G. M., Tatarenkov, V. M., (1964), Sov. Phys. J.E.T.P. 18, 1211, and Quantum Electronics III, (Paris, Dunod), 377.

Basov. et al (1963), as above.

Li Tie-Cheng, Fang Li-Zhi (1964), Acta Phys. Sinica, 20, 753-60.

Senitzky, I. R. (1958), Phys. Rev. 111, 3.

Basov, N. G., Oraevskii, A. N., Uspenskii, A. V. (1967), Optics and Spectroscopy, 23, 504.

Wells, W. H. (1958), J. App. Phys. 29, 714-7.

Lainé, D. C. (1966), Proc. Phys. Soc. 87, 855-7

Bloom, S. (1956), J. App. Phys. 27, 785-8.

Krause, W. H. U. (1968) Phys. Lett. 28A, 380-1.

Kukolich, S. G. (1965) Phys. Rev. 138, A1322-5.

## CHAPTER IV

### THE EXPERIMENTAL INVESTIGATION OF TRANSIENT EFFECTS.

#### 4.1 The oscillation transient

##### (a) Quenching with an injected signal

In Chapter II it was described how the detection technique may be used to inject a stimulating signal into the maser cavity. Since the klystron is frequency modulated the stimulating signal sweeps across the molecular resonance. This probing signal permits operation of the maser as a sensitive spectrometer below oscillation threshold (Gordon, 1955). It may also be used for spectroscopy when the maser is oscillating (Shimoda and Wang, 1955). A reduction in the oscillation amplitude at the main line frequency is seen when the signal is swept across the quadrupole satellite frequencies. The quadrupole transitions occur between energy levels which are involved in the main line transitions, and the change in populations of these energy levels induced by the probing signal is reflected by a reduction in the main line oscillation amplitude. Shimoda and Wang report that it is possible to quench the oscillation by excitation at the quadrupole frequency.

This mode of quenching by population depletion involves excitation and detection of quenching at two quite different frequencies. It is also possible to quench the oscillation by injection of a signal within the linewidth of the maser signal

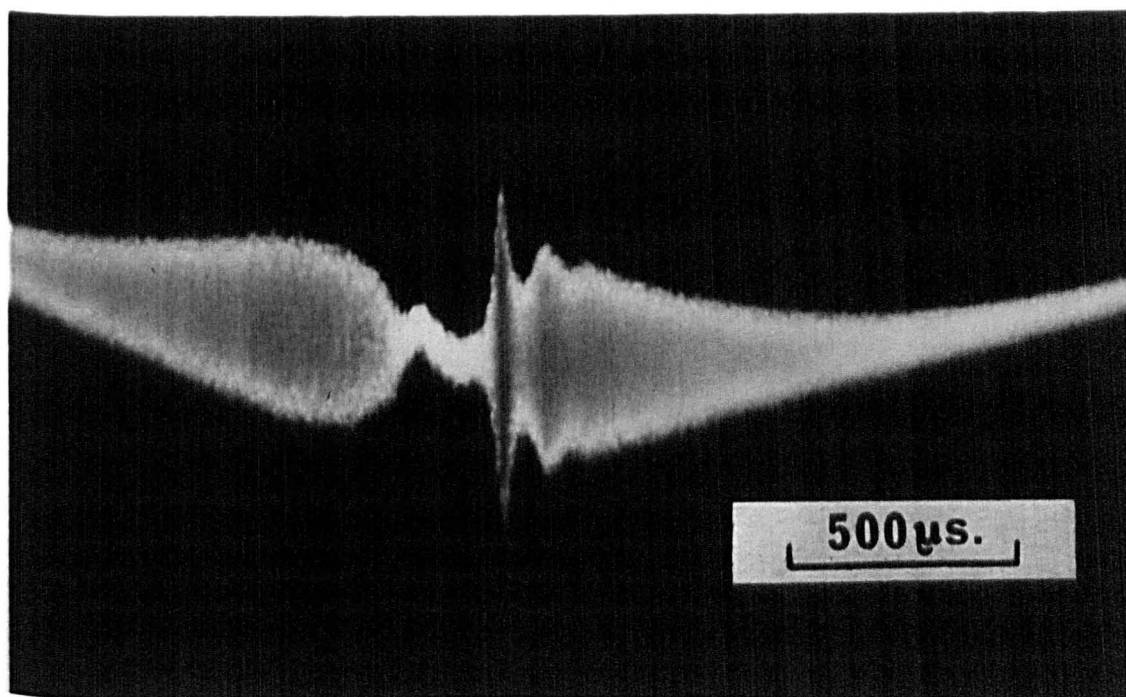


Figure 4.1 Oscillation transient following quenching

(Lainé, 1967). At low levels of the injected signal,  $\nu_s$ , its presence is registered by the changing beat frequency it produces with the maser oscillation, passing through a zero frequency beat when it is momentarily at the maser frequency, Figure 2.9(c). At a higher level, the oscillation is quenched when  $\nu_s$  is close to the molecular resonance frequency, and a stimulated emission signal appears in place of the zero frequency beat. As the probing signal recedes from the maser oscillation frequency the oscillation appears again and approaches its steady state amplitude, as evidenced by the amplitude of the beat signal in Figure 4.1. At low beam intensities the approach to the steady state is monotonic, but for an intense beam the approach has the damped oscillatory character seen in Figure 4.1 (it should be noted that the changing beat frequency amplitude is subject to amplifier bandpass restrictions).

Evidently the use of an injected signal affords an efficient method of fast switching of the maser oscillation. It was remarked in Chapter III that the attempt by Grasyuk and Oraevskii to switch a molecular beam, by the application of a high-voltage pulse to the focuser, failed probably because of the relatively long time required for the establishment of the active beam of upper state molecules, the subsequent smearing effect due to the velocity distribution, and finally the time required for penetration into the cavity. The success of the present method is attributable, in large part,

to the fact that the molecules are perturbed within the cavity, where they are all coupled to a common radiation field, and where the effects of the finite magnitude of the velocity and its distribution are minimised.

The transient was first observed as a slight overshoot like that seen on the right hand side of Figure 4.4C. This occurred within the cavity referred to as cavity 2 (Chapter II) which has a  $Q$  of about 6,000. From the theoretical considerations of Chapter III it is seen that the transient should be more pronounced if the  $Q$  is increased. Accordingly cavity 1 was fabricated, with a small coupling hole in order to retain as high a value of loaded  $Q$  as possible, commensurate with a reasonable signal to noise ratio for the oscillation. It is also possible to argue that "the effect is not prominent in the ammonia maser" (to quote Singer and Wang, 1961) because the excited molecules are usually supplied at a greater rate than the depopulation rate due to coherent induced emission. It would seem that conditions favouring the transient can be approached by increasing the depopulation rate and simultaneously decreasing the rate of supply of the molecules. However, decreasing the number of molecules flowing into the cavity would decrease the depopulation rate. The two factors appear to be immutably opposed. The problem is better viewed in another way. The frequency of the amplitude modulation of the transient is linearly related to the

field in the cavity,

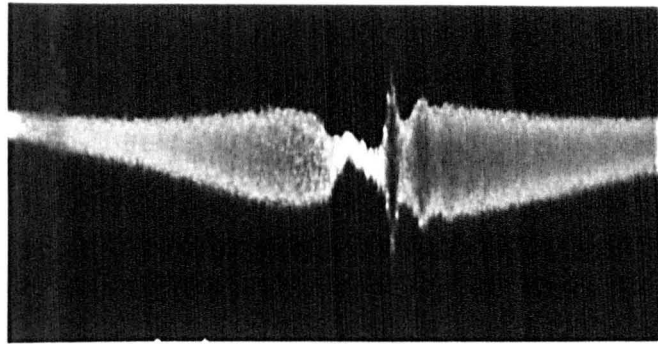
$$\omega_1 \sim \frac{\mu E_1}{\hbar} .$$

Normally the radiation energy density in the cavity is too low for the effect to be seen, since the period of amplitude modulation is greater than the mean time of flight of the molecules. The period of modulation may be decreased by increasing the electric field; this by such measures as increasing the Q of the cavity, and increasing the intensity of the beam. The mean time of flight of the molecules can be increased by cooling the beam. It was seen that this latter course also augments the beam intensity by increasing the population of the 3,3 inversion levels, thus increasing the field in the cavity. Here is the justification for the cooled beam. Figure 4.1 shows the transient obtained with cavity 1 (12.4cm. long,  $Q \sim 9,000$ ), and a beam cooled to 170°K, at a pressure of 2.8torr behind the nozzle (0.1cm. channel) and with a focuser voltage of 55kV. Since the velocity varies as the square root of the absolute temperature the expected increase in transit time resulting from cooling of the nozzle is a factor of about 1.3. The mean velocity is about  $3 \times 10^4$  cm. sec.<sup>-1</sup> at room temperature (Jaynes and Cummings, 1963) corresponding to a transit time of about 0.4msec. This would be increased to about 0.5ms. for the cooled beam.

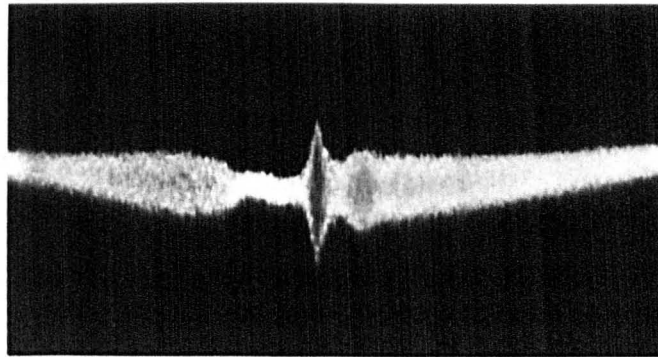
The frequency of the modulation seen in the photograph Figure 4.1 is estimated to be 9.5kHz. The signal to noise ratio presently obtainable does not permit a reliable calculation of relaxation times (coupled with the errors in correction for band-pass effects). Figures 4.2(a) and 4.2(b) show the change in the transient period and amplitude for the change in focuser voltage from 55kV. down to 20kV. The decrease in the modulation frequency with decreasing focuser voltage can be clearly seen. Figure 4.2(c) shows the incipient transient produced under conditions of operation without liquid nitrogen pumping and the necessarily much reduced beam flux.

There is an interesting feature of the appearance of the transient. The stimulated emission peak is followed by a ringing signal appearing as a changing beat frequency. Normally the microwave bridge is set so that the oscillation grows from that ringing signal and is seen to be locked to it on the oscilloscope presentation of frequency (time) variation. If, however, the conditions are such that the beat signal decreases to below the level of thermal noise before the onset of the oscillation, the starting time of the oscillation is observed to "jitter" on the trace. Presumably the oscillation is then initiated by noise and the point of time at which this occurs varies slightly between the successive 50Hz. repetitive sweeps.

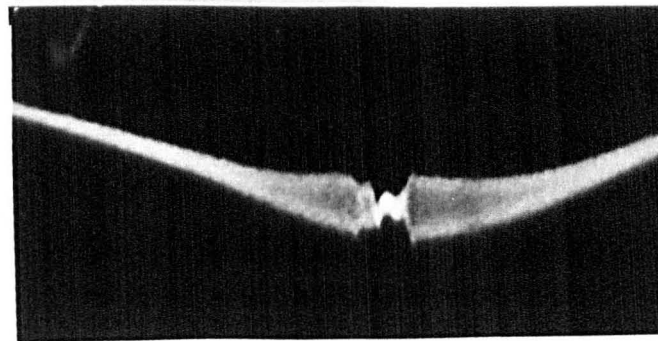




(a) 55kV



(b) 20kV



(c) without liquid nitrogen

Figure 4.2 Oscillation transient

(b) The transient that follows Stark switching

It was indicated in the last section that it was considered that much of the efficiency of the method of switching derived from the circumstance that a beam parameter was varied during the passage of molecules through the cavity. It seemed worthwhile investigating this proposition by attempting another method of switching in the cavity: that of quenching the oscillation by applying a square wave pulse to a metal probe projecting into the cavity, in the path of the beam. The application of a pulse of electric field means that the molecules suddenly experience a region of inhomogeneous field, causing a degree of Stark splitting and spreading of the spectral line. This then may be termed "molecular Q switching", though it should be noted that the previous method involved molecular Q switching, in that the line is spread by saturation during the signal injection.

The probe is shown in Figure 4.3. It consists of silver wire 0.51mm. in diameter, partly sheathed in a glass tube, and mounted through a nylon screw. The assembly is mounted in a tapped hole in the wall of the cavity, which terminates in a 1mm. diameter hole into the cavity. The glass sheath projects just into the cavity and the probe extends across two-thirds of the cavity diameter. The probe is mounted opposite the coupling hole and exerts a considerable tuning effect.

Figures 4.4(a) to (i) display the change in transient as

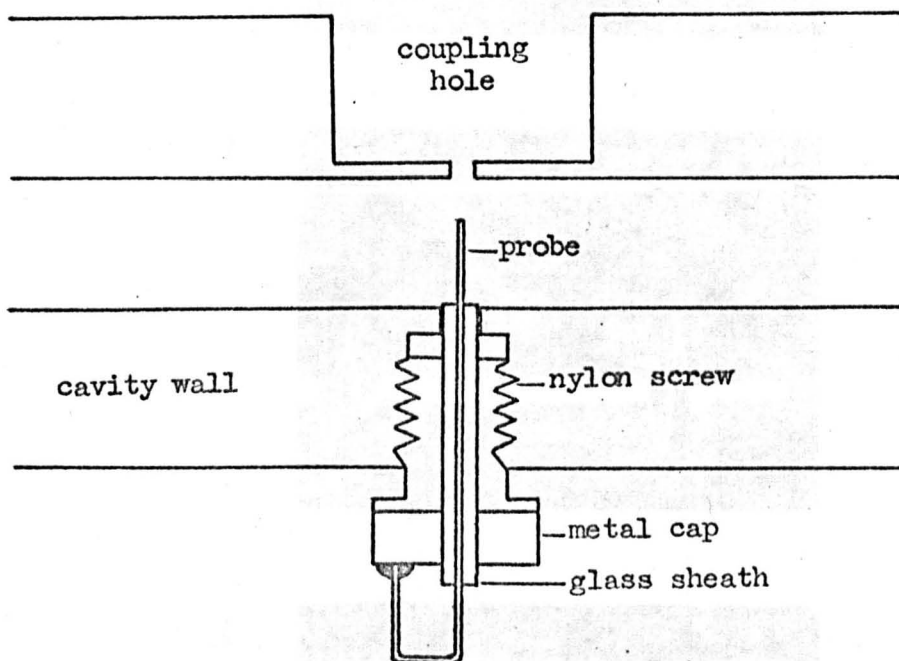


Figure 4.3. The probe mounted in the cavity.

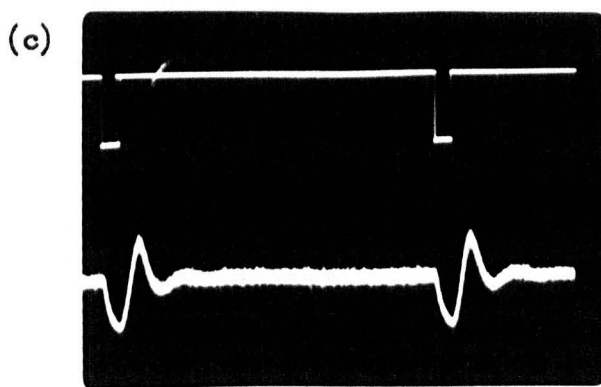
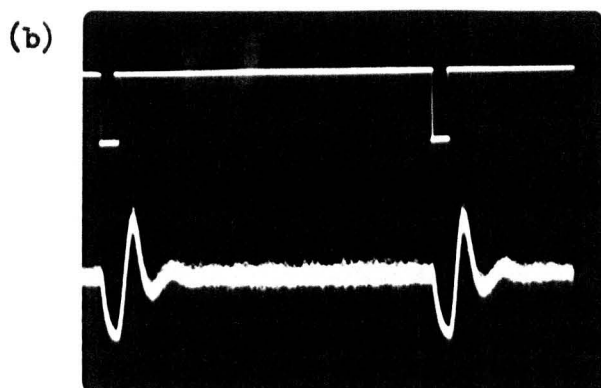
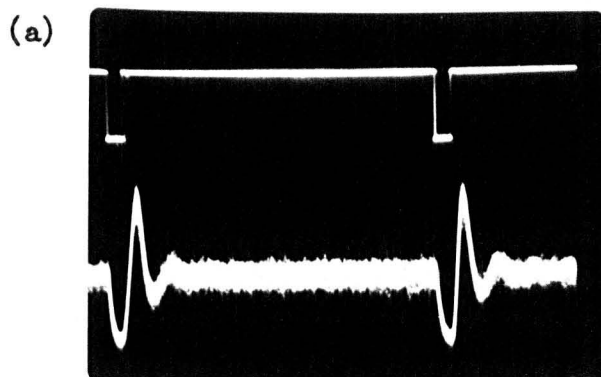


Figure 4.4 Transient following Stark switching

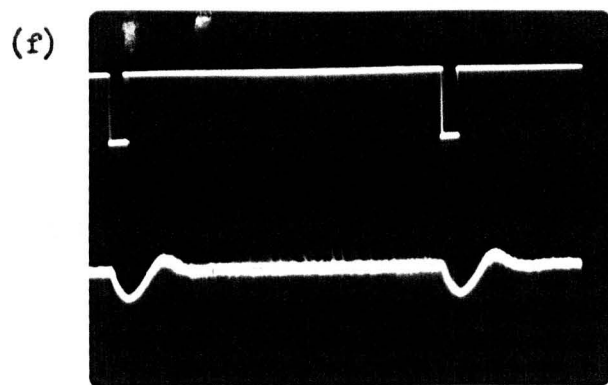
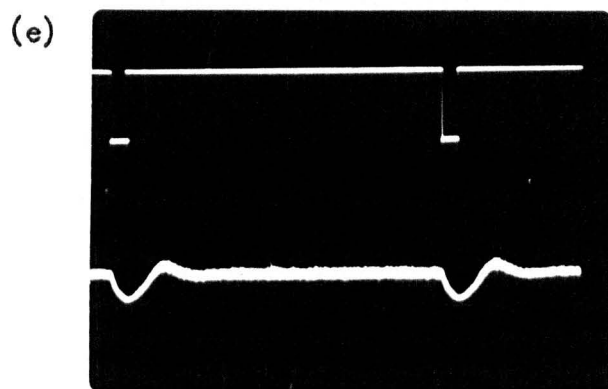
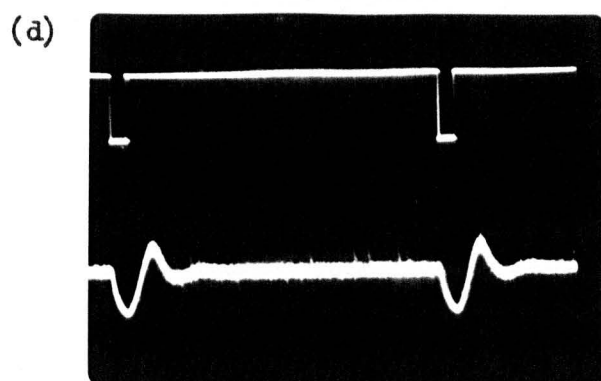


Figure 4.4

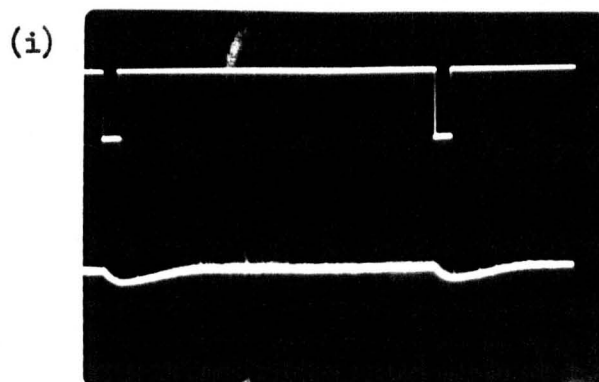
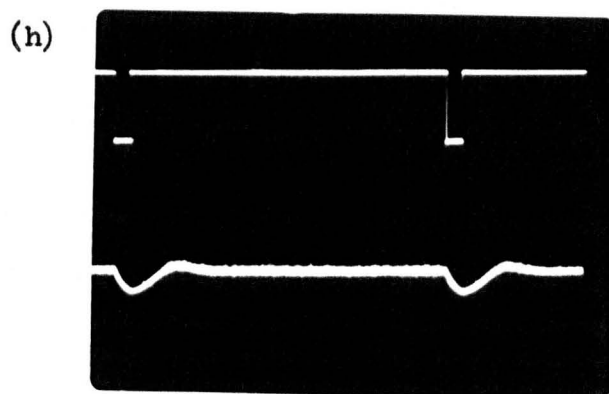
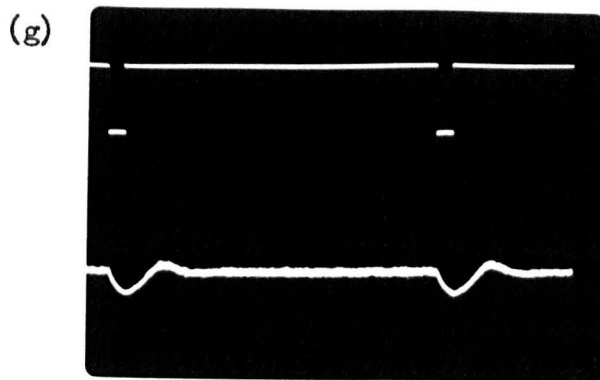


Figure 4.4

the focuser is varied through the respective focuser voltages; 50, 40, 30, 27.5, 25, 22, 21, 20 and 18kV. (for a beam pressure of 2.3 torr behind the nozzle). The pulse has an amplitude of 100volts, a width of 50  $\mu$ seconds and a pulse repetition frequency of 1kHz. The change in the frequency of modulation is clearly seen. However, with the present signal to noise ratio the determination of the frequency from the photograph is subject to a large error derived from the thickness of the traces. Figure 4.5 shows the variation of the modulation frequency with focuser voltage, replete with possible errors. The change from an oscillatory character to an aperiodic one is seen to occur at about 25kV.

It was not possible to quench the oscillation completely using this probe. The quenching resulted in a change of about 40% in the level of oscillation. This is not surprising since the region of inhomogeneous field is a very small one. In consequence the photographs depict not one transient, but the composite of two - a switching-off transient, and a switching-on transient. Following the leading edge of the applied pulse there is a switching-off transient as the oscillation level drops to a lower level; then following the trailing edge there is a switching-on transient as the oscillation is restored to its former high level. For this reason the results cannot, in their present form, yield values of rise time, and other parameters. Figure 4.6(a) shows an expanded trace of the

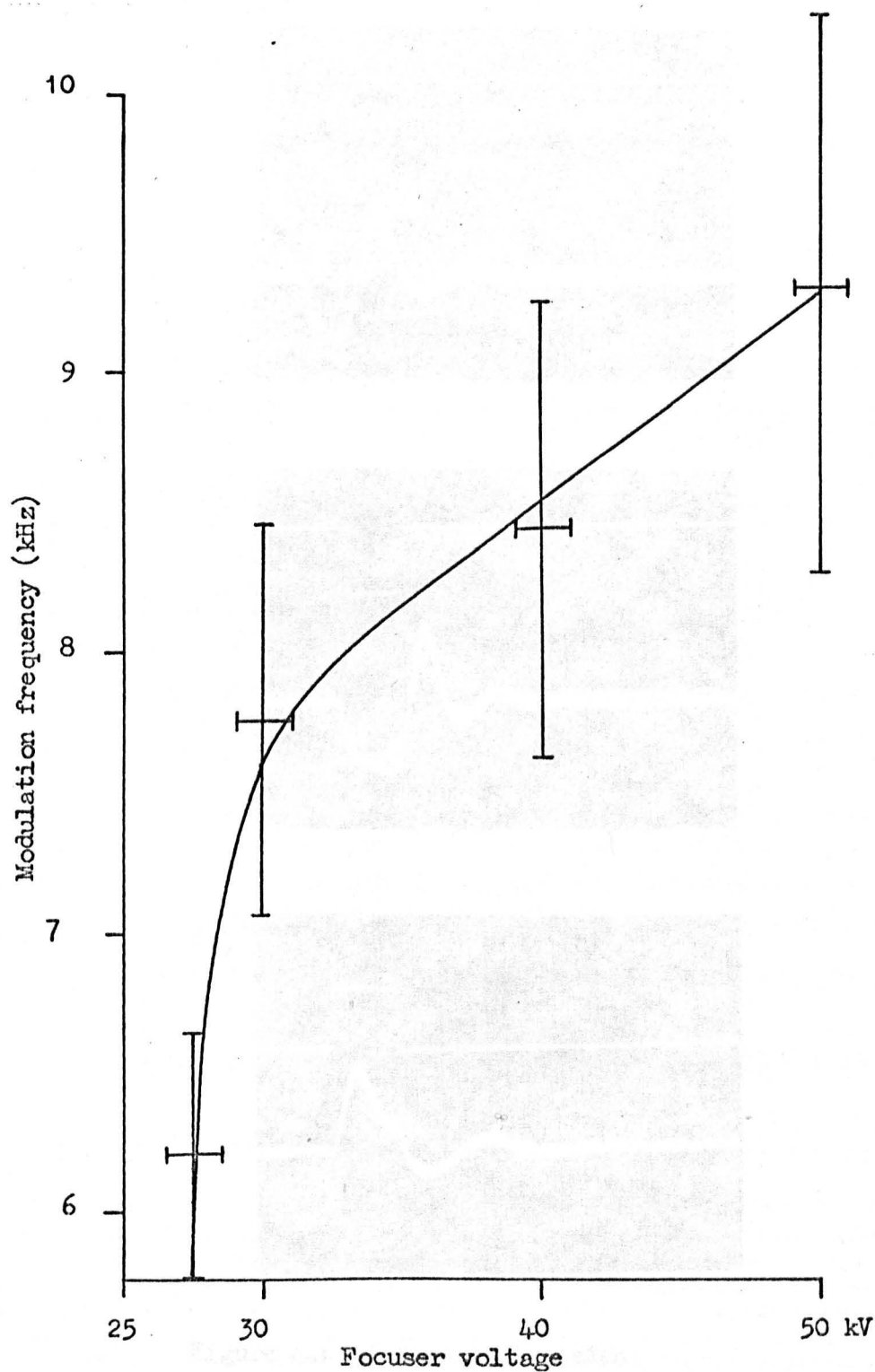


Figure 4.5. The variation of transient modulation frequency with focuser voltage.



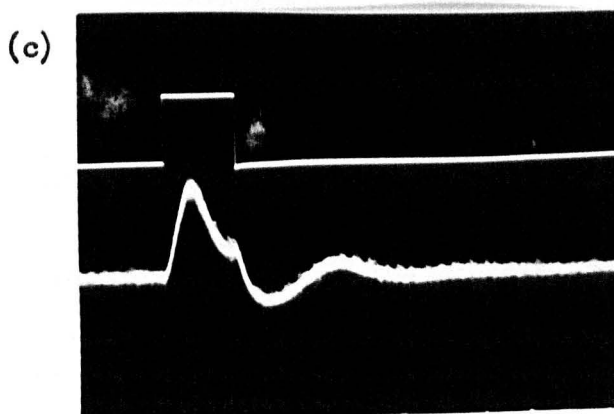
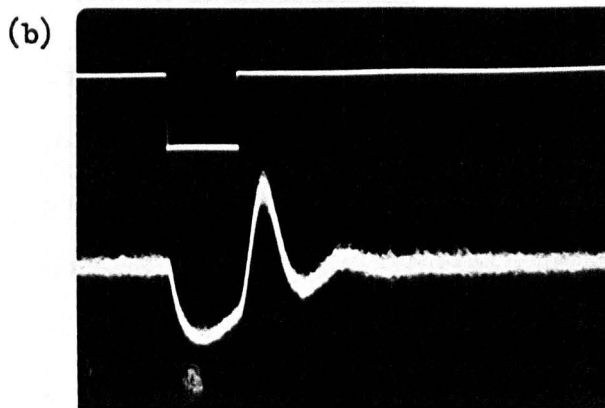
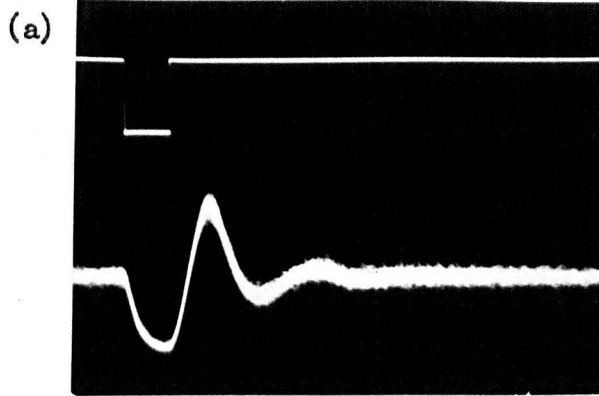


Figure 4.6 Composite transient

phenomenon. Figures 4.6(b) and (c) in which a  $100\mu$ second pulse is applied, display the effect even better; the discontinuity between the two transients is clearly visible. The effect has also been verified by coalescing two pulses of the maximum width,  $100\mu$ seconds, to yield a pulse of  $200\mu$ seconds duration, whereupon further development of each transient is visible (not illustrated here). Since the transients have a duration of about  $300\mu$ seconds it has not been possible to separate the two. Complete quenching of the oscillation would permit reliable measurements to be made of relaxation and rise times (knowing the response law of the complete detection system).

There is a potentially confusing feature of the photographs 4.6(b) and (c) in which the pulses apparently have reversed polarity. The Mullard signal generator used to provide the pulse did not reverse the polarity of the pulse, but exchanged the mark-space sections of the pulse train. Thus in Figure 4.6(b) the field is applied for  $100\mu$ seconds, and a partial switching-off is followed by a switching-on; whereas, in Figure 4.6(c) the field is switched off for  $100\mu$ seconds and a switching-on of the transient is followed by a switching-off.

#### 4.2 Induced "spiking".

The oscillation transient following quenching by an injected signal is observed under conditions of a relatively wide frequency sweep of the injected signal across the natural maser

oscillation frequency  $\nu_0$ . Then the beat frequency signal upon which the oscillation transient (frequency  $\nu_t \sim 10\text{kHz.}$ ) is superimposed is in general greater than  $80\text{kHz.}$  in order that the transient phenomenon can be distinguished easily from the magnetic satellites of the  $J = K = 3$  inversion transition which lie between  $50$  and  $80\text{kHz.}$  from the main transition.

If, now, a relatively narrow frequency sweep is used, such that the beat frequency is  $\lesssim 10\text{kHz.}$  before and after quenching, a series of spikes of oscillation of relatively large amplitude can be produced. These spikes occur before and after the region of oscillation quenching, as shown in Figure 4.7. The risetime of an individual spike is  $\sim 10\ \mu\text{s}$ , and the decay time  $\sim 20\ \mu\text{s}$ . The repetition frequency of the spikes follows that of the beat frequency (between the maser oscillation frequency  $\nu_0$  and the frequency modulated exciting signal  $\nu_s$ ) up to  $\sim 10\text{kHz.}$  The duration of the train of spikes appears to be limited by the time for which the beat signal is less than  $10\text{kHz.}$ , the natural period of the oscillation transient. Consequently, the duration of spiking is dependent upon the rate of frequency sweep of the excitation signal. The longest period of continuous spiking observed so far is  $\sim 2\text{ms}$ . This time is considerably longer than the mean time of flight of an individual molecule through the cavity ( $\sim 0.5\text{ms.}$ ), in contrast to the case of the transient phenomenon. It is also of interest to note that the

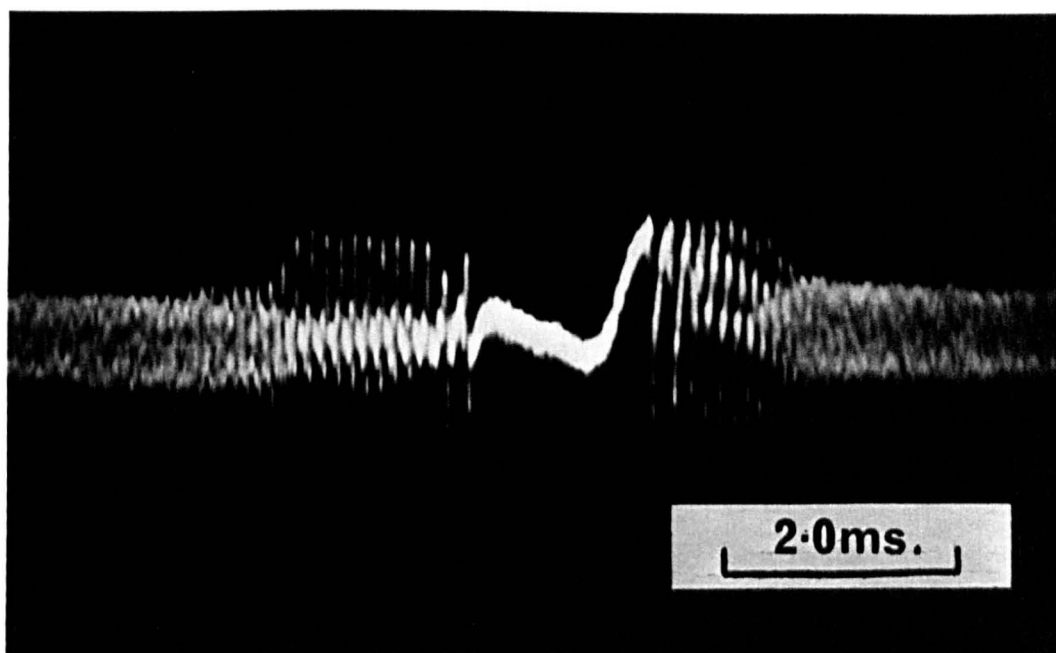


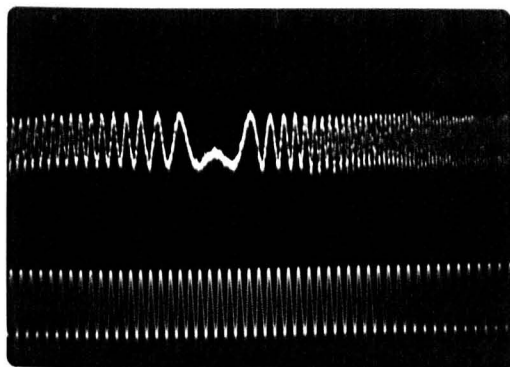
Figure 4.7. Induced spiking

amplitudes of the spikes of oscillation are somewhat greater than the level of continuous oscillation as shown by the amplitude of the beat signal on the extreme left and right hand sides of Figure 4.7.

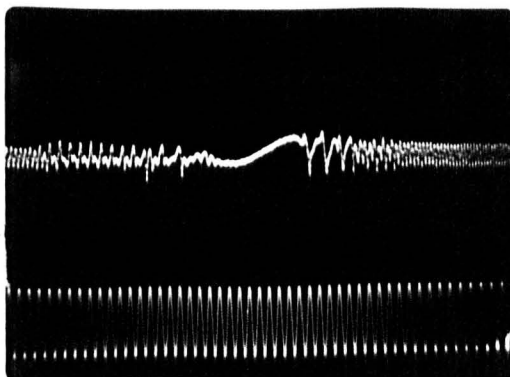
The dependence of spiking upon the presence of the externally applied signal is clearly shown by the fact that at low levels of applied signal neither spiking nor quenching occur. In their place a beat signal is obtained which passes through zero beat frequency when the applied signal of frequency  $\nu_s$  is instantaneously at the maser oscillator frequency  $\nu_o$ . Figure 4.8(a) shows the zero beat obtained when the injected signal level is low: Figure 4.8(b) shows the appearance of spiking when that level is increased.

Figure 4.8(c) demonstrates decisively the relation between the transient and the spikes. On the left is the transient produced by the rapid frequency sweep from the sharply rising leading edge of the saw-tooth voltage applied to the klystron reflector, and on the right is the spiking induced by the slower sweep from the trailing edge of the saw-tooth.

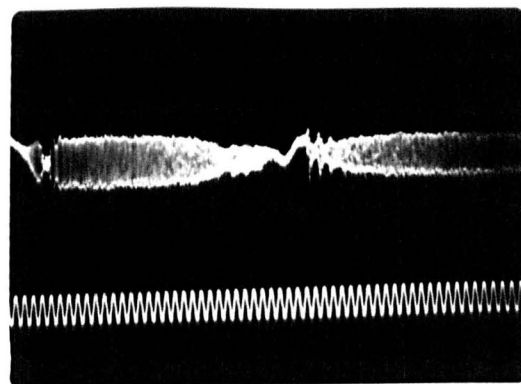
It will be noted from Figure 4.7 that the spiking phenomenon precedes and follows the quenched oscillation region. Furthermore, the spiking decays as the amplitude of oscillation grows to its steady state level on the right hand side, and vice versa on the left hand side. On close examination of an expanded trace it is



(a) zero beat



(b) spikes



(c) transient and spikes

Figure 4.8

evident from the superimposition of the growing beat frequency and the spiking signal, that the spiking repetition frequency follows the beat frequency. Thus the effect may be attributed to the externally applied signal going in and out of phase with the growing oscillation, and leading to a periodic modulation of the microwave electric field within the cavity at the beat frequency.

(Alternatively the system may be regarded as being partially quenched with a periodic modulation at the beat frequency). Figures 4.9(a) and 4.9(b) display the situation where the beat frequency exhibits harmonic relationships with the spiking frequency, over a small range of frequency. Figure 4.9(c) shows an expanded trace where the spiking frequency gradually increases until the spiking can no longer be sustained.

Comparison is invited between this series of photographs of the transient and the spiking phenomenon, and the photographs in Figure 4.10. The latter show the behaviour of an RC oscillator subjected to a small disturbance.

The correspondence is not fortuitous. A simple RC audio oscillator has many essential features in common with a maser, particularly an amplification mechanism combined with a feedback mechanism of which the round-trip phase is strongly frequency dependent. It also has a saturation mechanism to reduce the round-trip gain as the power level increases. In a simple RC oscillator

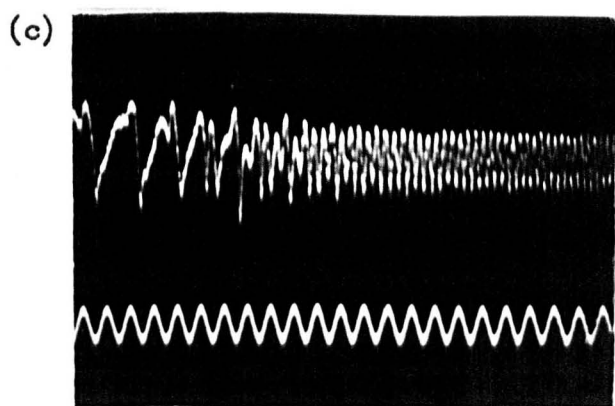
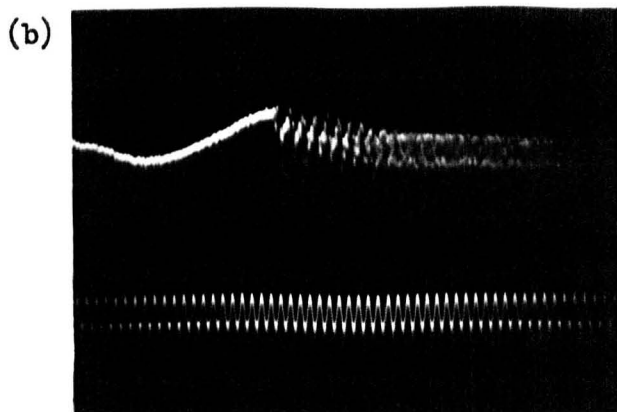
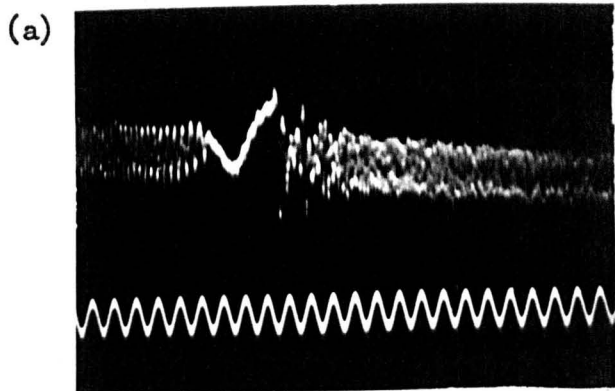
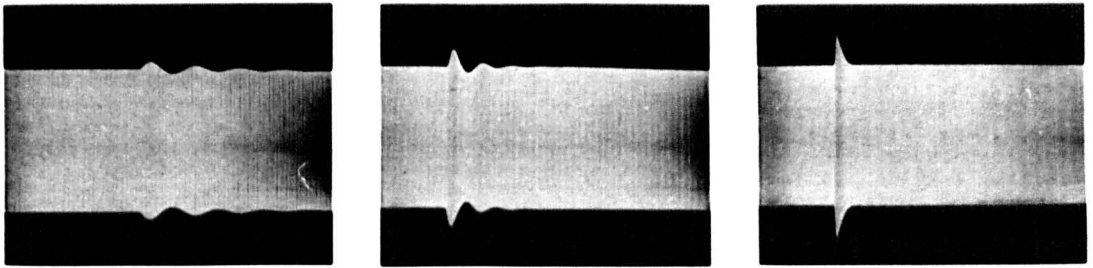
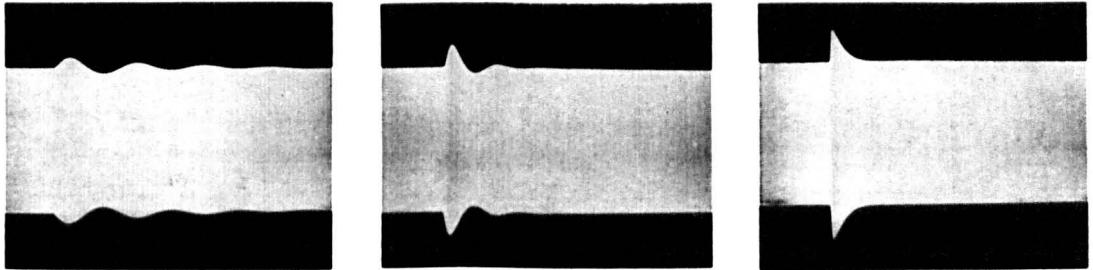


Figure 4.9 Intermediate stages of spiking

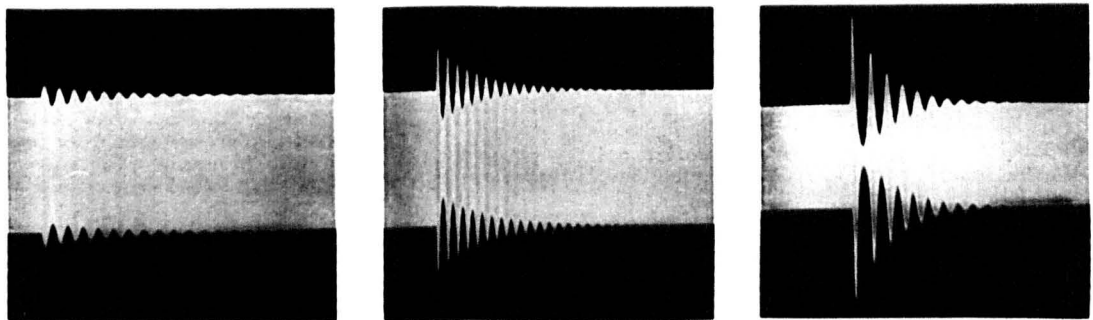




(a) Envelope response typical of RC oscillator to slight amplitude disturbances within circuit. Oscillation frequency is 100 cps (left), 1 kc (middle), and 10 kc (right). Sweep times are 200, 100, and 50 millsec/cm, respectively. Oscillator distortion is 66 db below oscillation level.



(b) Envelope response to internal disturbance when lamp circuit time constant is increased, showing slower envelope transients. Distortion, sweep times, and oscillator frequencies are same as in (a).



(c) Envelope response when oscillation level is reduced to obtain very high effective linearity in amplifier portion of circuit. Distortion is about 90 db below oscillation level. Sweep times are 1 sec/cm (left), 500 millsec/cm (middle), and 100 millsec/cm (right). Oscillator frequencies are same as in (a).

Figure 4.10 Transients in an RC oscillator (after Oliver, 1960)

this saturation mechanism is a variable resistance in the feedback loop, in the form of a small lamp the temperature and resistance of which change with the average signal power dissipated in it, so that the feedback round the loop is reduced.

Another point of contact between the oscillator and its familiar solid state laser counterpart is that the time constant of its saturation mechanism (determined by the thermal time constant of the lamp) is relatively long, to be compared with the long meta-stable lifetime in the laser case. For this reason it is expected that "spiking" behaviour would be seen in the output of such an oscillator. However, this form of instability is not often seen. Oliver (1960) has shown that there is usually a weak saturation mechanism in the amplifier stages, and this small compression effect for large signals is usually sufficient to eliminate the spiking. If the oscillator is made with a highly linear amplifier section then the spiking is manifested. Figure 4.10 shows the envelope responses under various conditions of time constant and distortion. This discussion of the analogy follows that of Siegman (1968).

#### 4.3 The spectroscopic investigation of the state of the beam emerging from the first cavity.

The observation of the transient indicates that molecules are oscillating between the two levels during the course of their transit through the resonator. It is thus reasonable to expect that

the emerging beam will exhibit changes in its relative populations as the beam intensity is varied, that is, it should change from emissive to absorptive as the electric field within the cavity increases.

Figure 4.11 depicts schematically the arrangement used to examine the emergent beam. It will be recalled from the discussions of Chapter III that the oscillating polarisation possessed by the beam emerging from the first cavity can initiate oscillations in the second cavity for a focuser voltage well below that of the threshold for the cavity acting alone. For the arrangement used here (first cavity  $Q \sim 9,000$ , second cavity  $Q \sim 6,000$ ) the effect is quite pronounced. With the first cavity detuned by about 10 MHz. so that the beam is unpolarised the second cavity oscillates freely at 17.5kV. for a nozzle pressure of 1.6 torr (the optimum pressure, with the iris aperture optimised at 1.1mm): when the first cavity is tuned to the molecular resonance frequency the threshold for forced oscillation in the second cavity is about 10kV. Since, for the purposes of a spectroscopic examination the presence of an oscillation in the second cavity is an embarrassment, with its concomitant beat frequency superimposed on the oscilloscope trace, it is desirable to remove the polarisation of the beam. This can be achieved by projecting the beam through an inhomogeneous electric field, such as that provided by a state focuser (Basov et al, 1964). If the

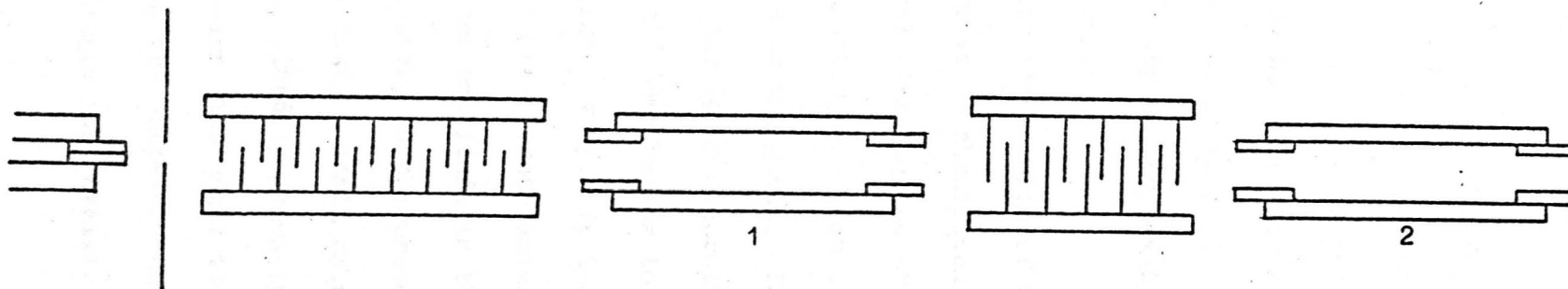


Figure 4.11. The arrangement of cavities and focusers used for the spectroscopic examination of the beam.

field is maintained at a low level then the polarisation may be removed without any sensible disturbance of the level populations. The onset of free oscillation in the second cavity can be deferred a little, without prejudice to the cavity's function as a spectrometer, by detuning it (the second cavity) a little. In the experiment described below the second cavity did not oscillate throughout the range of focuser voltage.

Figure 4.12 shows the results of the spectroscopic examination. Below 2kV. there is an absorption (not visible) corresponding to the near thermal distribution of populations. Above 2kV. some focusing action is exerted, the beam is emissive in the first cavity, and still emissive on emergence. The emissive signal increases and then wanes, and gives way to an absorptive signal after 10.5kV. The absorption increases and then begins to decrease when a transient is just visible in the first cavity. By the time the transient is well established the system has become emissive again. Throughout this process the oscillation amplitude in the first cavity displays a monotonic increase. However, in the process the spectral line exhibits a splitting. At 22kV. a small emissive-going notch appears in the absorptive line and steadily grows in amplitude and width at the expense of the absorption line until it changes into an emissive signal. Figure 4.13 shows the shape of the spectral line for a succession of focuser voltages (the available signal to noise ratio

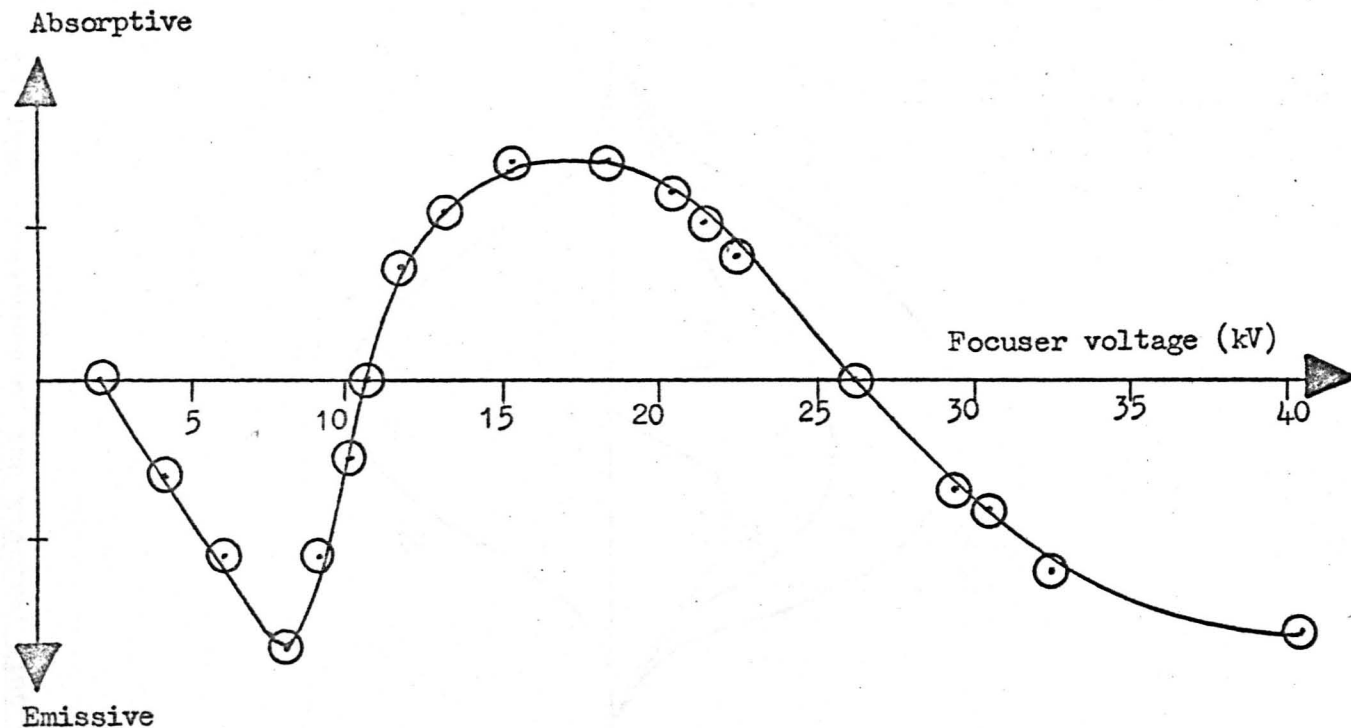


Figure 4.12. The variation with the main focuser voltage of the state of the beam leaving the first cavity.

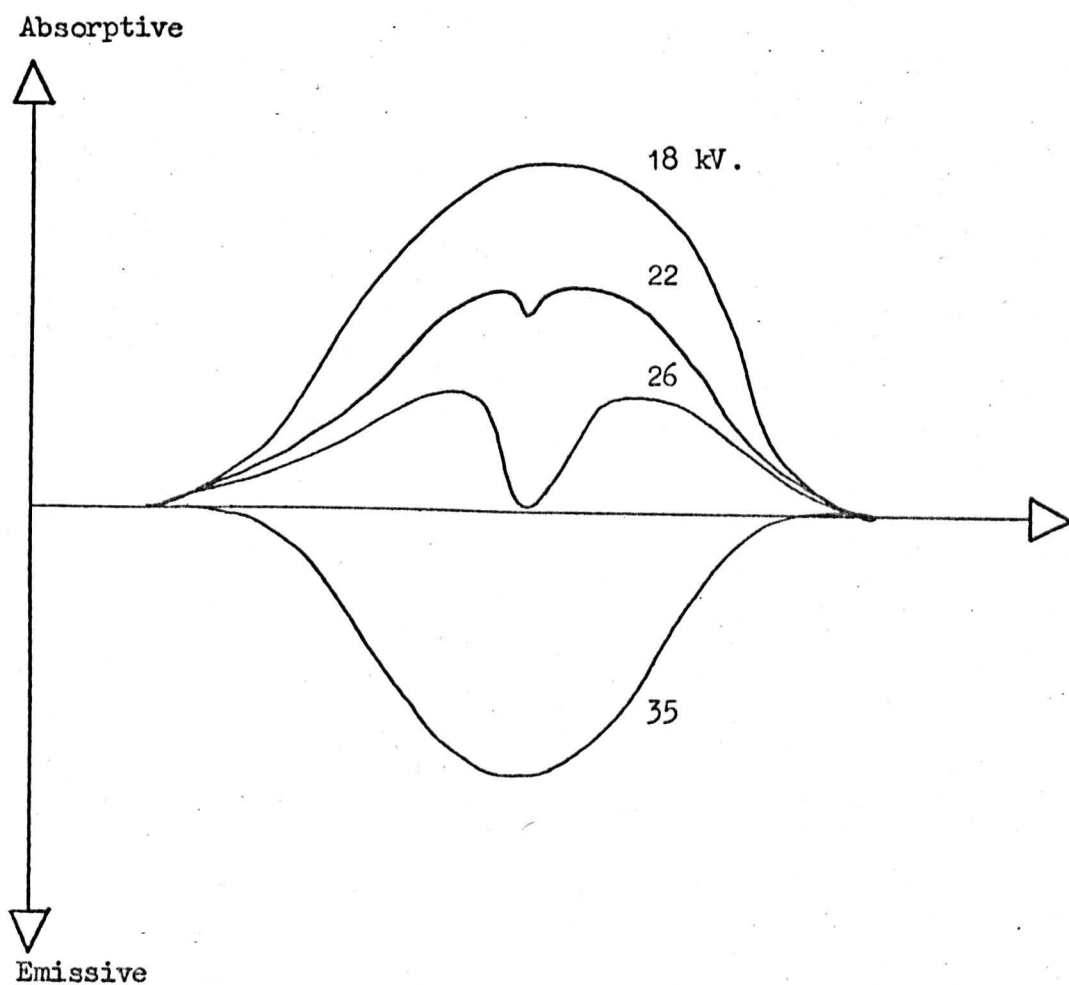


Figure 4.13. The appearance of the spectral line observed in the second cavity for various magnitudes of focuser voltage.

did not permit photographs).

It thus appears that an emissive line is superimposed upon an absorptive one; a kind of "hole-burning". The relative widths of the two lines give an indication of the possible mechanism. The narrow width of the emissive line at about 22kV. indicates that the emitted radiation is originating from relatively slow molecules. If this is, in fact, the case, then their transition probability (a function of time) could be quite different from that appropriate to faster molecules. The hypothesis is given further support by the observation that the emissive line is easily saturated by an increase in sideband power.

For the purpose of analysis assume first that an unsorted beam passes through the first cavity, which is tuned to the molecular resonance frequency  $\nu_0$ , then the excess population will oscillate between the two levels. At time  $t$ , the probability of the excess population in the upper and lower levels,  $a$  and  $b$  respectively will be given by

$$|a|^2 = \sin^2 \omega t,$$

$$|b|^2 = \cos^2 \omega t,$$

where

$$\omega = \frac{\mu_{12} E}{\hbar}$$

and  $\mu_{12}$  is the dipole matrix element for the transition,  $E$  the magnitude of the oscillating electric field in the resonator,  $t$  the



interaction time of the molecules with the radiation field. At time  $t = 0$ ,  $|b|^2 = 1$ ,  $|a|^2 = 0$ , and the excess population at the entrance to the cavity is in the lower energy state. At the time  $t = \tau$  given by  $2\omega\tau = \pi$ ,  $|b|^2 = 0$ ,  $|a|^2 = 1$ , and the excess population will be transferred to the upper energy state. In the frame of reference in which the molecules are stationary, the time  $\tau = \pi/2\omega$  corresponds to a  $\pi$  pulse. Similarly  $\tau = \pi/\omega$  corresponds to a  $2\pi$  pulse, in which case the excess population will be restored to the lower energy state.

The interaction time, however, is not the same for all molecules, for there is a velocity distribution. If two groups of molecules are considered such that  $2\tau_1 = \tau_2$ , where  $\tau_1, \tau_2$  are the interaction times of slow and fast molecules respectively, then if  $2\omega\tau_1 = 2\pi$ ,  $2\omega\tau_2 = \pi$  and the population of slow molecules will be inverted with respect to the fast molecules. If both fast and slow molecules pass into a second resonant cavity of length  $L$  used as a spectrometer cell, the spectral linewidth  $\Delta\nu$  given by  $V_{1,2}/L$  will be narrower for slow molecules (velocity  $V_1$ ) than for fast molecules (velocity  $V_2$ ). Moreover, for the present example where the initial beam is absorptive, the slow molecules will be absorptive, whereas the fast molecules will be emissive on emerging from the first cavity, and consequently the spectral line of the fast molecules will be subject to "hole-burning" by the slow molecules.

In the maser experiment described above the beam entering the cavity is emissive and the slow molecules subject to the  $2\pi$  pulse are emissive, in contrast with the fast molecules receiving a  $\pi$  pulse which are absorptive.

The pulse excitation of the molecules in the maser situation arises from the strong self-oscillation, but the excitation could equally well be derived from pulses of an externally applied signal at  $\nu_0$ . The latter process is the one applicable to the initially absorptive system of molecules.

The maser system possesses the added virtue that the second focuser can be employed selectively to defocus the fast molecules, and to focus the slow molecules into the cavity. Such an attempt was made in the experiment, but full separation could not be observed owing to the limitations imposed by the signal to noise ratio, governed mainly by klystron frequency instabilities.

The technique of utilisation of slow molecules is general to beam systems, and not restricted to maser systems, though the latter do offer the advantage of space focusing. The improvement in spectral resolution yielded by the slow molecules has implications both for spectroscopy and for frequency standard development. The production of such a beam and its use in a spectrometer of the Ramsey separated fields type offers an enhanced spectral resolution without increase of the separation between the cavities. The experiment

described above showed that a compromise must be made between degree of resolution and amplitude of signal.

A number of frequency standards employ velocity selection of molecules; for example, caesium beam standards may incorporate selection of molecules following curved trajectories in magnetic fields: the path in the field depends upon velocity. Selection of a greater number of molecules involves increasing the beam divergence. Also, in Chapter II it was described how attempts have been made to select slow molecules in masers by injecting molecules into a focuser at an angle to its axis. The present method avoids the difficulty of such methods, though it is true that there is the compromise between signal amplitude and spectral resolution, as more of the velocity distribution is utilised to provide slow molecules.

The analysis given above has been restricted to a consideration of two groups of molecules having a simple ratio of transit times. Obviously the analysis could be extended to include the velocity distribution. However, in the case of the maser cognisance should also be taken of the non-Maxwellian distributions produced by the state focuser. Furthermore, the dipole matrix element is not a constant, but depends upon the particular sublevel the molecule occupies. Molecules are focused differentially according to their occupation of the sublevels, and so there is an additional distribution factor to be taken into account - that of the dipole moments.

These observations of the self-excitation beyond the  $\pi$  pulse condition of the molecules in the cavity may be used to explain an anomalous saturation effect observed by Helmer et al (1960 a,b). They investigated the increase of flux of lower state molecules occurring when the maser oscillated on the 3,3 line, using a coaxial lower state focuser and ionization detector. The anomalous saturation effect they observed they attributed tentatively to the presence of infrared oscillation at 0.125mm. wavelength through the interference of the rotation inversion transition  $J = 4, K = 3 \rightarrow J = 3, K = 3$  which terminates on the lower maser level.

Now the method of Helmer et al is capable only of detecting lower state molecules, and so the magnitude of the ion current proportional to the flux of low state molecules would vary less rapidly as a function of focuser voltage than the signal observed spectroscopically which is proportional to the molecular population difference between levels. However, the flux of lower state molecules focused into the ionisation detector would pass through a maximum once the  $\pi$  pulse condition was exceeded, although at a higher voltage than the peak of absorption observed in the spectroscopic mode of operation. The maximum value of ionization detector current would consequently appear as an anomalous saturation effect, if the maser oscillation signal was not sufficiently strong to exceed the  $\pi$  pulse condition for state inversion of the molecular beam as a

whole. Thus it may be concluded that the presence of an infrared oscillation need not be invoked to interpret the results of Helmer et al.

#### 4.4 Further investigations of the state of the beam emerging from the first cavity.

The experiment described in section 4.3 monitors the state of the beam in terms only of the relative populations of the levels, registering net absorption or emission. The polarisation information is lost by the action of the inhomogeneous electric field created by the ancillary state focuser.

It was shown in Chapter III that the change in oscillation amplitude in the second cavity as a function of the detuning of the first cavity is an indication of the magnitude of the pulse received in the first cavity. Thus the Strakhovskii - Tatarenkov (S - T) curves provide information which is complementary to that yielded by spectroscopic examination. The relationship between the two methods of examination is explored, and the S - T curves that are usually obtained are explained in terms of the spectroscopic diagram. Furthermore a new series of S - T curves is predicted, which would exhibit shapes not seen before. Part of these predictions has been verified. Confirmation of the set of predictions awaits further investigation.

The predictions concern the S - T curves which should be

attained with a maser which can oscillate sufficiently strongly to produce up to a  $2\pi$  pulse. The familiar S - T curves are obtained with conventional masers which appear to have produced less than a  $\pi$  pulse.

It should be emphasised that the graph showing the relation between the emission or absorption signal in the second cavity as a function of the focuser voltage represents measurements made with the first cavity tuned to the molecular frequency,  $\nu_0$ . In order to provide an accurate correlation between the S - T curves and the spectroscopic results it is necessary to examine the emission and absorption in the second cavity as a function of focuser voltage for a series of detunings of the first cavity. However, in the absence of this information, qualitative estimates of the relation between detuning and the spectroscopic results can be made.

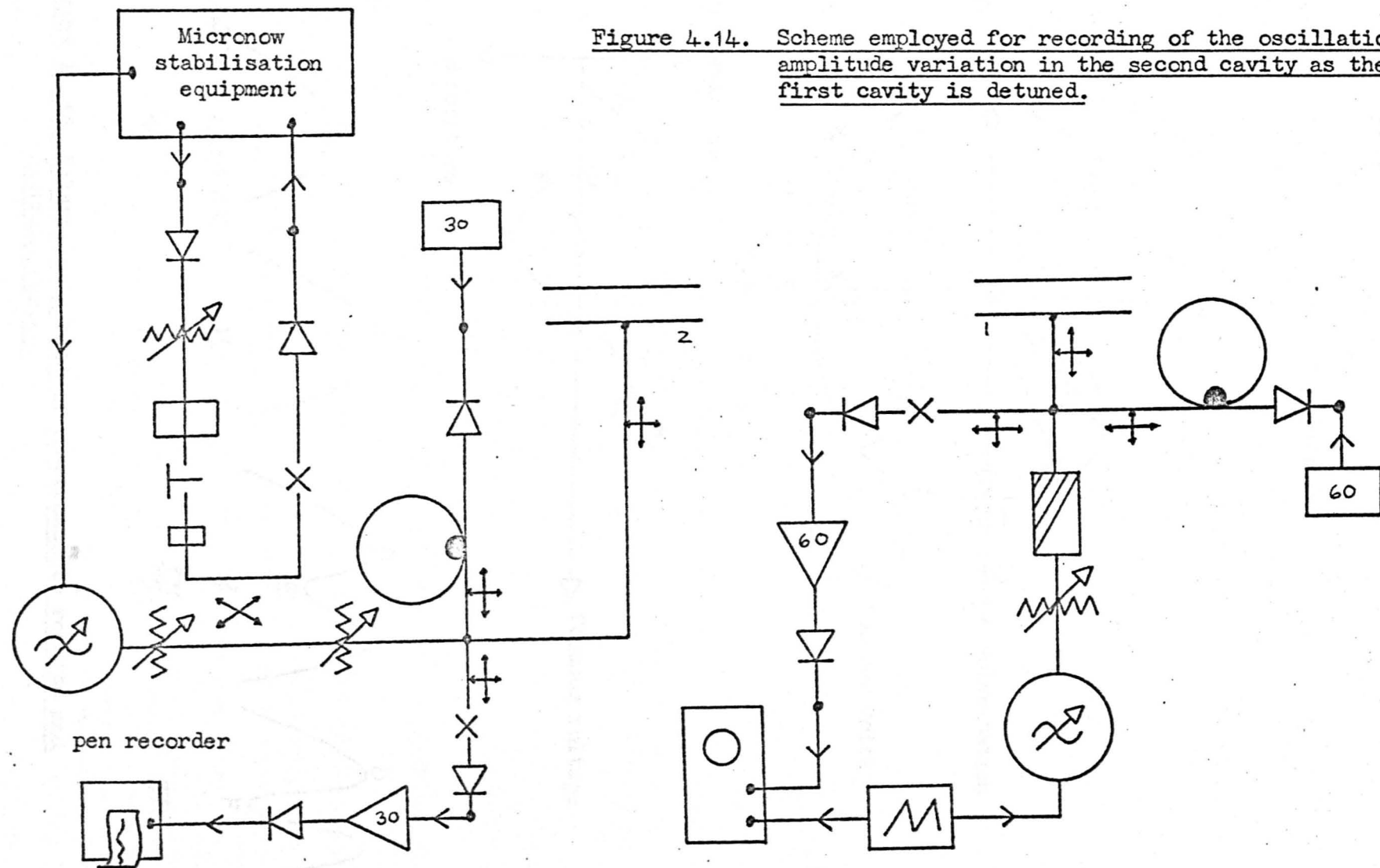
The electric field within the first cavity varies with the detuning as a semi-ellipse; this is why the theoretical S - T curves appear to suffer a contraction of shape near the maximum detuning. This implies that the pulse  $\left(\int_0^{\tau} E dt\right)$  experienced by the molecules in travelling through the cavity is subject to modification by the semi-elliptical function. Thus the spectroscopic graphs would exhibit with detuning a change of scale and shape. However, for a qualitative examination it is permissible to regard the effect of detuning as a tracing backwards of the locus of the spectroscopic graph for  $\nu_0$  as

the detuning is increased.

The form of the spectroscopic graph can be derived from a consideration of the locus of the pseudo-dipole moment in the sense of the analogy established by Feynman et al (1957). Figure 4.15(a) shows the expected form for the locus of the dipole moment as the focuser voltage is increased and the electric field within the cavity grows. The vector grows and turns in a clockwise sense as the molecules experience a greater pulse in the first cavity. The growth of the vector is at first rapid, but after a certain time becomes slow owing to the onset of saturation. The representation is one in which the component of the vector along one axis represents the excess population (population difference between the two levels) and the other axis represents one of the components of the oscillating dipole moment; the third axis has been transformed away by transferring to the rotating frame of reference. The spectroscopic experiment records the time evolution of the population component, and the transverse component decides the form of the S - T detuning curves.

Compare Figure 4.15(a) with 4.15(b). The dipole vector grows and rotates through the position A, and then through B at which the population emissive component is a maximum. The vector continues through C and then D where the population component is zero, but the transverse component is a maximum. The system then becomes absorptive. Somewhere in the second quadrant the locus will begin to approximate

Figure 4.14. Scheme employed for recording of the oscillation amplitude variation in the second cavity as the first cavity is detuned.





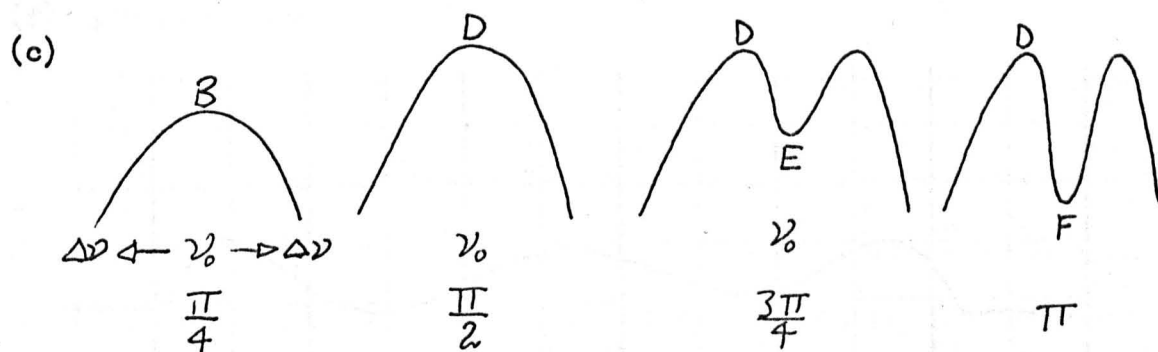
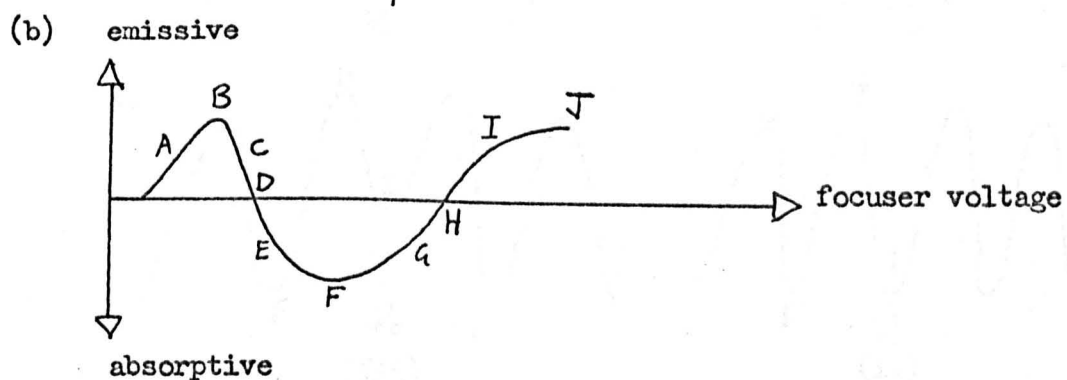
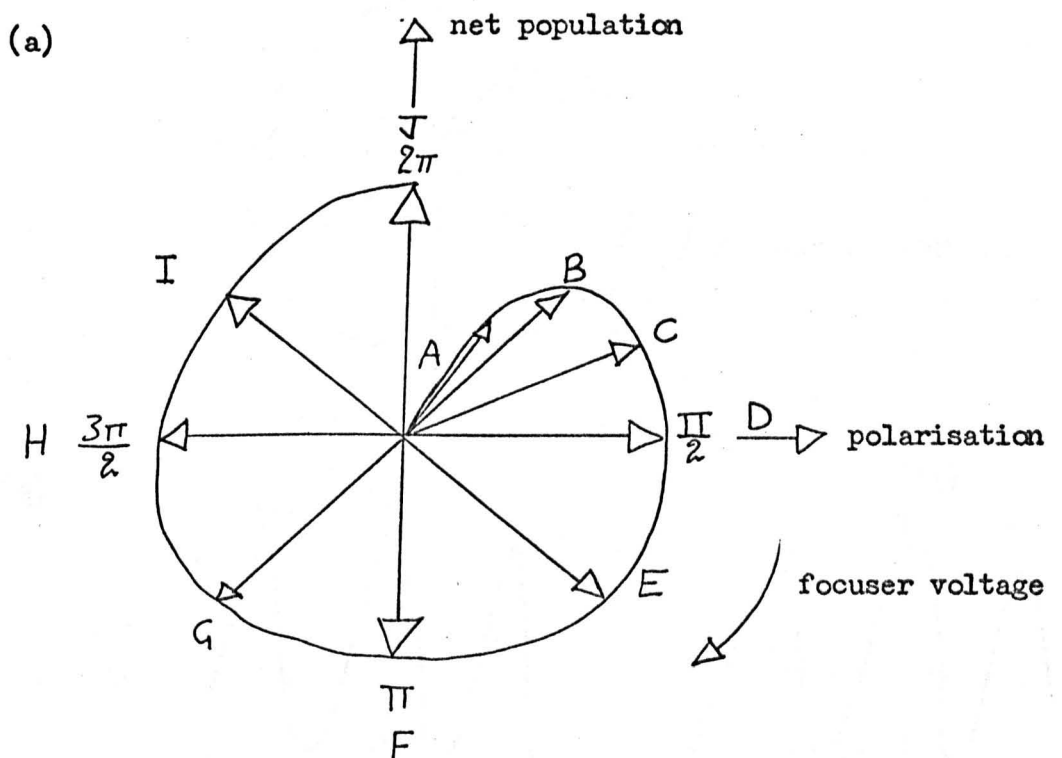
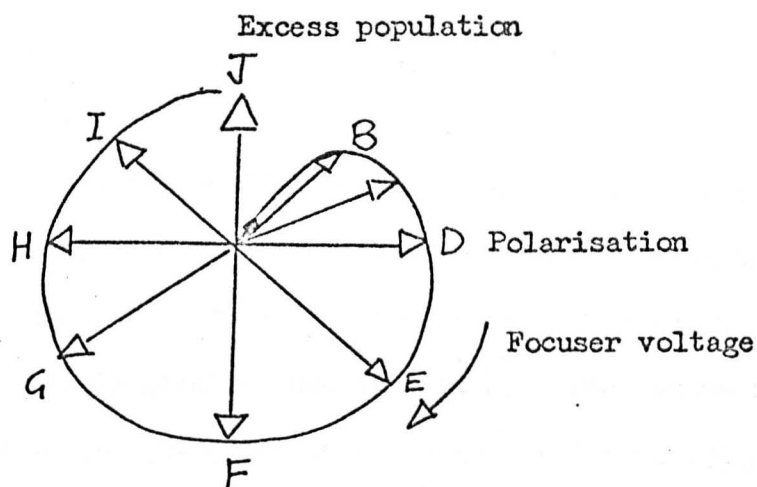
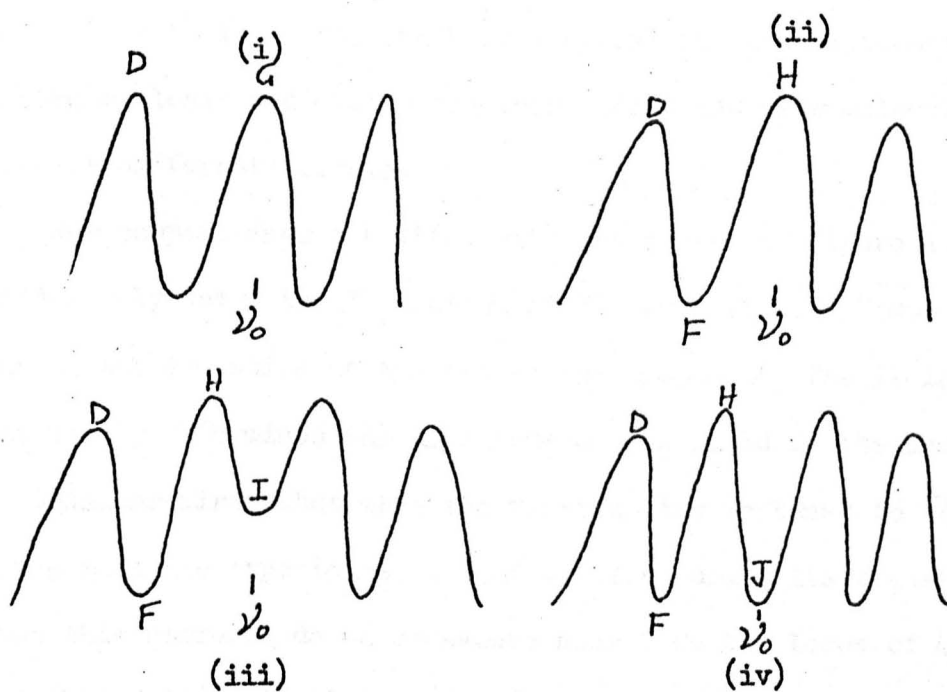


Figure 4. 15 Relationship between spectroscopic results and detuning curves.

(a)



(e)



(f) pen recording

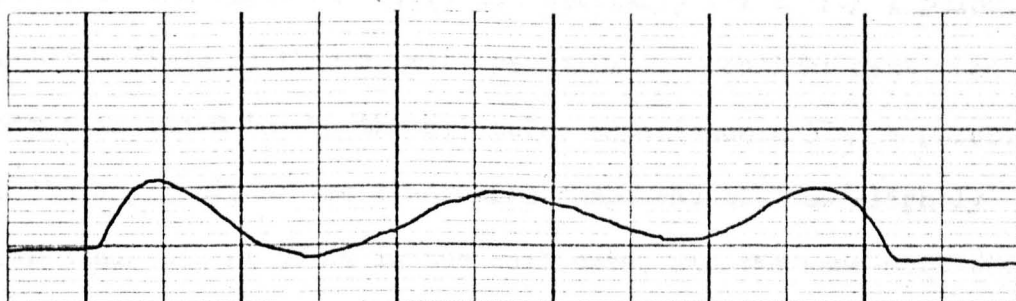


Figure 4.15 Predicted detuning curves

to a circle as saturation limits the growth of the vector. As the vector turns through  $F$  the absorption becomes a maximum and then decreases to zero at  $H$ , where the transverse component is again a maximum (possibly greater than that at  $D$ ). The system then becomes emissive once again and grows to a maximum at  $J$ , the  $2\pi$  position. Further regions of the spectroscopic graph could be traced out by continuing the rotation. The graph is a spiral in which successive spirals become closer and closer together. Fast and slow molecules will describe different spirals.

Now compare Figure 4.15(a) with the graphs of Figure 4.15(c), and consider only the  $0$  to  $\pi$  section of Figure 4.15(a). Focus attention on the evolution of the transverse component, for it is this that mainly determines the amplitude of the field in the second cavity. Consider first that when the first cavity is tuned to  $\nu_0$  the average molecule experiences a  $\pi/4$  pulse during its transit time; then this corresponds to somewhere near  $B$  on the locus of 4.15(a). As cavity 1 is detuned the transverse moment decreases monotonically and with it the field in cavity 2. Similarly for a  $\pi/2$  pulse, though the field is then a relative maximum. Consider next when cavity 1 is tuned to  $\nu_0$  the molecules experience a  $3\pi/4$  pulse. Then the amplitude of the transverse component will be slightly larger than that at  $\pi/4$  in the real case, and the same magnitude in the theoretical simplification. As the cavity is detuned the

transverse component increases to a maximum at  $\pi / 2$  and then decreases. For an exact  $\pi$  pulse at  $\nu_0$  there is no transverse component at  $\nu_0$  and the field within the second cavity is zero; the molecules are purely absorptive. As the cavity is detuned the transverse component grows to a maximum at  $\pi / 2$  and then decreases again.

This description accounts qualitatively for the types of S - T curves that have been observed before (remembering that the amplitude of the signal for experimental graphs may not be linear with electric field). Consider now the type of S - T curves that would be obtained with a maser that can produce up to a  $2\pi$  pulse when the cavity is tuned to the molecular resonance (the argument can of course be extended for pulses greater than  $2\pi$  ).

Figure 4.15(d) reproduces 4.15(a) to facilitate comparison. The series of curves in 4.15(e) display the expected form of S - T curves for different pulses applicable to zero detuning. The points on the curves are labelled with the letters indicating the sequence of points on the locus of 4.15(a) as the vector evolves in time with the detuning.

Another point must be made. Whenever the system is emissive, that is when it is in the quadrants A-D or H-J, it is possible that the second cavity may break into free oscillations. For this reason part of the proposed S - T curves may be obscured: for instance

curve (ii) may be obscured to some extent by the second cavity breaking into oscillation soon after point D is reached. For curve (iii) this may occur before much of the curve can be traced out. Thus, in order to display as much as possible of these extended S - T characteristics it is necessary to select conditions that favour the dominance of the first cavity over the second. The condition where the first cavity fails to phase lock the field of the second cavity and allows it to oscillate freely is a rather extraneous consideration. The domination of the first cavity over the second can be achieved by using a very high Q cavity for the first resonator, and a low Q cavity for the second. Previous investigators seem to have used either cavities of comparable Q, or a second cavity having a higher Q than the first.

Figure 4.14 shows the microwave scheme employed in the investigation of the S - T curves. Cavity 2 ( $Q \sim 6,000$ ) is stabilised at the molecular resonance frequency, and the oscillations in it are monitored with a klystron stabilised with the Micronow equipment (described in Appendix B). The variation of the oscillation amplitude is traced on a pen recorder. Cavity 1 ( $Q \sim 9,000$ ) is detuned through a wide frequency range by heating and then cooling so that its resonance sweeps slowly across the molecular resonance. Its dominance over the second cavity is demonstrated by the fact that Higa beats and subsequent forced oscillation occur in cavity 2 when

cavity 1 is detuned about 8 MHz. from  $\nu_0$ . The Higa beats region seems to have occurred at no more than about 6 MHz. away from  $\nu_0$  in previous investigations.

For conditions known to be close to G (same focuser voltage and nozzle pressure), by comparison of the focuser voltage with the spectroscopic graph, the qualitative shape of the predicted detuning curve has been verified. Figure 4.15(f) shows the pen recording obtained. The remaining series of curves have yet to be verified.

It is seen that the spectroscopic results permit a reasonably accurate calibration of the locus of the vector in 4.15(a). This relation between the focuser voltage and the S - T curves permits a comparison of relative efficiencies for different masers. For example the present maser gives (at  $\nu_0$ ) a  $\pi/2$  pulse at  $\sim 10.5\text{kV}$ , a  $\pi$  pulse at  $\sim 17.5\text{kV}$ , and a  $3\pi/2$  pulse at  $\sim 26\text{kV}$ . Judging from the S - T curves shown in the paper by Lainé and Smith (1966) their maser gave a  $\pi/2$  pulse at about 17kV.

It is interesting to note that they observed a splitting at about 16kV. Since this seems to occur below the  $\pi/2$  condition it does not seem possible to interpret this structure in terms of the fundamental processes underlying the S - T curves. Their tentative explanation still seems plausible. They suggest that the S - T curves may be reflecting the structure of the ammonia spectrum, since the various components of the line are focused differentially and

also slower molecules contribute more to the oscillation as the focuser voltage is decreased.

#### 4.5 Suggestions for further work

Proposals for further investigations are most conveniently discussed under a series of headings appropriate to each topic.

##### A Oscillation transient

###### (a) Molecular Q switching with an injected signal

Consider means of obtaining a more pronounced transient. The most important parameter to be considered is the cavity Q. It should be possible to increase the Q by cooling the cavity, and decreasing the wall losses. The gain in Q that can be obtained by cooling is limited by the onset of the anomalous skin effect. In the absence of accurate information about the resistivity of the wall material it is not possible to predict the temperature at which the anomalous skin effect occurs. However an improvement factor of 2 or 3 in Q should be possible in cooling the cavity down to temperatures of the order of 170°K. The amount of cooling is also limited by the consideration that solid ammonia must not be deposited on the cavity walls. It can collect charge and exert a Stark spreading of the spectral line, and can also detune the cavity.

An increase in the electric field in the cavity can possibly be obtained by directing a second active beam into the cavity in the opposite direction.

The efficiency of the focusing action can possibly be improved by scattering out of the beam the axial  $M_J = 0$  molecules which are not subject to focusing action. This may be done using a small beam stop on the axis. This must be earthed since objects within the maser box rapidly accumulate charge when the focuser is on (the second focuser used in the spectroscopic experiment was found to charge up sufficiently within a few seconds of being disconnected from earth to exert a depolarising effect on the beam). It must also be borne in mind that the insertion of an earthed beam stop changes the fringe field of the focuser, which is most influential in determining the interaction of the dipoles with the cavity field.

(b) molecular Q switching with a Stark field

The considerations of (a) apply here, but in addition the effect of the probe can be enhanced considerably by extending the region of inhomogeneous field. This can be done by creating the electric field between two probes spaced, say, about 1cm apart, as well as between one probe and the cavity wall.

In observing the spikes it is desirable to use a stable microwave source which can be swept over a very restricted frequency range. The limitations of the present scheme are imposed by the instability of the klystron resulting from ripple on its high voltage supply, and not the sweep unit.



When the period of spiking has been extended sufficiently for it to be observed in the second cavity it would be interesting to feed the output back into the first cavity, as a kind of analogue of the pulses circulating in lasers. The experiment could also be conducted on the N.M.R. analogue.

B The spectroscopic examination of the beam emerging from the first cavity

Since the slow molecules exhibit a very small linewidth, it should be possible to discern structure on the emissive-going spectral line, with an increased signal to noise ratio. Again this is limited by klystron instabilities. It should be possible to conduct a slow sweep through the line using a far more stable source.

C Verification of the predictions for the new detuning curves

This should be attempted using cavities with more disparate values of  $Q$ . The spectroscopic curves for different amounts of detuning should be constructed. It is stressed that the oscillation amplitude in the first cavity must be monitored to ensure that it is monotonic increasing throughout, otherwise focuser breakdown may cause the system to trace out the reverse locus. Once constructed these curves should be correlated with S - T curves constructed under the identical conditions.

Attempts should be made to obtain these effects on the nuclear maser analogue.

D Examination of a nozzle exhibiting a peculiar discontinuous effusion

During the pilot experiments required to establish the optimum dimensions for a nozzle, one nozzle was observed to emit its effusion in a series of "puffs". It consisted of a tube of about 3mm internal diameter, 0.5cm long, terminating in a channel 0.5mm diameter and 0.75cm long.

The oscillation in the maser cavity was observed to switch on very rapidly and switch off very rapidly. The frequency of puffing seemed to depend only on the pressure behind the nozzle and increased with that pressure from about 1 every 20 seconds to several per second. This behaviour could only be initiated by increasing the pressure from below. The pressure behind the nozzle was observed to rise slowly then drop precipitately as the oscillation signal appeared. The ion gauge registered an increase in pressure in the two chambers soon after the oscillation signal appeared.

It is possible that the dimensions of the nozzle and the nozzle pressures (a few torr) are such that the flow is intermediate between viscous and molecular flow. Two further observations: there is drill "chatter" visible at the entrance to the narrow channel; and the surfaces are usually covered in diffusion pump oil.

It would be worthwhile investigating this phenomenon by  
(a) trying to fabricate another nozzle with the same property, and

then altering the nozzle dimensions;

- (b) investigating the variation of the effect with cooling, and
- (c) with change in volume of the source chamber.

The time constants involved may be measures of thermal processes.

#### E Investigations of an alternating gradient focuser

Kakati and Lainé (1967, 1969) have recently investigated an alternating gradient focuser which can focus absorptive beams. Since the maser described here can produce an absorptive beam, the A.G. focuser parameters can be investigated by interposing it between the two cavities and monitoring its focusing action in the second cavity.

#### F Investigation of microwave echoes

Preparations are being made to investigate echoes in the ammonia maser. The pulses of microwave radiation are produced by applying voltage pulses to microwave switching diodes.

One of the major considerations to be examined is that of the required frequency stability. No firm conclusion can be reached, but among the factors to be taken into account are the following.

The effect of frequency instabilities on the pseudo-dipole vector may be viewed in the rotating frame. The change in frequency  $\Delta\omega$  is represented by a vector at right angles to a vector  $\mu E/\hbar$ . The angle  $\theta$  between the direction of the effective field and

$\mu E_1 / \hbar$  is given by

$$\tan \theta = \frac{\Delta \omega}{\mu E_1 / \hbar}$$

Now  $\tan \theta$  should be  $\ll 1$ ,

$$\text{i.e. } \frac{\Delta \omega}{\mu E_1 / \hbar} \ll 1$$

For a  $\pi/2$  pulse the pulse length is given by

$$\frac{\mu E_1}{\hbar} \tau_1 = \frac{\pi}{2} \Rightarrow \Delta \omega \ll \frac{\pi}{2 \tau_1}$$

$$\text{or } \Delta \nu \ll 1 / 4 \tau_1$$

The duration of the pulse should be very much less than the transit time of molecules through the cavity which is of the order of 300-500  $\mu$ s. Consider a pulse of 1  $\mu$ s duration then the above condition becomes  $\Delta \nu \ll 250 \text{ kHz}$ .

or better than 1 in  $10^5$  parts over a period of 1  $\mu$ s.

It can be seen that the relationship between  $\Delta \omega$  and  $\tau_1$  is a Fourier one.

These considerations are incomplete since the rate of change of the frequency is not examined in its effects upon the vector. Nor is the filtering action of the cavity considered.

Another maser would provide stability within the linewidth but the problem then arises of coupling enough power through two coupling holes.

Two pulses from an external source can be administered successively to a beam as it passes through two cavities in succession. However, there is the difficulty of arranging that the dephasing and rephasing of the components of the polarisation occurs in the same region of inhomogeneity.

#### G Transient nutation

An attempt could be made to observe transient nutation either directly in the form of the modification of a pulse transmitted through ammonia in a gas cell, or in derived form using the scheme of Macomber (discussed in Chapter III).

## REFERENCES

- Gordon, J. P. (1955), Phys. Rev. 99, 1253.
- Shimoda, K., Wang, T. C. (1955), Rev. Sci. Instr. 26, 1148-9.
- Laine, D. C. (1967), Electronics Letters, 3, 454-5.
- Singer, J. R., Wang, S. (1961), Phys. Rev. Lett. 6, 351-4.
- Jaynes, E. T., Cummings, F. W. (1963) Proc. I.E.E.E. 51, 89.
- Oliver, B. (1960), Hewlett-Packard J. 11, 1-8.
- Siegman, A. E. (1968), An Introduction to Lasers and Masers,  
(Preliminary Ed.) New York, McGraw-Hill.
- Basov, N. G., Oraevskii, A. N., Strakhovskii, G. M., Tatarenkov, V. M.  
(1964), Sov. Phys. J.E.T.P., 18, 1211.
- Helmer, J. C., Jacobus, F. B., Sturrock, P. A. (1960a) J. App. Phys.  
31, 458-63.
- (1960b), Quantum Electronics, New York, Columbia, 78-80.
- Laine, D. C., Smith, A. L. S. (1966), Phys. Lett. 20, 374-6.
- Kakati, D., Laine, D. C. (1967), Phys. Lett. 24A, No 12.
- (1969), Phys. Lett. 28A, No 11.

KEY

Symbols employed in the microwave circuit diagrams.



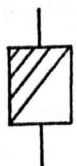
amplifier



or




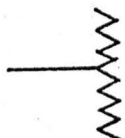
diode (microwave crystal detector, or  
second detector following r.f.  
amplifier.)



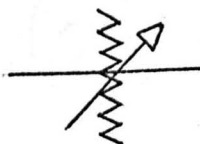
or



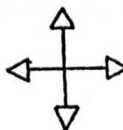
ferrite isolator (forward direction )



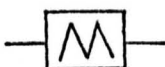
matched load



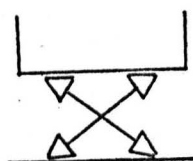
attenuator (variable)



or



matching unit

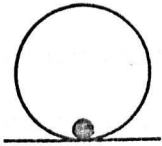


directional coupler

20 dB



junction (magic tee)



wavemeter



transition (specifically a taper from X-band  
to K-band waveguide).



variable frequency generator (including klystrons)



d.c. block.



APPENDIX A

Electroforming cavities

Copper is deposited electrolytically from an acidic copper sulphate solution on to the stainless steel mandrel. The anode is oxygen free high conductivity copper.

The composition of the solution is:

copper sulphate $\text{CuSO}_4 \cdot 5\text{H}_2\text{O}$	200g
potassium aluminium sulphate	12g
pure sulphuric acid (S.G. 1.84)	56g or 31ml
water to	1 litre

(from Canning's Handbook on Electroplating 19th.Edn.)

This reference indicates that a charge of 108 ampere-minutes per square foot is required to deposit 0.0001 inch of copper.

The mandrel is rotated slowly. The direction of the current is reversed periodically for about one third of the time, to minimise the degree of uneven deposition.

## APPENDIX B

A method for determining the loaded Q factors of microwave cavities  
(devised in collaboration with G. D. S. Smart).

The loaded Q factor of a resonator is determined by measuring the frequency separation  $\Delta\omega$  between the half-power points on the Q response curve, and using the relation  $Q = \omega_0 / \Delta\omega$ .

Two difficulties arise in determining  $\Delta\omega$ . One is that of resolution of the frequency separation which may be difficult when using a resonant cavity wavemeter possessing a Q lower than that which is being measured; the second is that of determining the half-power points on the response curve, since the absorption response seen on an oscilloscope or on a meter is modified by the klystron mode shape.

Figure B.1 shows a microwave arrangement which is commonly used to determine the Q of a cavity. The cavity is placed in a side arm of a magic T junction and the absorption is monitored in the fourth arm. The klystron mode shape is observed by coupling power from the main waveguide-run. As the klystron is tuned (by changing the reflector voltage) across the cavity resonance, the power to the cavity is maintained constant by altering the first attenuator. The second (calibrated) attenuator settings for the maximum and minimum points of the absorption are found and the attenuator settings for the half-power points calculated.

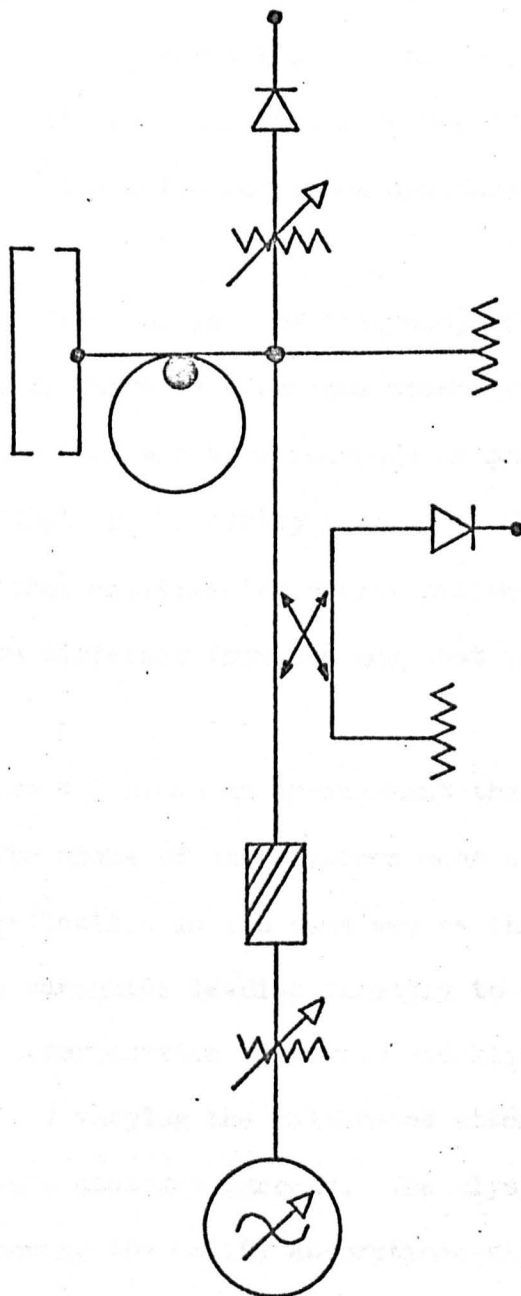


Figure B.1 Arrangement for Q measurement.

The attenuator is altered accordingly and the resonance is scanned from one side of the point of maximum absorption to the other side to give in each case a current at the detector crystal of the same magnitude as that pertaining to the centre frequency. The frequencies corresponding to these two positions are found with the cavity wave-meter.

Apart from the lack of frequency resolution obtainable with a wavemeter, there is a serious drawback to this method, and that is the fact that the klystron mode is monitored in a different location from that of the cavity resonance. The shape of the klystron mode that modifies the cavity response may, because of reflections, be different from the one that is monitored nearer the klystron.

Figure B.2 shows an arrangement that overcomes this deficiency. The shape of the klystron mode at the cavity is monitored by reflection in the same way as the resonance by coupling power from the waveguide leading directly to the cavity.

The superposition of cavity and klystron mode is plotted in terms of dB by varying the calibrated attenuator in the directional coupler to give a constant current. The klystron mode alone is then plotted by removing the cavity absorption: this is done by heating the cavity to tune it beyond the frequency limit of the mode.

Allowance may then be made for the effect of the klystron

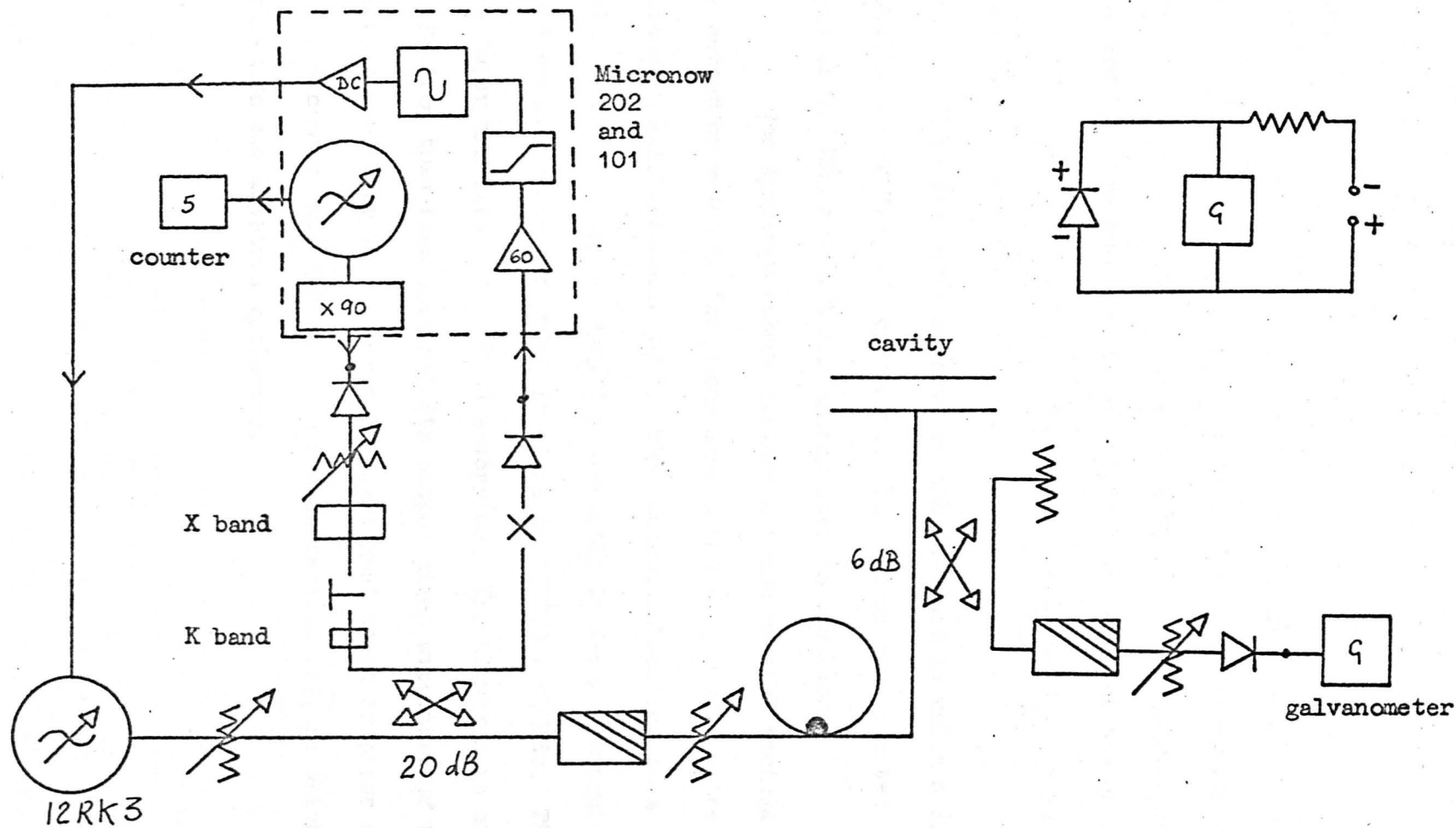


Figure B.2 Scheme employed for determining cavity Q values

mode.

In the case of the high Q cavity where the coupling was very small, it was necessary to "back off" most of the voltage developed across the galvanometer in order to retain sufficient sensitivity. The two curves were plotted in terms of the galvanometer scale readings, and the scale was in turn calibrated in terms of dB using the calibrated attenuator.

High frequency resolution was obtained by using a klystron stabilised with Micronow equipment. The curves were plotted in steps of 0.5 MHz and 0.25 MHz appropriate to the two Qs.

The Micronow scheme employs a 5 MHz crystal oscillator, the output of which is frequency multiplied to 450 MHz in the Micronow multiplier chain 101C. This output is applied to a Hewlett-Packard step-recovery diode mounted in X-band waveguide to yield harmonics, one of which is close to  $23,870 \pm 60$  MHz. There is a taper transition to K-band waveguide. The klystron is offset 60 MHz from this frequency and its output mixes with that of the harmonic generator to produce a 60 MHz signal which is phase detected in the Micronow unit 202 to produce a correction voltage which is applied to the klystron reflector.